| | |
|---|---|
| **Titre:** Title: | Attachment of Therapeutic and Imaging Agents to Flagellated Magneto-Aerotactic Bacteria Cells for Tumor Treatment and Targeting Purposes |
| **Auteur:** Author: | Yasamin Majedi |
| **Date:** | 2018 |
| **Type:** | Mémoire ou thèse / Dissertation or Thesis |
| **Référence:** Citation: | Majedi, Y. (2018). Attachment of Therapeutic and Imaging Agents to Flagellated Magneto-Aerotactic Bacteria Cells for Tumor Treatment and Targeting Purposes [Mémoire de maîtrise, École Polytechnique de Montréal]. PolyPublie. https://publications.polymtl.ca/3723/ |

UNIVERSITÉ DE MONTRÉAL

# ATTACHMENT OF THERAPEUTIC AND IMAGING AGENTS TO FLAGELLATED MAGNETO-AEROTACTIC BACTERIA CELLS FOR TUMOR TREATMENT AND TARGETING PURPOSES

YASAMIN MAJEDI

INSTITUT DE GÉNIE BIOMÉDICAL

ÉCOLE POLYTECHNIQUE DE MONTRÉAL

MÉMOIRE PRÉSENTÉ EN VUE DE L'OBTENTION

DU DIPLÔME DE MAÎTRISE ÈS SCIENCES APPLIQUÉES

(GÉNIE BIOMÉDICAL)

DÉCEMBRE 2018

UNIVERSITÉ DE MONTRÉAL

ÉCOLE POLYTECHNIQUE DE MONTRÉAL

Ce mémoire intitulé :

# ATTACHMENT OF THERAPEUTIC AND IMAGING AGENTS TO FLAGELLATED MAGNETO-AEROTACTIC BACTERIA CELLS FOR TUMOR TREATMENT AND TARGETING PURPOSES

présenté par : MAJEDI Yasamin

en vue de l'obtention du diplôme de: Maîtrise ès sciences appliquées

a été dûment accepté par le jury d'examen constitué de :

Mme CHERIET Farida, Ph. D., présidente

M. MARTEL Sylvain, Ph. D., membre et directeur de recherche

M. LAFLEUR Michel, Ph. D., membre et codirecteur de recherche

M. MOHAMMADI Mahmood, Ph. D., membre et codirecteur de recherche

M. STIKOV Nikola, Ph. D., membre

# DEDICATION

I dedicate this thesis to my beloved parents, family, teachers, friends and fellow laboratory colleagues without whom it was impossible for me to complete this work.

# ACKNOWLEDGMENT

I would like to express my deepest gratitude to my main supervisor Prof. Sylvain Martel, the director of the Nanorobotics Laboratory for giving me the opportunity to work on this project. I am truly honored to have had the privilege to work under the supervision of such an outstanding scholar. I am especially thankful to my co-supervisor, Prof. Michel Lafleur, for his continuous guidance, valuable advice and encouragement throughout the course of the project and for reviewing my thesis. This research project would not have been possible without his abundant support, invaluable guidance and valued knowledge. Very special thanks go to my other co-supervisor, Dr. Mahmood Mohammadi, for his guidance and comments that were essential for the accomplishment of this work. Special gratitude goes to Dr. Samira Taherkhani, Mr. Dumitru Loghin, Mr. Charles Tremblay, Ms. Kelly Wang, Mr. Jean-Philippe Masse, Ms. Marie-Christine Tang, Mrs. Dainelys Guadarrama Bello and Mr. Philippe Plamondon who were abundantly helpful and offered invaluable assistance, particularly in laboratory work and analysis.

Deepest gratitude is also due to my dear professors in the United Arab Emirates University; Prof. Thies Thiemann and Prof. Ali Hassan Al-Marzouqi for opening the door for me to pursue my studies in Polytechnique Montreal.

I am especially thankful to my parents, family and friends; particularly, Donia Majedi and her son Yousef Altahan, Farah Majedi, Murtada Kadhim, Ahmed Naceur, Kawthar Learning Circle, Amina Faisal, Marianna Gamba, Maryam Tabatabaei, Nahid Mohammadi, Noor Shehadeh, Raheleh Daneshi, Sangaré Alima Mantala and Sara Hosseini Kolkooh who supported me in every way during the completion of my master's studies.

My deepest gratitude goes to all the Nanorobotics Laboratory members; particularly, Mr. Arash Azizi and Mr. Kévin Gagné for their professional support.

Above all, I am grateful to God the Most Merciful.

# RÉSUMÉ

Malgré les progrès significatifs dans le domaine technologique et la compréhension du cancer (au niveau biologique), il y aura toujours des défis qui ralentiront le développement et l'implémentation de certaines options de traitements dans les essais cliniques. Les chercheurs dans les secteurs de l'administration du médicament et du génie tissulaire font face à des problèmes majeurs. Ceux-ci incluent notamment l'absence d'un système conventionnel et sélectif d'administration et de diffusion du médicament, les barrières physiologiques rencontrées par les agents antitumeur hématogènes avant de parvenir aux cellules cancéreuses dans les tumeurs solides et la séquestration des médicaments par le système immunitaire qui fait en sorte qu'une petite portion de la dose totale administrée atteint le site ciblé. Ainsi, un dosage fréquent est requis pour l'obtention de l'effet thérapeutique escompté, ce qui cause des effets adverses. Cela résulte ultimement par l'échec du traitement. De plus, l'imagerie médicale est essentielle dans le diagnostic et le traitement du cancer. Toutefois, dû à la complexité structurale des tumeurs et à la profondeur de pénétration limitée dans les tumeurs des agents de contraste disponibles, ceci était infaisable. Avec les développements récents, l'obtention d'images détaillées et à hautes résolutions a été facilitée.

L'attachement et l'imagerie d'agents thérapeutiques nanométriques aux microorganismes magnéto-aerotactiques connus sous le nom de BN-1 magnetotactic bacteria (MTB) pour le ciblage des tumeurs ont été étudiés au cours de ce projet de maîtrise. Les microrobots MTB semblent être des agents de ciblage autopropulsés et navigable idéaux. Ils sont capables de voyager contre la pression du fluide interstitiel de la tumeur (TIFP) afin de cibler les régions profondes des tumeurs solides. Les complexes de MTB ont été formulés en attachant aux MTB (i) des liposomes encapsulés avec du SN38 (MTB-LP-SN38) et (ii) des nanoparticules fluidMAG-ARA superparamagnétique d'oxyde de fer magnétiques de 200 nm de diamètre (MTB-MNP). Puisque les nanoparticules magnétiques se comportent comme des agents d'imagerie par résonnance magnétique (IRM), les complexes MTB-MNP facilitent le monitoring de la structure de la tumeur et des zones hypoxiques, tout en agissant comme rétroaction dans les opérations de navigation des MTB.

D'une part, les MTB-LP ont été développés par conjugaison covalente directe de liposomes fonctionnalisés à des groupements amine ($–NH_2$) qui sont naturellement présents à la surface des bactéries MTB, via un couplage carbodiimide. D'autre part, le complexe MTB-MNP a été préparé

selon une procédure en deux étapes. Tout d'abord, les nanoparticules magnétiques ont été fonctionnalisées avec l'anticorps BN-1 (AB) contre la protéine en surface des MTB en utilisant la chimie des carbodiimide. Par la suite, les MNP-AB ont été attachés aux MTB.

Les échantillons de LP, LP-SN38 et MTB-LP-SN38 ont été analysés par chromatographie liquide/spectroscopie de mass (LC/MS), spectroscopie UV, diffusion dynamique de la lumière (DLS) et potentiel zeta (ZP).

De plus, l'efficacité de l'attachement, l'alignement suivant le champ magnétique et la vitesse moyenne de natation d'échantillons de MTB-MNP soumis à un champ magnétique externe ont été examinés.

Subséquemment, les résultats ont montré que les cellules de bactéries MTB sont capables de transporter des quantités thérapeutiques de médicaments et d'agents d'imagerie sans compromettre leur capacité naturelle de nager.

# ABSTRACT

Despite the significant progress in technology and in the biological understanding of cancer, there are still multiple challenges that slow down the development and implementation of certain treatment options in clinical trials. The researchers in the fields of drug delivery and tissue engineering are facing major problems. Some of these include the lack of a conventional and selective drug delivery and release system, the physiological barriers that the bloodborne antitumor agents encounter before reaching cancer cells in a solid tumor and sequestration of the drugs by the immune system that makes only a few percent of the total administered dose reaching the intended target site. Hence, there is a necessity for a frequent dosing to achieve the desired therapeutic effect, which can cause adverse side effects or sometimes even treatment failure. Furthermore, medical imaging is essential in cancer diagnosis and treatment. However, current medical imaging methods have limited use due to the structural complexity of the tumor and the limited penetration depth of the previously available contrast agents into tumor tissues. With recent developments, obtaining a high-resolution and detailed image of a tumor has been facilitated.

The attachment of therapeutic and imaging nanosize agents to the magneto-aerotactic microorganisms known as BN-1 magnetotactic bacteria (MTB) for tumor targeting purposes has been studied during the accomplishment of this master's project. MTB microbiorobots appear to be ideal self-propelling and navigable targeting agents. They are capable of traveling against the Tumor Interstitial Fluid Pressure (TIFP) to target deep regions in solid tumors. MTB complexes were formulated by attaching to MTB (i) SN38 anticancer drug encapsulated liposomes (MTB-LP-SN38) and (ii) 200 nm fluidMAG-ARA superparamagnetic iron oxide magnetic nanoparticles (MTB-MNP). As the magnetic nanoparticles act as magnetic resonance imaging (MRI) contrast agents, MTB-MNP complexes facilitate monitoring the tumor structure and hypoxic zones while acting as feedback control in the MTB navigation operations.

On one hand, the MTB-LP was developed by direct covalent conjugation of functionalized liposomes to amine ($–NH_2$) groups that are naturally present on the surface of MTB bacteria, via carbodiimide-mediated coupling. On the other hand, the MTB-MNP was prepared via a two-step procedure. First, the magnetic nanoparticles were functionalized with the BN-1 antibody (AB) against the MTB protein surface using carbodiimide chemistry, then the MNP-AB were attached to the MTB.

The LP, LP-SN38 and MTB-LP-SN38 samples were analyzed with liquid chromatography/mass spectroscopy (LC/MS), UV-Spectroscopy, dynamic light scattering (DLS) and zeta potential (ZP). In addition, the attachment efficiency, alignment in the magnetic field and average swimming velocity of the MTB-MNP samples submitted to an external magnetic field were investigated. Subsequently, results showed that MTB bacteria cells are capable of carrying sufficient therapeutic and imaging agents without altering their natural swimming capability.

# TABLE OF CONTENTS

# LIST OF TABLES

# LIST OF FIGURES

# LIST OF SYMBOLS AND ABBREVIATIONS

| | |
|---|---|
| 2D | Two-dimensional |
| 3D | Three-dimensional |
| AB | Antibody |
| CDI | N,N′-carbonyldiimidazole |
| Chol | Cholesterol |
| CMC | 1-cyclohexyl-3-(2-morpholinoethyl)carbodiimide |
| COBALT | Cobalt Combination bacteriolytic therapy |
| CPT-11 | Irinotecan hydrochloride |
| DCC | Dicyclohexylcarbodiimide |
| DIC | Diisopropyl carbodiimide |
| DLS | Dynamic light scattering |
| DSPC | Distearoylphosphatidylcholine |
| DSPE-PEG(2000)-COOH | 1,2-distearoyl-sn-glycero-3-phosphoethanolamine-N-[carboxy(polyethylene glycol)2000] |
| EDC or EDAC | 1-Ethyl-3-(3-dimethylaminopropyl)carbodiimide hydrochloride |
| EPR | Enhanced permeation and retention |
| FE-SEM | Field-emission scanning electron microscope |
| GUV | Giant unilamellar vesicle |
| HDLs | High-density lipoproteins |
| HPLC | High-performance liquid chromatography |
| LC/MS | Liquid Chromatography/Mass Spectroscopy |
| LOD | Limit of detection |
| LP | Liposome |

| | |
|---|---|
| LUV | Large unilamellar vesicle |
| BN-1 MTB | BN-1 magnetotactic bacteria |
| MDT | Magnetic Drug Targeting |
| MES | 2-(N-morpholino) ethanesulfonic acid |
| MFC | Magnetic field configuration |
| MLV or LMV | Multilamellar vesicle |
| MNP | Magnetic nanoparticle |
| MP | Magnetic Particles |
| MNP-AB | Magnetic nanoparticle-antibody |
| MRI | Magnetic resonance imaging |
| MRN | Magnetic Resonance Navigation |
| MTB | Magnetotactic bacteria |
| MTB-LP | MTB-Liposome |
| MTB-LP-SN38 | MTB-Liposome-SN38 complex |
| MTB-MNP | MTB-Magnetic nanoparticle |
| NHS | N-hydroxysuccinimide |
| OATZ | Oxic-anoxic transition zone |
| PB | Phosphate buffer |
| PBS | Phosphate buffered saline |
| PDI | Polydispersity index |
| PS | Particle size |
| SEM | Scanning electron microscopy |
| S/N | Signal to noise ratio |
| SN38 | 7-Ethyl-10-hydroxycamptothecin |

| | |
|---|---|
| SPION | Superparamagnetic iron oxide nanoparticle |
| Sulfo-NHS | Sulfo-N-hydroxysulfosuccinimide |
| SUV | Small unilamellar vesicles |
| TEM | Transmission electron microscopy |
| TIFP | Tumor interstitial fluid pressure |
| ZP | Zeta potential |

---

| | |
|---|---|
| θ | Angle |
| A | Ampere |
| $B_o$ | Applied magnetic field |
| cm | Centimeter |
| G | Gauss |
| g | Gram |
| h | Hour |
| k | Kilo |
| L | U-turn diameter |
| l | Liter |
| m | Magnetic moment |
| m | Meter |
| min | Minute |
| ml | Milliliter |
| mm | Millimeter |
| $\eta$ | Viscosity of the medium |

| | |
|---|---|
| Pa | Pascal |
| pN | Piconewton |
| R | Radius of a sphere |
| sec | Second |
| T | Tesla |
| V | Velocity at an applied magnetic field |

# CHAPTER 1 INTRODUCTION

Cancer is a major and public health issue worldwide. The World Health Organization (WHO) predicts that there will be 21.6 million deadly cancer cases by 2030 annually worldwide (World Health Organization, 2017). Cancer is going to strike one in two Canadians, annual cancer statistics of Canadian Cancer Society reported in 2017 (Canadian Cancer Society, 2017). Treatment options depend on the tumor's type, size, location, stage of cancer and the overall health of the patient. Traditional cancer treatment options available are surgery, radiotherapy and chemotherapy with chemotherapy being the most common treatment for cancer.

Systemic administration of therapeutic agents with short biological half-life and narrow therapeutic index can lead to acute or cumulative toxicity. Moreover, there are many physiological obstacles and barriers that impede the delivery of therapeutics at effective concentrations to all cancer cells. For instance, upon systemic administration, some therapeutic agents will be taken up by the immune cells of the liver, spleen and other parts of the reticuloendothelial system. Other barriers to the penetration of therapeutic agents to solid tumors are intracellular tight junctions (Choi, Strauss, Richter, Yun, & Lieber, 2013) and high tumor cell density (Au, Jang, & Wientjes, 2002; Kuh, Jang, Wientjes, Weaver, & Au, 1999; Trédan, Galmarini, Patel, & Tannock, 2007). Nanoencapsulation of drug molecules in PEGylated nanocarriers (e.g. liposomes, nanoparticles, polymeric, micelles, etc.) can increase the systemic circulation, promote tumor targeting and uptake via enhanced permeation and retention effect (EPR) and ultimately minimize drug-originated systemic toxicity effects (Kaminskas et al., 2012). However, only a small fraction of the total administered doses (~ 2%) is actually delivered to the tumor (Bae & Park, 2011; Hong, Zhu, Jiang, Tang, & Pei, 2009).

Cancerous cells have the ability to spread throughout the body through the bloodstreams or the lymphatic system. This process known as metastasis creates hard-to-treat conditions. Rapid growth accompanied by inadequate vascular bed or angiogenesis is the reason why most solid tumors contain hypoxic microenvironments that act as tumoral barriers (Junttila & de Sauvage, 2013). The hypoxic regions of tumors are characterized by low oxygen levels (~ 0.7% $O_2$) and known to be resistant not only to radiation treatments, but also chemotherapy (Brown & Wilson, 2004) as these hypoxic regions are located well beyond the diffusion limits of large drug molecules. The main reason is that convection as a means of transport in the tumor interstitial space is quasi-inexistent

due to the lack of flow caused by an inefficient drainage through the lymphatic system. This causes an increase in the tumor interstitial fluid pressure (TIFP) that creates an obstacle for the delivery of therapeutics such as during chemotherapy (Minchinton & Tannock, 2006). There have been continuous efforts to increase the targeting of active agents to hypoxic regions of solid tumors (e.g. targeting exogenous and endogenous hypoxia-associated molecular markers (Bussink, Kaanders, & van der Kogel, 2003), manipulating the extracellular matrix (Minchinton & Tannock, 2006) using bio-reductive hypoxia-activated prodrugs (Weiss et al., 2011), reducing tumoral pressure (Ariffin, Forde, Jahangeer, Soden, & Hinchion, 2014), using multistage nanoparticle delivery system (C. Wong et al., 2011), etc.). However, high passive targeting efficacy cannot be achieved by the systemic treatment of these agents.

A high-efficient targeted drug delivery mechanism is still an unmet goal but is being worked upon extensively. The main problem with current mechanisms is that they lack efficient targeting and tracking systems. Magnetic targeting techniques have received much attention; however, they are not fully effective. For example, Magnetic drug targeting (MDT) and Magnetic resonance navigation (MRN) approaches are not yet feasible for a highly effective application into the tumoral microenvironments (Martel et al., 2007; Polyak & Friedman, 2009; Rotariu & Strachan, 2005). Depth-dependent MDT is more effective for near-to-skin solid tumors only because of the relatively fast decay of the magnetic field as going further away from the magnetic source. The depth-independent MRN is not highly efficient for direct delivery of therapeutics because the magnetic induction volume of the magnetic agents at the capillary level is not sufficient (Martel, 2014). Researchers have engineered artificial bacteria to deliver cancer drugs, but despite the numerous potential benefits that the synthetic bacteria therapy can offer, they still lack an autonomous unit and a precise navigation mechanism. On the other hand, some studies showed that some of the aerotaxis (behavioural response to an oxygen gradient) and chemotaxis (response to environment's chemical composition change) bacteria found in nature could be promising therapeutic agents vectors. For instance, different studies showed that Clostridia (Fox et al., 1996; St Jean, Zhang, & Forbes, 2008), Salmonella (Forbes, Munn, Fukumura, & Jain, 2003; Ganai, Arenas, Sauer, Bentley, & Forbes, 2011; Kasinskas & Forbes, 2006), Bifidobacterium (Yin et al., 2013) and Escherichia coli (Forbes, 2010) bacteria successfully delivered therapeutic molecules to tumor tissues.

In 2016, Felfoul and colleagues showed that BN-1 magnetotactic bacteria (MTB) (Frankel, Bazylinski, Johnson, & Taylor, 1997) have the required characteristics to act as medical microrobots for applications in targeted cancer therapy in the field of medical nanorobotics (Felfoul et al., 2016). The goal is to enhance the delivery or uptake by the targeted cells while reducing the toxicity of the free drug and/or of the nanocarriers for the healthy tissues. MTB are spherical cells with diameters less than the diameter of the smallest blood vessel in the human body (1-2 μm in diameter). They naturally contain a chain of single-domain membranous iron oxide magnetic nanoparticles (MNP) known as magnetosomes that causes the bacteria to align in the direction of the applied magnetic field (0.5-100 Gauss). In a clinical setting, such direction is ultimately set towards the tumor. Furthermore, MTB are microaerophilic organisms. By means of their oxygen sensing mechanism, they are able to detect low oxygen gradients (~ 0.5% oxygen level) and swim towards the low oxygen regions of active cancer cells via two flagella bundles that can generate tenfold more propulsive force (~ 4.0 - 4.7 piconewtons (pN)) compared with other flagellated bacteria, a factor facilitating deep penetration in tumor tissues. In addition, the flagella provide the bacteria with an average swimming velocity of 200 $\mu m.s^{-1}$.

While MTB appear to be ideal self-propelling and navigable targeting agents, capable of traveling against the TIFP to target deep regions in solid tumors, these magneto-aerotactic bacteria can be loaded with drug-containing nanoscale particles attached to the surface of the cells prior to be injected near the tumor with superior delivery ratios and minimized systemic circulation (Felfoul et al., 2016) compared to all the other known targeting modalities such as drug-encapsulated micro/nanoparticles (Kumari, Yadav, & Yadav, 2010; Malam, Loizidou, & Seifalian, 2009) and bacterial therapies.

In the first part of this work, drug-loaded liposomes were successfully attached to the surface of MTB for tumor targeting and treatment purposes. The attachment efficiency of drug-loaded liposomes to the surface of MTB was studied. In the second part, a magnetic resonance imaging (MRI) contrast agent was successfully attached to the MTB for tracking loaded bacteria and tumor visualization purposes. The swimming velocity, magnetic sensitivity or alignment in the magnetic field and the U-turn characteristics of the swarms of control MTB versus MTB complex were studied.

## 1.1 Thesis outline

This thesis work is in the framework of a major research project aiming to develop a novel approach for cancer treatment using MTB. The preliminary works of the current project were done by Taherkhani, Essa and their colleagues (Felfoul et al., 2016). The main role of the candidate was to reproduce the attachment of payload to the surface of MTB to enable targeted drug delivery as microcarriers that can also be employed in different fields such as drug delivery, gene delivery, real-time imaging, etc. The thesis is organized into five chapters, as elaborated below.

Chapter 1 presents a general introduction and it brings forward the need for developing MTB liposomal-based drug delivery system and MTB-magnetic nanoparticles for tumor targeting and MRI imaging purposes, respectively. This chapter also presents the research hypothesis and objectives.

Chapter 2 presents a comprehensive literature review and background information. The purpose of this chapter is to highlight the current therapeutic technologies and tumor imaging modality approaches for cancer therapy. The role of bacteria as biocarriers in cancer therapy, liposomes as drug carriers and the role of superparamagnetic iron oxide nanoparticles in imaging applications were specifically discussed in this chapter.

Chapter 3 consists of the research methodology of the thesis. In more details, in this part, the author outlines the research strategy, the research approach, for the formulation of functionalized liposomes, development of MTB liposomal-based delivery system for carrying therapeutics and MTB-magnetic particles for MRI imaging purposes in cancer therapy.

Chapter 4 addresses the produced experimental findings and results during the candidate's masters study. The drug entrapment efficiency in liposomes, characterization of the drug-loaded liposomes attached to the MTB, attachment efficiency of the magnetic nanoparticles to MTB and characterization of the control MTB versus MTB complex were presented in this chapter. This chapter is also dedicated to discussing the findings and highlight the main results of this master project.

Chapter 5 presents a concise conclusion drawn from the research results followed by recommendations and future perspective.

## 1.2 Thesis hypothesis and objectives

### 1.2.1 Thesis hypothesis

Development of bacteria-based complexes without compromising the bacteria cells' capabilities (e.g. magnetic response, motility, etc.).

### 1.2.2 Thesis objectives

The goal of this master's work was to study and assess the attachment of the therapeutic and imaging nanoparticles to the surface of live MTB as a self-propelled microrobot for tumor targeting, treatment and imaging purposes.

**Objective 1:**

Provide instructions on the formulation of functionalized liposomes.

**Objective 2:**

Provide the protocol for loading the liposomes with the SN38 antitumor drug.

**Objective 3:**

Provide the procedure of attachment of the SN38 loaded liposomes to the MTB.

**Objective 4:**

Provide the procedure of attachment of the superparamagnetic iron oxide nanoparticles to the MTB.

# CHAPTER 2 BACKGROUND AND LITERATURE REVIEW

The following chapter provides a comprehensive literature review for this project. The first part of this literature review covers the current cancer therapy modalities. The second part discusses targeted cancer therapy, specifically magnetic targeting. The third part presents the clinical applications of bacteria-based therapy and addresses the use of BN-1 magnetotactic bacteria as a new approach to overcome the limitations of other types of bacteria in cancer therapy. The fourth part tackles SN38 as an anti-cancer drug while the fifth part discusses liposomes as a drug carrier. The sixth part describes carbodiimide chemistry as a common bioconjugation technique employed to attach nanoparticles to the surface of the MTB cells. Finally, the last part of this literature review discusses the role of magnetic particles (MP) as MRI contrast agents and the motivation behind the use of superparamagnetic iron oxide nanoparticles in tumor imaging.

## 2.1 Cancer treatment options

With all the improvements in overcoming various diseases, cancer still stands as one of the leading causes of death worldwide. Radiation therapy, surgery and chemotherapy are the main classifications of current therapies widely used for cancer treatment. Cancer therapy by surgery is an invasive treatment leading to the complete elimination of the tumor which involves removing the healthy tissue surrounding the tumor as well (S. A. Hussain, Feb 2001). This type of treatment includes difficulties such as the size or the location of the tumor, damaging of the healthy tissue located around the tumor, metastasis and the potential risk of host-pathogen interactions. On the other hand, some radiation therapies lack the ability to target a specific location in the body, resulting in severe side effects for the patient. In such therapies, the radioactive substances along with a high dose of ionizing radiation move throughout the body and affect both the cancerous cells as well as the normal tissues. In addition, cancer cells in the hypoxic oxygen-deficient sections of the tumor are resistant to both radiotherapy and chemotherapy (Moeller, Richardson, & Dewhirst, 2007; Znati et al., 1996). Chemotherapy often involves systemic side effects with no specific distribution and unfavorable pharmacokinetics. High concentrations of the anti-tumor drug are required in order to reach an effective dose, but this can lead to an unsustainable drug level, drug resistance, dangerous side effects and ultimately organ failures. Furthermore, following extravasation from the tumor vessels, the drugs often attach to the cellular barriers preventing them

from reaching the inaccessible region of the tumor. Thus, the chemotherapy drug is withheld to affect the quiescent cancer cells in hypoxic sections situated far away from the tumor vessels (Brown & Wilson, 2004). Sometimes the association of different treatment methods is needed to enhance the therapeutic indices (O'Connell et al., 1994; Peddareddigari, Wang, & DuBois, 2010). Therefore, improvement of the therapeutic benefits by employing an active transport vehicle that prevents healthy cells from being exposed to the anti-tumor drugs and delivers the drug substances directly to the target site is necessary.

## 2.2 Targeted therapy for cancer

The systemic therapy's efficiency depends on the adequate amount of the pharmaceutical agent's transportation to the tumor site. To achieve this efficiency, the active agent has to reach the vascular system of the tumor, secrete in the interstitium and then, move to the tumor tissue in order to be in straight contact with the tumor cells (Jain, 2012). Improvement of the active or passive tumor targeting methods assists in increasing the effectiveness of the diagnostic or therapeutic agent's delivery to the tumor cells that can be reached by magnetic navigation (Furlani & Furlani, 2007; Mishima, Takeda, Izumi, & Nishijima, 2006), particulate-based drug formulation (e. g. polymers, dendrimer and liposomes) (Kumari et al., 2010; Malam, Loizidou, & Seifalian, Nov 2009) or chemoembolization (Maleux et al., 2009).

### 2.2.1 Magnetic targeting delivery

In order to transfer the therapeutic agents to the tumor, proper steering delivery systems are in need and this can be obtained with magnetic targeting methods such as MRN and MDT (Gleich et al., 2007; Mishima et al., 2006). The current method for magnetic targeting involves encapsulating the therapeutic agents in the polymeric-magnetic particles' hybrids or liposome nanoparticles and guide them towards the tumor site using the magnetic force generated by the gradient coils of the MRI system (Martel et al., 2007; Pouponneau, Leroux, & Martel, 2009) or by an external magnet (Furlani & Furlani, 2007; Mishima et al., 2006). In MDT, therapeutics are being loaded in magnetic particles and trapped near the tumor via external magnets. Because of higher gradient intensity near the magnet, the targeting efficiency of this technique greatly relies on how close the tumor site is to the magnet. In order to enhance the targeting efficacy for tumors located deep inside the body, the MRN technique for navigation of an untethered device was proposed by Martel and colleagues

(2009) (Martel et al., 2009). MRN technique relies on the induction of 3D directional magnetic propulsion force on magnetic materials generated from three magnetic gradient coils of the MRI.

The MRN system was used in the presence of a magnetic gradient by Martel and colleagues (2009) to apply a magnetic force on magnetized magnetic particles, guiding them in the main vascular system of a live pig (Martel et al., 2009). MRN merged with chemoembolization demonstrates a considerable improvement in the MRI-based navigation of microdevices to targeted regions (Pouponneau et al., 2009).

Although MRN has advantages over MDT, the navigational control of both techniques decreases dramatically in the tumor complex microvasculature, while higher force is required to diffuse the small therapeutic carriers inside the capillaries of the microvasculature (Felfoul, Mathieu, & Martel, 2008; Martel et al., 2007).

## 2.3 The role of bacteria in cancer therapy

The application of bacteria in cancer therapy was accidentally discovered by Coley in 1891 (Coley, 1891) which was the beginning for other researchers to verify different strategies in order to make a progress towards the treatment of cancer (Baban, Cronin, O'Hanlon, O'Sullivan, & Tangney, 2010; Bettegowda et al., 2003; Forbes, 2010; Gardlik, Behuliak, Palffy, Celec, & Li, 2011; Kasinskas & Forbes, 2006; Patyar et al., 2010). The main specifications of the bacteria that make them a potential agent in cancer therapy are that the bacteria possess self-powered and self-propulsion properties and they can specifically proliferate, target and accumulate within the solid tumor areas. They are capable of swimming in low Reynolds number hydrodynamics similar to the tumor microenvironments and human capillaries. Bacteria can generate toxins that are able to destruct and lyse the tumor tissues. They generate an externally detectable signal while the sensory apparatus of the bacteria allows them to react to internal signals and/or external stimuli in the tumor microenvironment (Bettegowda et al., 2003; Forbes, 2010; Kasinskas & Forbes, 2006; St Jean et al., 2008).

The strains of Bifidobacterium (Yin et al., 2013), Clostridia (Fox et al., 1996; St Jean et al., 2008) and Salmonella (Forbes et al., 2003; Ganai et al., 2011; Kasinskas & Forbes, 2006) bacteria, are generally used as potential candidates to penetrate deeply and accumulate into the preferred hypoxic regions. Research on animal models demonstrated that Salmonella is able to arrive at the

tumor through the broken vessels when intravenously administrated. After entering the tumor region, because of the suitable environment, Salmonella is able to form colonies and induce apoptosis (Ganai et al., 2011; Kasinskas & Forbes, 2006). In addition, bacteria can be utilized as vehicles for gene therapy or their genes can be modified in order to exhibit genes that induce antitumor effects (Baban et al., 2010; Fox et al., 1996; Gardlik et al., 2011). Bacteria can also play the role of a vehicle that delivers therapeutic agents to the target (St Jean et al., 2008). Some techniques to defeat cancer by using bacteria-based technology is demonstrated in Figure 2.1 (S. Liu et al., 2014). Schematic depiction of the hypothetical process of solid tumor invasion and colonization by Salmonella is presented in Figure 2.2 (Felgner, Kocijancic, Frahm, & Weiss, 2016).

Regardless of the massive research done on bacteria in cancer therapy, the method still faces many difficulties before it can be effective in clinical applications. For example, a high dose of bacteria is needed in order to induce a significant therapeutic effect which may result in intense toxic side effects. Furthermore, the lack of the hypoxic areas at the primary stage of the tumor can significantly decrease the effectiveness of anaerobic bacteria that are administered via intravenous injection. This influences the bacteria to target, form colonies and generate toxins in the central areas of solid tumors (Baban et al., 2010; S. Liu et al., 2014). For example, in a phase I clinical trials, the application of a genetically modified anaerobe Salmonella typhimurium (VNP20009) to target small tumors with an absent necrotic zone demonstrated that tumor colonization of bacteria can be reached at very high dose but with no antitumor effects (Toso et al., 2002).

Anaerobic bacteria often accumulate and influence the necrotic and hypoxic cells (Moese & Moese, 1964) while the radiation therapy and chemotherapy possess limitations toward destroying the cells in these areas (Gray, Conger, Ebert, Hornsey, & Scott, 1953; Roizin-Towle & Hall, 1978). “Combination bacteriolytic therapy” (COBALT) was suggested to improve the results of the previously mentioned treatment, which combines bacterial therapy and conventional cancer treatments such as radiotherapy and chemotherapy (Dang, Bettegowda, Huso, Kinzler, & Vogelstein, 2001). For example, Clostridium novyi bacteria have been studied along with the radiotherapy agents (Bettegowda et al., 2003). Cheong and colleagues (2006) demonstrated that the release of liposomes encapsulating a drug in the necrotic area of the tumor can be increased by using cell membrane-disrupting properties of bacteria proteins (Cheong et al., 2006). Using aerotaxis or chemotaxis, these types of bacteria are able to arrive and accumulate in the tumor sites without computer-assisted navigation (Forbes et al., 2003; Kasinskas & Forbes, 2006).

Magnetotactic bacteria are suggested as remotely computer-controllable agents to deliver drugs to solid tumors (Taherkhani, 2015).

### 2.3.1 BN-1 magnetotactic bacteria

Martel and colleagues (2009) used flagellated BN-1 MTB as a delivery system that possesses the main specifications needed to deliver the therapeutic agents into the unreachable regions of the tumor sites (Felfoul et al., 2016; Martel, Mohammadi, Felfoul, Lu, & Pouponneau, 2009). In one of the studies, nanoliposomes were attached on the surface of the MTB and injected near the tumors in mice. Swarms of the bacteria complexes were guided under an applied magnetic field and the results showed that up to 55% of total drug loaded MTB reached into regions of active cancer cells in colorectal tumors (Felfoul et al., 2016). This was a huge improvement over the 0.7% achieved by standard chemotherapy. Such result means that a much lower dose will lead to much enhanced therapeutic effects for a given therapeutic leading to much less toxicity for the patients, which might ultimately lead to significant reductions in health care cost considering that toxicity-related issues contribute significantly to an increase of the treatment for the patients. This approach applies to many therapeutics and cancers where injections near the tumor are possible. When the injection near the tumor is too complex or invasive, an approach based on exploiting the magnetic field of a clinical MRI scanner has been developed and validated by Martel, 2017 (Martel, 2017). But this approach can only target near the tumor and not the regions of active cancer cells inside a tumor.
Figure 2.3 demonstrates the BN-1 MTB cells with a spherical shape and 1-2 μm in diameter. These properties provide the ability for the BN-1 MTB cells to extravasate into the tumor site from the tumor's blood vessels which have pores sizes of 0.38 to 2 μm (Hobbs et al., 1998; McDonald & Baluk, 2002). Furthermore, the suitable size of the cells allows a maximum surface area that enables the attachment of nanoscale components on its surface (Taherkhani, 2015). The BN-1 MTB cells can play the role of microrobots with a directional self-propelling system which is generated by two bundles of nine flagella located at one side (Felfoul et al., 2016). The ~ 4 pN propelling force of the BN-1 MTB cells are produced by the flagella. This can be very effective when functioning in the tumor microenvironment and the smallest blood vessels that have Reynolds number hydrodynamic conditions (Koumoutsakos, Pivkin, & Milde, 2013). BN-1 MTB cells have relatively higher propelling force compared to other flagellated bacteria with the thrust force of 0.3

- 0.5 pN (Martel et al., 2009). Furthermore, the average swimming speed of the MTB is about 200 $\mu m.s^{-1}$ at room temperature (Martel et al., 2009).

As demonstrated in Figure 2.3a, the BN-1 MTB cells have a single magnetosome chain which is made from 10 - 15 magnetite ($Fe_3O_4$) nanoparticles in the size range of 30 - 80 nm. The embedded remote-control interface in the BN-1 MTB, as well as efficient motor sensory and actuation capabilities, support the idea of the BN-1 MTB as a microrobot in the field of targeted delivery (Martel, 2012).

As can be observed in Figure 2.4, when the BN-1 MTB cell is in contact with an external directional magnetic field a little higher than 0.5 Gauss (the Earth's magnetic field), the magnetic dipole moment (m) is provided by the magnetized chain. The BN-1 MTB cells possess a magnetic moment of almost $10^{-15}$ $A.m^2$ (or $J.T^{-1}$), that allows them to respond to magnetic fields as low as 50 μT ($5 \times 10^{-20}$ J) (Blakemore, 1982). Once there is an angle (θ) between the applied magnetic field (B) and the magnetic dipole of the chain, the magnetic torque is employed (De Lanauze, 2013; Felfoul, 2011b; Nadkarni, Barkley, & Fradin, 2013). The induced magnetic torque allows the magnetosome chain to act as a compass and aligns the MTB cells in the magnetic field (Felfoul, Pouponneau, Mathieu, & Martel, 2007; Martel, 2006).

The behavior of the MTB cells in the applied magnetic field depends on the magnetic moment. The value of the magnetic moment is influenced by the properties of the magnetosome chain (e.g. size and a number of the magnetic nanoparticles). The arrangement of the $Fe_3O_4$ nanoparticles within the MTB cells in a linear format maximizes the magnetic moment of the bacteria. The BN-1 MTB inherently shift in the direction of the oxic-anoxic transition zone (OATZ) in reaction to the Earth's magnetic field. In OATZ, BN-1 cells prefer low oxygen concentrations (~ 1 - 2% $O_2$), this action is named magneto-aerotaxis behavior (Frankel et al., 1997). To use MTB in the controlling purposes for *in vivo* drug delivery into hypoxic areas and tumor microenvironments, the mentioned specifications are very important. Magnetotaxis (response to magnetic field's lines) in combination with aerotaxis is able to influence the BN-1 MTB swimming orientation and the bacteria response is based on a balance of these stimuli (Denham, Blakemore, & Frankel, 1980; Frankel & Blakemore, 1980).

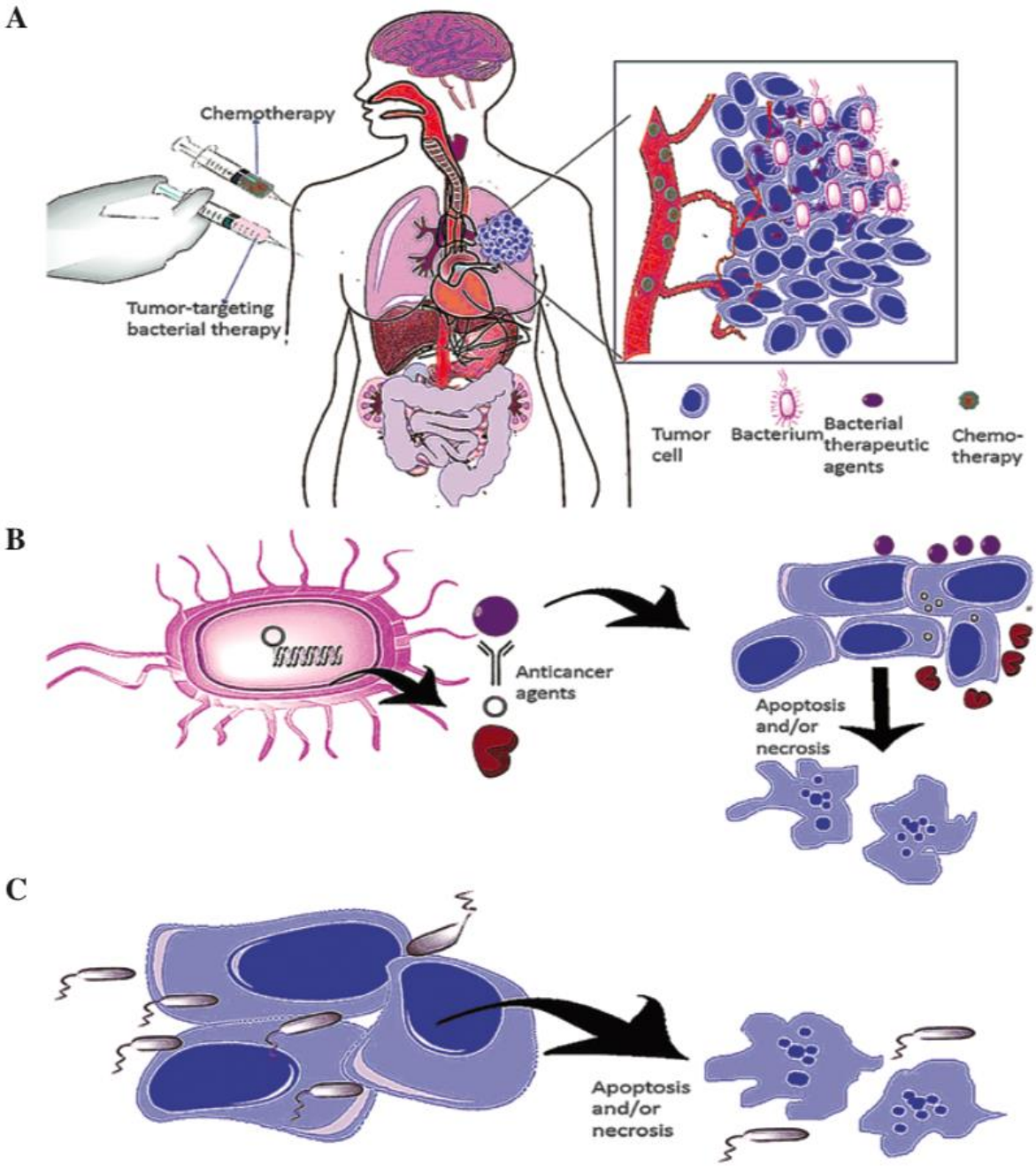


Figure 2.1: Bacteria cancer therapy strategies. (A) Bacteria have the ability to penetrate tissues. Anaerobic bacteria could actively penetrate deep into tumor tissue and accumulate following systematic injection (pink syringe), a property that the traditional chemotherapy (green syringe) does not possess. (B) Delivery of anti-tumoral agents. Bacteria are capable of delivering specific materials, which may be attached to particular anticancer agents. (C) Bacteria in oncolytic therapy. Anaerobic bacteria accumulate into tumor tissue and multiply in the hypoxic/necrotic regions while directly kill tumor cells. Adapted from (S. Liu et al., 2014).

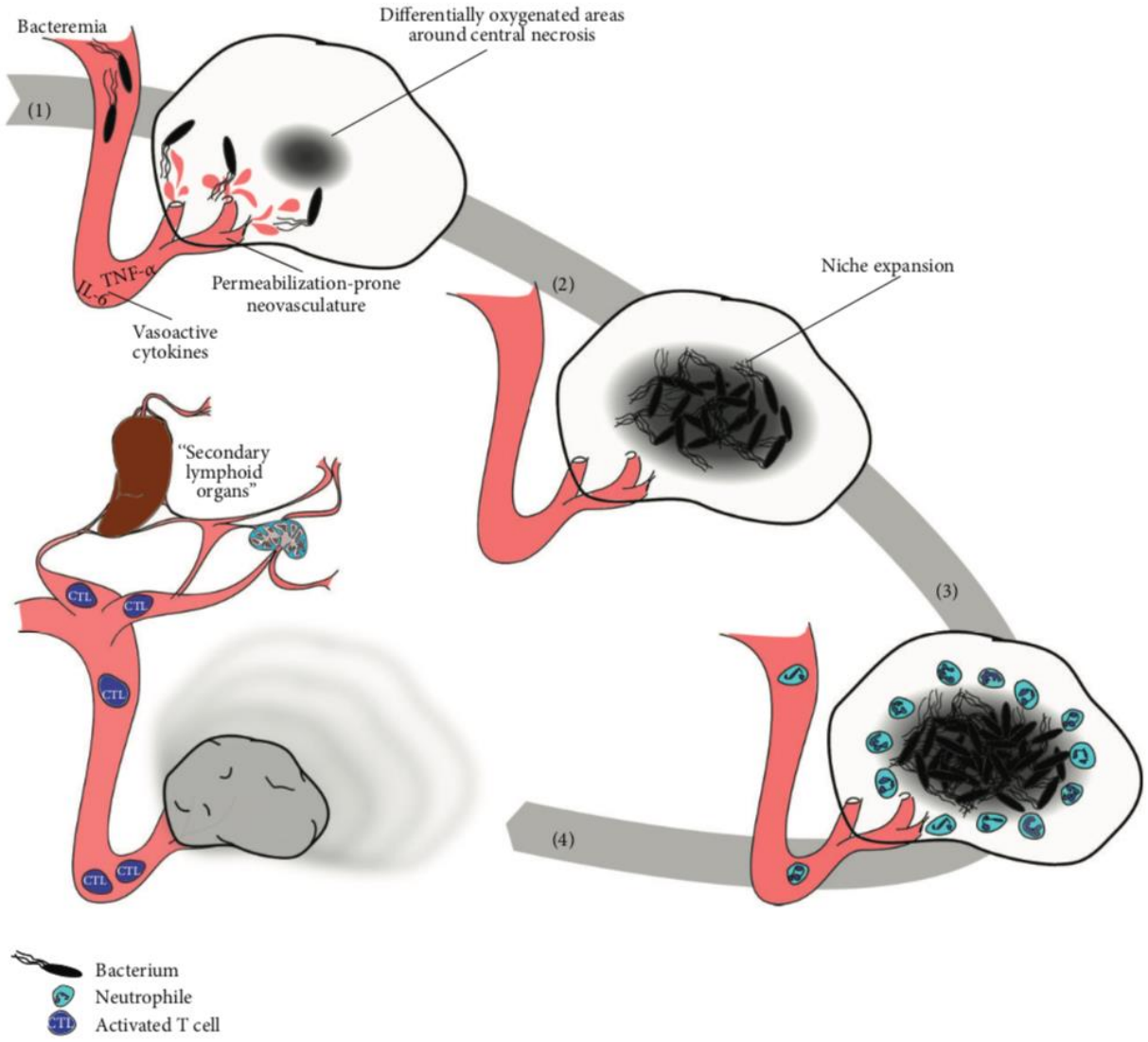


Figure 2.2: Major biological events associated with the antitumor therapeutic effect of Salmonella. (1) Tumor invasion. When bacteria are injected in the bloodstream, they induce a cytokine storm, which is dominated by vasoactive cytokines that enable passive deposition of bacteria in the tumor during the induced hemorrhage. (2) Colonization. Invading bacteria accumulate in the low oxygen concentration regions and proliferate to saturation. (3) Infection control. Colonization affects the tumor microenvironment by attraction and polarization of the innate effector cells and cytokines in favor of antibacterial control and tumor immune surveillance. (4) Antitumor response and tumor regression. Tumor regression takes place in response to multimodal therapeutic effects, including an adjuvant effect on the previously developed tumor immune surveillance, polarization of innate effectors' phenotype, direct cytotoxicity and passive effects. Adapted from (Felgner et al., 2016).

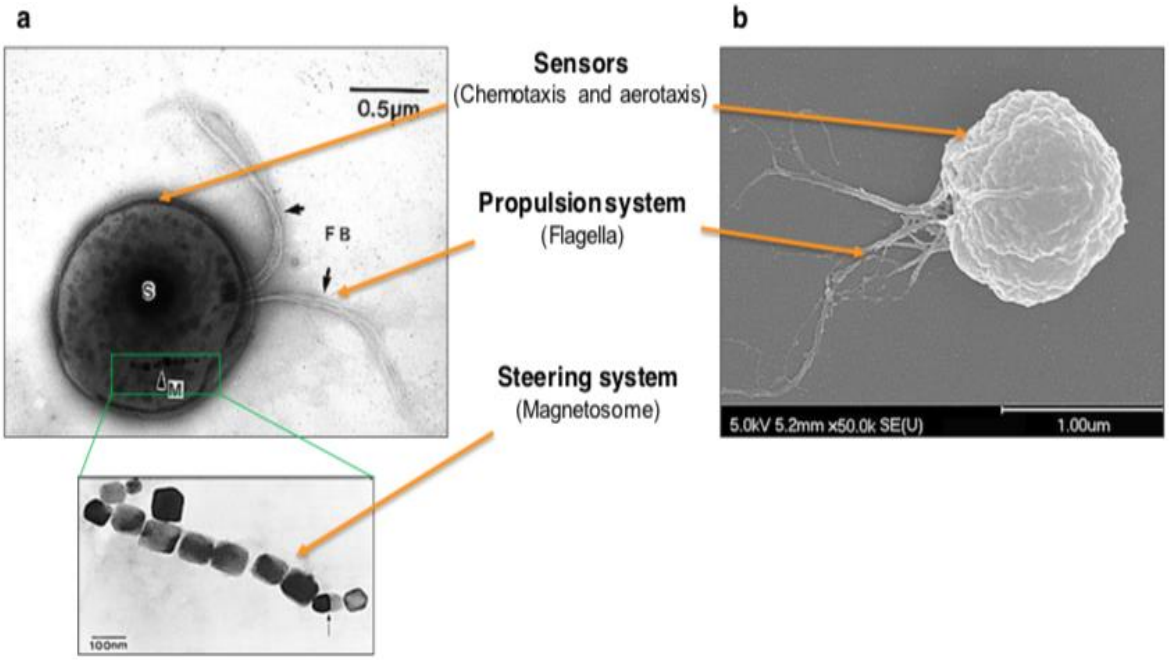


Figure 2.3: (a) MTB TEM (Frankel et al., 1997), its magnetosome chain (bottom) (Martel et al., 2009) and (b) SEM (Martel, Mohammadi, de Lanauze, & Felfoul, 2013) images with the main sensor and actuator components needed for delivering therapeutics deep into solid tumors. The photograms show the two flagella bundles that act as propulsion system (a, b) while the single chain of magnetosome with the size ranging from 30 - 80 nm as steering (a).

### 2.3.2 BN-1 MTB cells versus magnetic nanoparticles

From the microrobotics perspective, for a precisely targeted delivery to the tumor site, self-propulsion force, appropriate size and high velocities are the main required characteristics. Magnetite particles compared to the small magnetic bacteria with the same size and high swimming velocities need a much higher magnetic field to gain the same magnetophoretic velocity. The magnetic bacteria can be directionally controlled by applying a weak directional magnetic field (a little greater than the Earth's geomagnetic field) instead of using tens to hundreds of thousands of times higher field needed for any other magnetic targeting techniques (Frankel et al., 1997). Moreover, two bundles of flagella enable the propulsion force of the MTBs instead of an induced external force. For example, considering the BN-1 MTB and microcarriers at the same conditions (e.g. same velocity (200 $\mu m.s^{-1}$) and same size (2 $\mu m$)), the MTB bacteria are exposed to a much weaker magnetic field (Felfoul et al., 2008), which is higher than the threshold for clinical practices (Martel, 2013a).

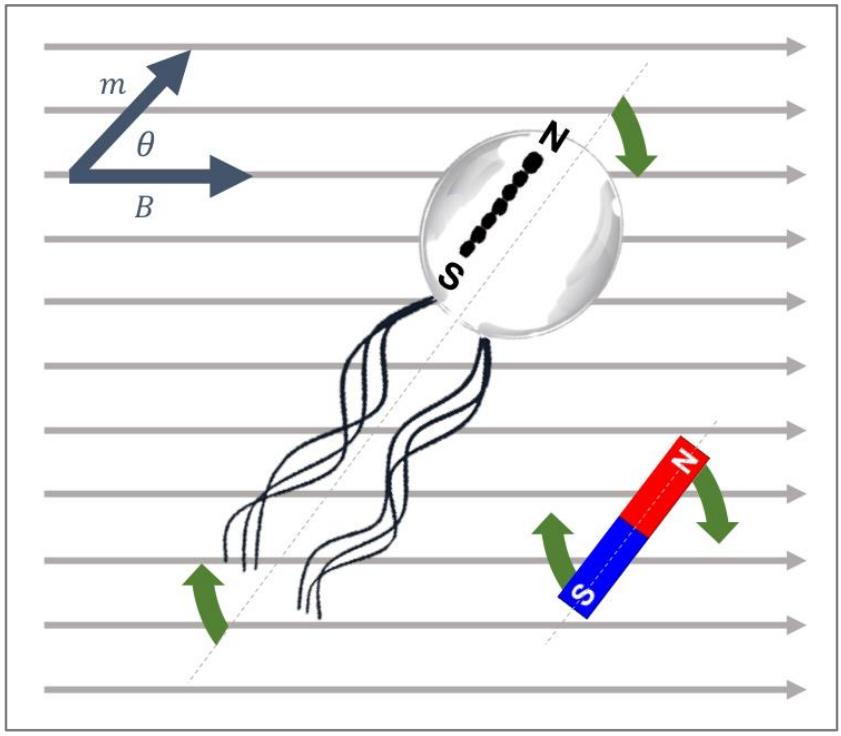


Figure 2.4: Schematic representation of the induced magnetic moment on the magnetosome chain of the polar BN-1 MTB cell in a homogeneous magnetic field. m is the magnetic moment of the MTB, B is the external magnetic field and θ is the angle between them (De Lanauze, 2013; Felfoul, 2011b; Nadkarni et al., 2013).

Despite MTB's appearance as a more promising method to increase the efficacy of tumor targeting and its possibility for deep penetration in comparison to magnetic particles using MRN and MDT methods (Martel et al., 2007; Polyak & Friedman, 2009; Rotariu & Strachan, 2005), it still encounters certain limitations when moving in the bloodstream. In order for the carrier to move through the blood vessels, its diameter should not exceed half the diameter of the smallest capillary (~ 4 μm) and it should attain a propulsion of ~ 4 pN (Felfoul et al., 2008; Martel, 2013b; Martel et al., 2009). Furthermore, usually, the leaky tumor vessels have openings of < 2 μm in size (Hobbs et al., 1998; McDonald & Baluk, 2002), which supports the requirement of the carrier diameter not exceeding 2 μm. Despite the much more effective function of BN-1 MTB in the microvasculature and in the tumor environment compared to the other known methods (S Martel, 2014; Martel et al., 2009), BN-1 MTB alone still has low efficiency because of the high blood flows in the large blood vessels. In theory, BN-1 MTB are not controllable at the fluidic turbulent motion and the flow leads to their disorientation (Taherkhani, 2015).

Thus, the usually applied intra-arterial or intravenous administration in chemotherapy is not the best choice for the MTB-based therapeutic interventions (Taherkhani, 2015). Flagellated bacteria are navigated through the larger blood vessels using methods such as balloon catheter or embolization to temporarily decrease the blood flow supplying the tumor (Felfoul et al., 2008). Compared to the previously mentioned techniques, magnetic microparticles with high saturation magnetization possess a higher effectivity in the larger blood vessels. When magnetic particles are larger in size, they must be exposed to a much lower magnetic gradient than a smaller particle (due to the material's magnetic volume) to obtain a similar magnetophoretic velocity. For example, the particle with a size of 10 μm or higher requires only < 500 mT/m magnetic gradients, which is among the acceptable targeting range, but its size is not appropriate for acting at the capillary level (Mathieu & Martel, 2007).

### 2.3.3 BN-1 MTB cells navigation via the magneto-aerotaxis system

Leading the MTBs to a tumor region to reach the dose of therapeutic agents and also the directional control movement of them needs generating a swarm aggregation of MTB in a three-dimensional volume. Software control systems, magnetic sequences, three-dimensional magnetic navigation platforms and physic theories for BN-1 MTB accumulation in a specific region were designed by De Lanauze and Felfoul (Figure 2.5) (De Lanauze, 2013; De Lanauze, Felfoul, Turcot, Mohammadi, & Martel, 2014; Felfoul, 2011a). Briefly, a magnetotaxis platform compromising six electromagnets is built with a configuration of three-axis orthogonal pairs of independent magnetic gradient coils and special time-varying sequences capable of producing a three-dimensional magnetic field. Maxwell configuration of the electric coils results in equal but opposite currents. Thus, in the magnetotaxis platform, by independent current ratio variations between each pair of electric coils, aggregation of MTB can be produced and its location can be controlled at the coil center. For example, when two electric coils positioned in a Maxwell configuration with equal but opposite currents are being used, a MTB aggregation plane at the center of these two coils can be produced. The aggregation can be shifted by changing the current ratio between these coils (De Lanauze et al., 2014). Figures 2.6 and 2.7 show the movement of the individual bacterium and an aggregation of MTB under an applied magnetic field, respectively.

The direct current power used to produce the magnetic field prevents overheating, radiation or any other side effects on the animals. Furthermore, the magnetic fields used to navigate the MTBs are

very weak, in the range of 10 - 100 Gauss (0.001 - 0.1 Tesla). When the MTBs are exposed to a magnetic field a little higher than the Earth's magnetic field, the concentration of oxygen has no influence on the swimming behaviors of the MTB cells and magnetotaxis exclusively affects the direction of the MTBs, which can be controlled by computers and electronics (Martel et al., 2009; Martel, Tremblay, Ngakeng, & Langlois, 2006). A three-dimensional field is able to induce a directional movement and torque on the MTB to generate an aggregate in a certain volume depending on the MTB concentration. Also, the movement and position of the MTB cells in the three-dimensional space is controlled by a computer software (De Lanauze et al., 2014; Sylvain Martel, 2014).

Figure 2.5 demonstrates the basics of the magnetotaxis system. As the distance from the coils increases (blue arrows), the directional magnetic field strength becomes weaker. The coils electrical current is adjusted to reach the aggregation zone outer boundary. This region correlates to the field intensity where the directional torque is induced insufficiently on the magnetosome chains and the direction of the swimming MTB is not influenced by the field. Therapeutic agent-loaded MTB will aggregate when any MTB leaving this 3D volumetric aggregation area is forced to come back within the zone. This is because of the induction of a sufficient directional torque on the chain of magnetosomes outside this area. Within the aggregation area, since a very weak directional torque is being induced on the magnetosomes, the magnetotaxis directional control is no more possible. Certainly, when the MTB assembles in the aggregation area, it continues to pursue a continual free circular motion. Within the tumor area, the displacements of MTB with the guidance of their microaerophilic behavior affects aerotaxis searching for hard-to-treat hypoxic regions of solid tumors (Felfoul et al., 2016).

When the BN-1 MTB enters the physiological environment, they become non-motile after ~ 40 minutes due to their changes in their growth culture environment and higher temperatures. This leads to a gradual reduction in the swimming velocity and the propelling force of BN-1 MTB (Martel et al., 2009). Thus, the short period during which the MTB is active and alive limits the whole *in vivo* process to target and navigate using BN-1 MTB (Taherkhani, 2015).

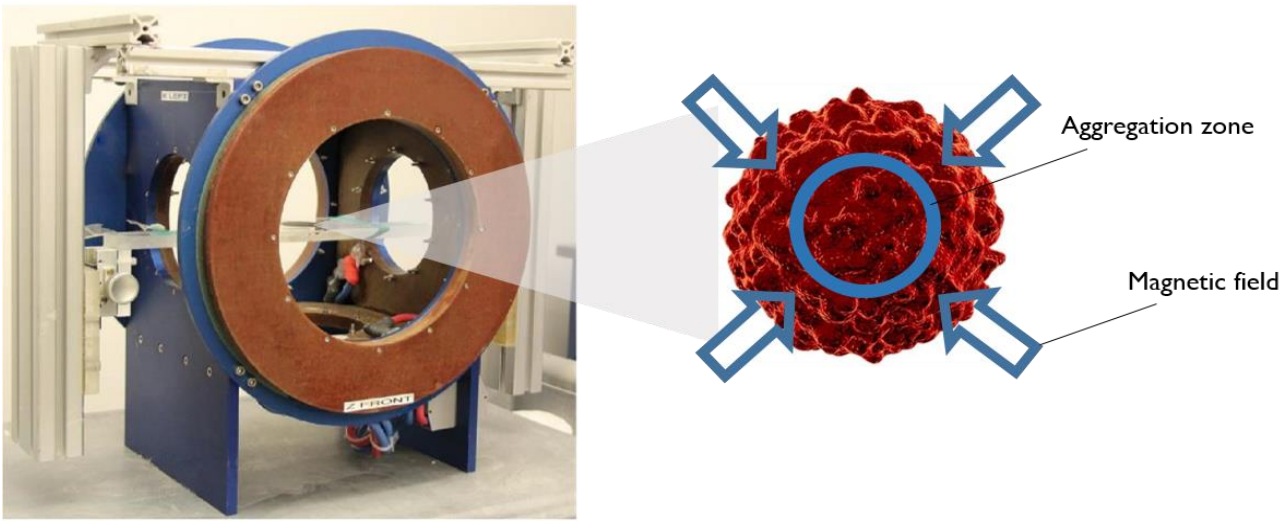


Figure 2.5: Representation of the magnetotaxis system with three independent magnetic gradient coils to test the capability of the MTB microactuator in transferring therapeutics into the hypoxic zones of solid tumors. Adapted from (Felfoul et al., 2016; De Lanauze, Felfoul, Turcot, Mohammadi, & Martel, 2014).

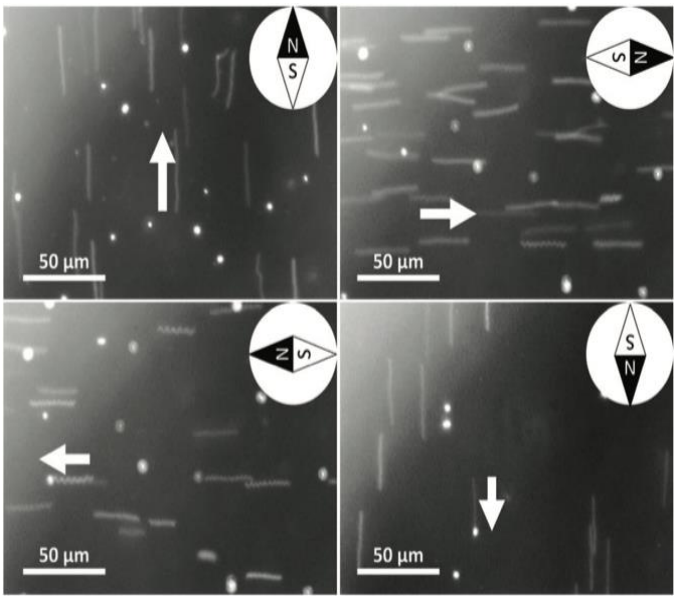


Figure 2.6: Microscopic images of MTB (white lines) responding to 2 mT magnetic field induction at various directions (the white dots should be disregarded as they are dead bacteria on the surface of the microscope slide). The swimming direction of the MTB is shown by white arrows. The compass north tip represents the direction of the applied magnetic field. Images were acquired by a Zeiss Imager.Z1 optical microscope in darkfield reflection mode via an exposure time of 200 msec. Adapted from (De Lanauze et al., 2014).

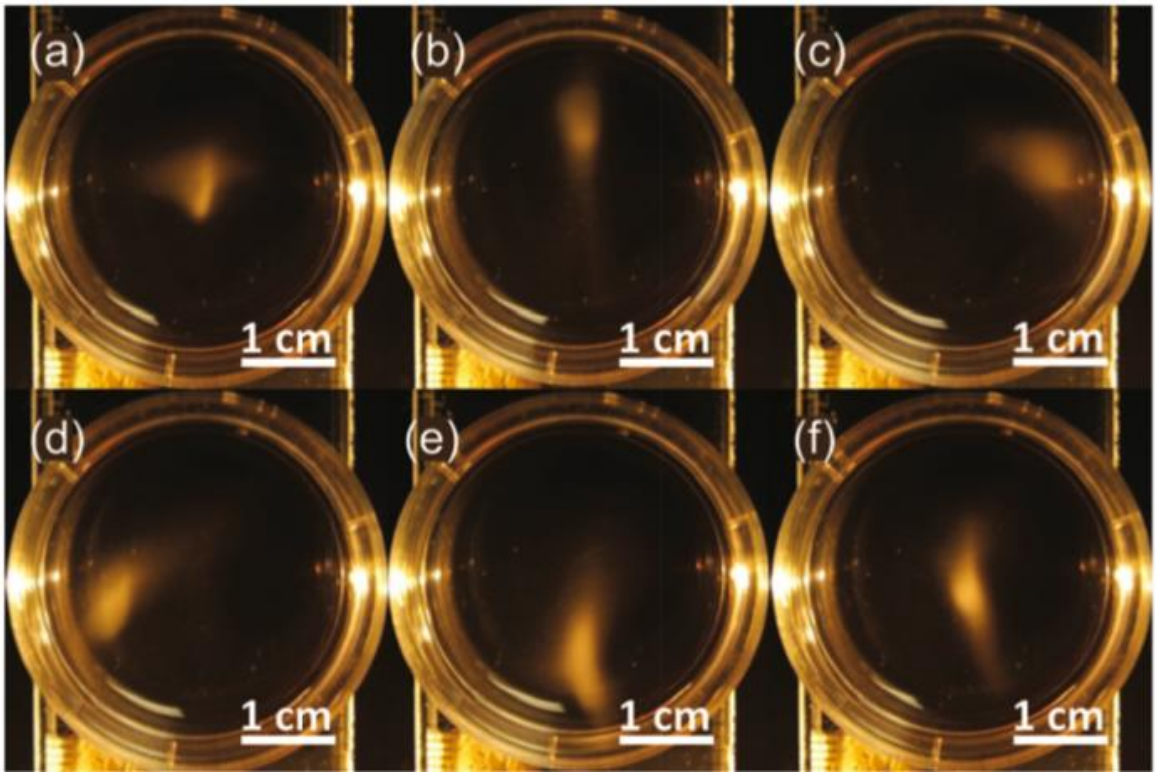


Figure 2.7: Images of the MTB aggregation movement along a predetermined cross-shaped path inside a petri dish located at the center of the magnetotaxis platform. This MTB aggregate was developed by current ratio variation technique with magnetic field exposure time of 3 seconds. Adapted from (De Lanauze et al., 2014).

## 2.4 SN38 as an anticancer drug

7-Ethyl-10-hydroxy-camptothecin (SN38) is a biologically active metabolite of irinotecan hydrochloride (CPT-11) which is a camptothecin derivative. The metabolic activation of CPT-11 to SN38 takes place in liver and tumor tissues (Slatter, Su, Sams, Schaaf, & Wienkers, 1997; Tobin et al., 2006). The clinical activity of the SN38 was found to be up to 1000-fold greater than CPT-11 in a number of cancer cell lines including colorectal, lung, lymphoma, gastric, cervical and ovarian cancer (Bodurka et al., 2003; Cunningham et al., 1998; Noda et al., 2002; J. Allen Zhang et al., 2004). SN38 induces apoptosis by stabilizing the cleavable complex formed between topoisomerase I (topoI) and DNA, resulting in double-strand DNA breakage and ultimately cell death (Figure 2.8) (Williams et al., 2003; Zeghari-Squalli, Raymond, Cvitkovic, & Goldwasser, 1999). Therefore, SN38 may be used for cancer treatment over CPT-11 as an effective anticancer agent.

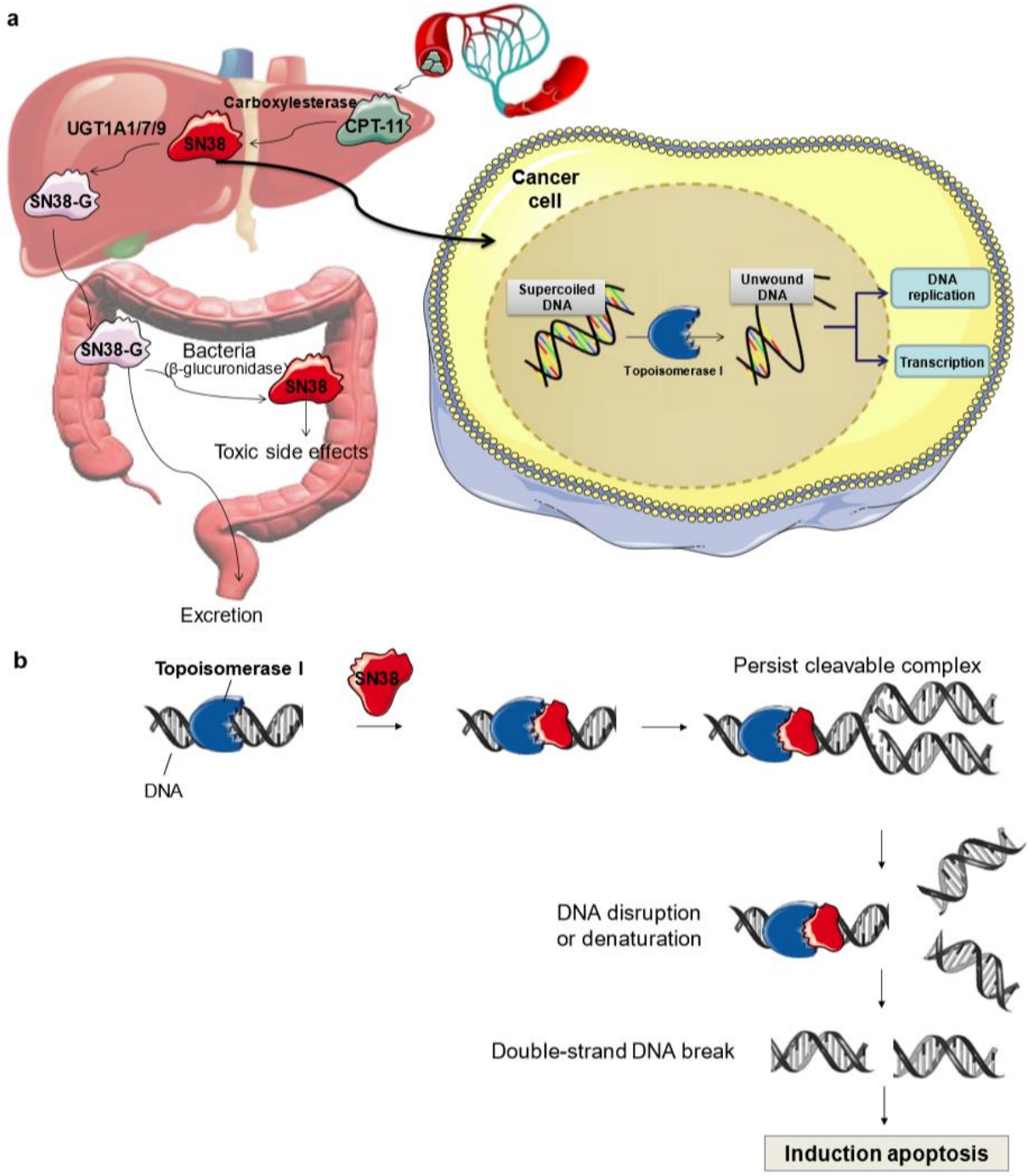


Figure 2.8: Metabolic pathways of CPT-11 and SN38. (a) CPT-11 is converted to its active metabolite (SN38) by liver carboxylesterase. UGT1A1 causes inactivation of SN38 by forming SN38 glucuronide (SN38-G). Then, β-glucuronidase intestinal bacteria convert SN38-G to SN38 and cause toxicity. (b) Inhibition of topoisomerase I activity by SN38. DNA synthesis is prevented by double-strand DNA break formation and apoptosis (Frese & Diamond, 2011).

### 2.4.1 Limitation of direct use of SN38

In comparison with CPT-11 parent drug, SN38 is considerably much more cytotoxic. SN38 has not yet been used in the clinical setting because it has some major challenges. Its insolubility in water, ethanol, polysorbate and cremophor, which are the most famous physiologically compatible liquids, and its short biological half-life have limited its direct clinical application (Duan et al., 2010; Manaspon, Hongeng, Boongird, & Nasongkla, 2012). In addition, SN38 is inactive in the physiological pH (pH 7.4) because of its pH-dependent behavior. At low pH, the SN38 is active and in the closed-ring neutral structure (lactone) form while at high pH, it is inactive and is in the form of an open-ring negatively charged structure (carboxylate) (Figure 2.9) (X. Yang et al., 2005). Figure 2.9 shows the pH-dependent equilibrium of SN38.

The half-life of conversion of the active SN38 form (hydroxy lactone, closed-ring structure) to the inactive SN38 form (carboxylate, open-ring structure) is ~ 12 min, where within 2 h, 99% of the active SN38 is converted to biologically inactive carboxylate SN38 at pH 7.4 at 37 ℃. To advance into clinical trials, developing a water-soluble form of SN38 is necessary (its solubility in water is < 5 μg/ml) (X. Yang et al., 2005). In addition, a drug delivery vehicle should be developed so that it can be loaded with SN38 by either chemical conjugation or physical entrapment. So far, liposomes, have shown promising results in delivery of SN38.

The integrity of the lactone moiety is structurally important for the passive diffusion of SN38 into cancerous cells and successful interaction with the topoisomerase target (Garcia-Carbonero & Supko, 2002; Tallman, Ritter, & Smith, 2005). In order to address the above challenges, various drug delivery technologies for SN38 delivery to the cancer tissues have been investigated (Ebrahimnejad, Dinarvand, Jafari, Tabasi, & Atyabi, 2011; Koizumi et al., 2006; R. Kolhatkar, Swaan, & Ghandehari, 2008; Z. Liu, Robinson, Sun, & Dai, 2008; Quanrong, James, Min, Chuan, & Jie, 2012).

## 2.5 Liposomal-based formulation for drug delivery applications

### 2.5.1 Liposome structure

Liposomes are lipid bilayer spherical vesicles that are biocompatible and degradable in a biological environment, making them a perfect candidate for carrying drugs into small vessels (Demetrios

Papahadjopoulos & Miller, 1967). They were initially discovered by Bangham and colleagues in 1965 (Bangham, Standish, & Watkins, 1965) and were used as nanocarriers for years (Jesorka & Orwar, 2008). Figure 2.10 illustrates phospholipids creating a bilayer. The hydrophobic tails are repelled from water and the hydrophilic heads are attracted towards the water, creating a bilayer (Jesorka & Orwar, 2008). Depending on their size and lamellarity, liposomes are divided into 4 groups: small unilamellar vesicles (SUVs; ~ diameter: 10 - 100 nm), large unilamellar vesicles (LUVs; diameter: ~ 100 - 1000 nm), giant unilamellar vesicles (GUV; diameter: > 1000 μm) and multilamellar vesicles (MLVs or LMVs) that are made of concentric layers. In this study, we prepared LUVs (diameter of 200 nm).

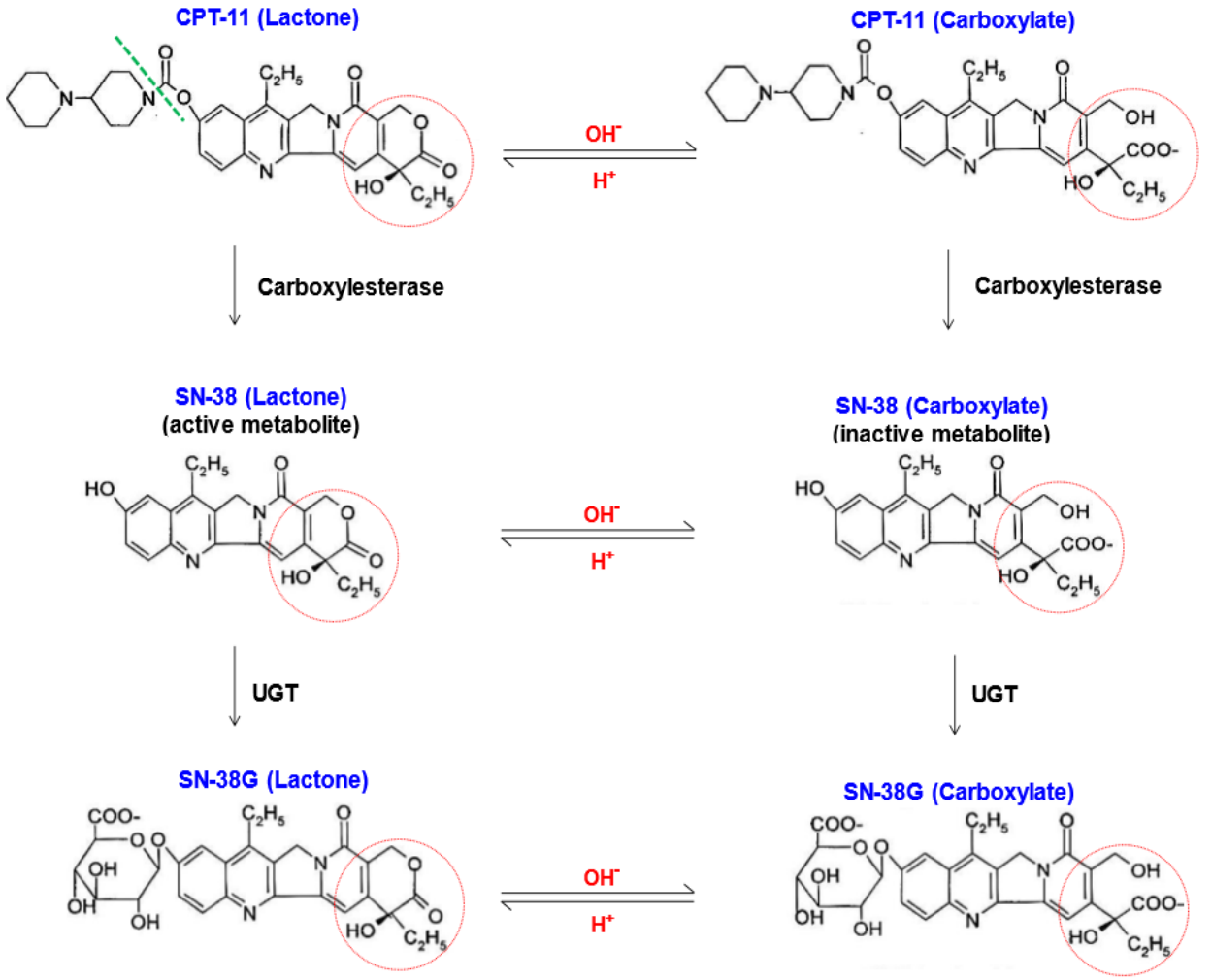


Figure 2.9: CPT-11 and SN38 pH-dependent equilibrium. At low pH, the SN38 is active and in the closed-ring neutral structure (lactone) form while at high pH, it is inactive and is in the form of an open-ring negatively charged structure (carboxylate) (J Allen Zhang et al., 2004).

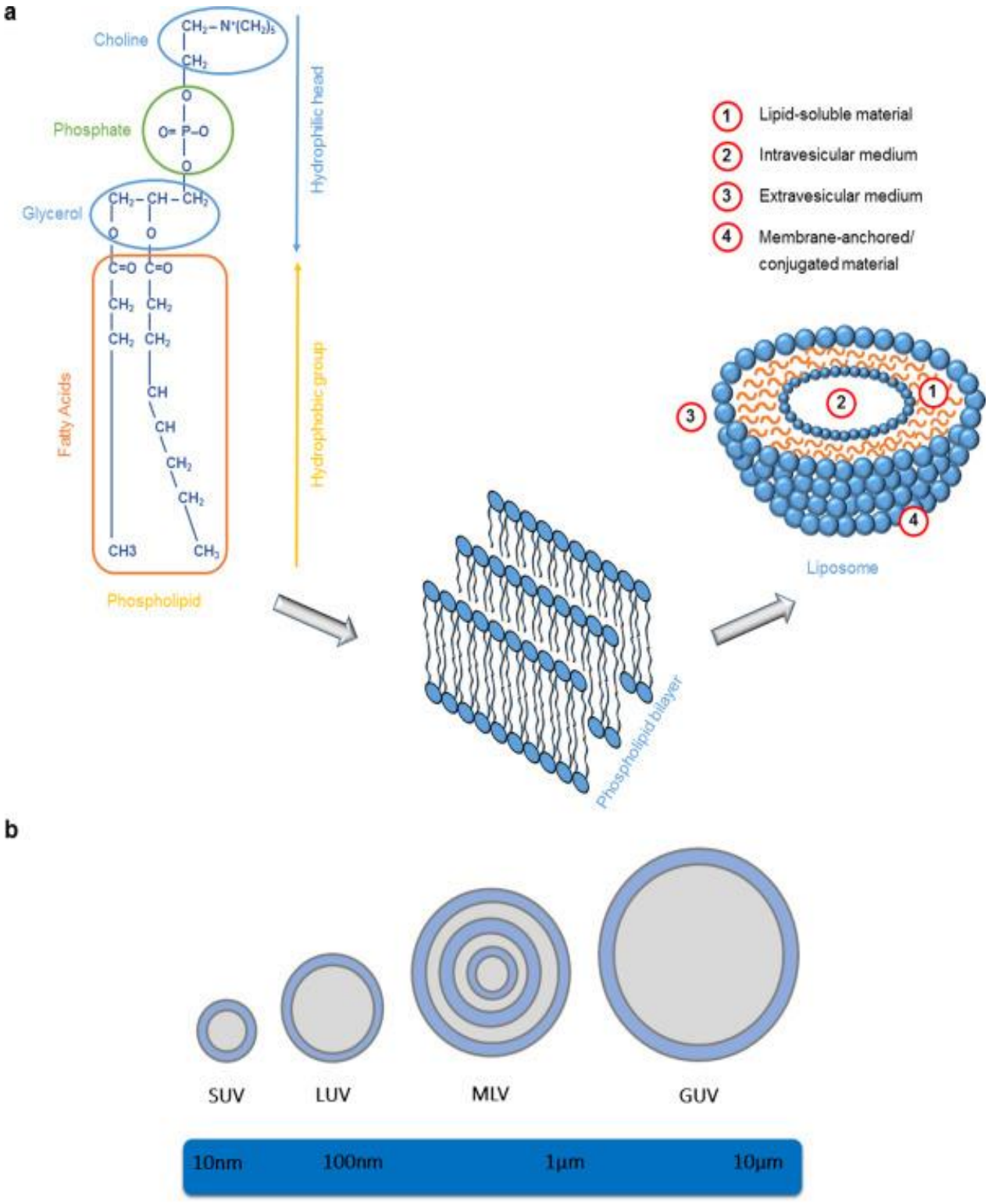


Figure 2.10: (a) Schematic representation of an individual phospholipid molecule, bilayer leaflets and liposomes. (b) Schematic illustration of the different liposomes categorized according to the size and number of lipid bilayers. Adapted from (Nogueira, Gomes, Preto, & Cavaco-Paulo, 2015).

### 2.5.2 Liposomes as drug delivery carriers

Liposomes as vesicles have been used in different research fields as drug carriers. For example, they were used as imaging contrast agents (Mikhaylov et al., 2011; Mitchell et al., 2013), vaccines (Channarong, Chaicumpa, Sinchaipanid, & Mitrevej, 2011), enzyme (Jesorka & Orwar, 2008; Yun, Maximov, Yu, Vertegel, & Kindy, 2013), carriers, as well as delivering anticancer drugs to the desired sites (Afergan et al., 2010; Andresen, Jensen, & Jørgensen, 2005; Immordino, Dosio, & Cattel, 2006; Jesorka & Orwar, 2008; Sawant & Torchilin, 2010). According to their structure, liposomes can carry both hydrophilic chemicals and molecules at the same time, inside the aqueous core and within the lipid bilayer domain, respectively (Torchilin, 2005). This allows lower drug toxic side effects (Al-Jamal & Kostarelos, 2011) and more control over drug release (Koçer, 2010). For instance, systemic administration of pharmaceutical substances that have short biological half-lives and negligible therapeutic indices leads to an increase in acute and cumulative toxicities. However, drug encapsulation in PEGylated nanocarriers (e.g. liposomes) as long-circulating pharmaceutical agents can improve the targeting efficiency through EPR effect (Kaminskas et al., 2012; Yallapu, Foy, Jain, & Labhasetwar, 2010). As mentioned before, SN38 is a pH-sensitive drug and PEGylated liposomes can protect the active metabolite status of this drug under varying physiological environment. However, only a small fraction of these carriers enter the tumors, by the EPR effect, due to poor lymphatic drainage (~ 2% after 4 h circulation) (Figure 2.11) (Hong et al., 2009; Jhaveri & Torchilin, 2014).

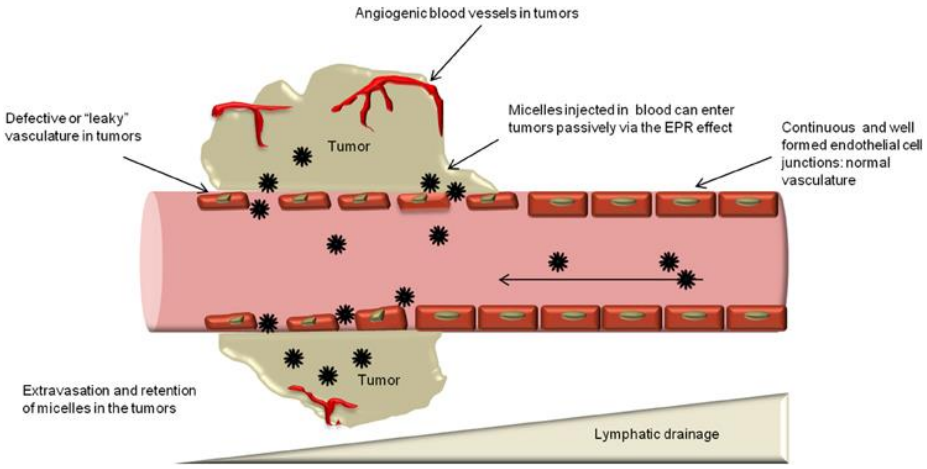


Figure 2.11: Schematic illustration of passive targeting via the EPR effect. Nanocarriers can extravasate into the tumors through the gaps between endothelial cells. Adapted from (Jhaveri & Torchilin, 2014).

### 2.5.3 Liposomes stability

The stability of liposomes is the main concern when it comes to biological applications. The size, coating, bilayer composition, surface charge and the lipid to active agent ratio can affect the physical properties of the liposomes. For example, like charges on the liposomes surfaces prevent their aggregation through like charge repulsion. The pH strength of the medium and unsaturated lipid chains can influence the chemical stability of the liposomes as they modulate the oxidation and the hydrolysis of the lipids. The risk of hydrolysis can be minimized in different ways such as the use of high molecular weight lipids or the addition of a sterol like cholesterol (Yang et al., 2013; Papahadjopoulos et al., 1972). The circulation half-life or the biological stability of liposomes can be influence by the size, composition and surface properties. For instance, liposomes with a radius of 10 – 100 nm are not rapidly recognized by the immune system and can avoid kidney filtration (Gil & Parak, 2008). As a consequence, different studies showed a high lifespan circulation of drug-loaded liposomes (Kaminskas et al., 2012).

### 2.5.4 Liposome manufacturing and synthesis techniques

Since the Bangham method (Bangham et al., 1965), there have been other techniques used to manufacture custom-designed liposomes such as detergent-depletion (Meure, Foster, & Dehghani, 2008), reverse-phase evaporation on thin film hydration (Szoka Jr, 1996), supercritical fluid techniques (Massing, Cicko, & Ziroli, 2008) and microfluidic method (Hood, DeVoe, Atencia, Vreeland, & Omiatek, 2014).

The common method to manufacture the liposomes is to disperse the lipid mixture by dissolving the lipids in an organic solvent, remove the organic solvent usually by evaporation to form a thin film of phospholipids and hydrate the lipid film in an aqueous solution through vigorous shaking to separate the swelling lamellae from the surface of the vessel and form sealed spherical structure. (Maherani et al., 2011).

In this study, we used the reverse phase evaporation/thin film hydration method. In this technique, the lipids and the cholesterol are dissolved in an organic solvent such as chloroform. Then, the solvent is evaporated by a rotary evaporator to create a thin dry film of the components on the inner wall of the rotary flask. The lipid film is then hydrated with an appropriate buffer at a temperature higher than the transition temperature of the lipid bilayers. When the obtained bilayers reach a

certain length though vigorous shaking, the sheets fold upon themselves and form liquid-filled large multilamellar vesicles of different sizes (Hernández-Zapata et al., 2010). SUVs can be obtained by sonication while (Figure 2.12), unilamellar large vesicles (LUVs) can be produced by extrusion through polycarbonate membranes above the transition temperature of lipids (Maherani et al., 2011).

### 2.5.5 Liposome drug loading strategies

Depending on the biocompatibility, solubility and the stability of the drug, different drug encapsulation technique can be employed (Mahapatro & Singh, 2011). There are two main methods to load drugs into the liposomes: passive and active encapsulation.

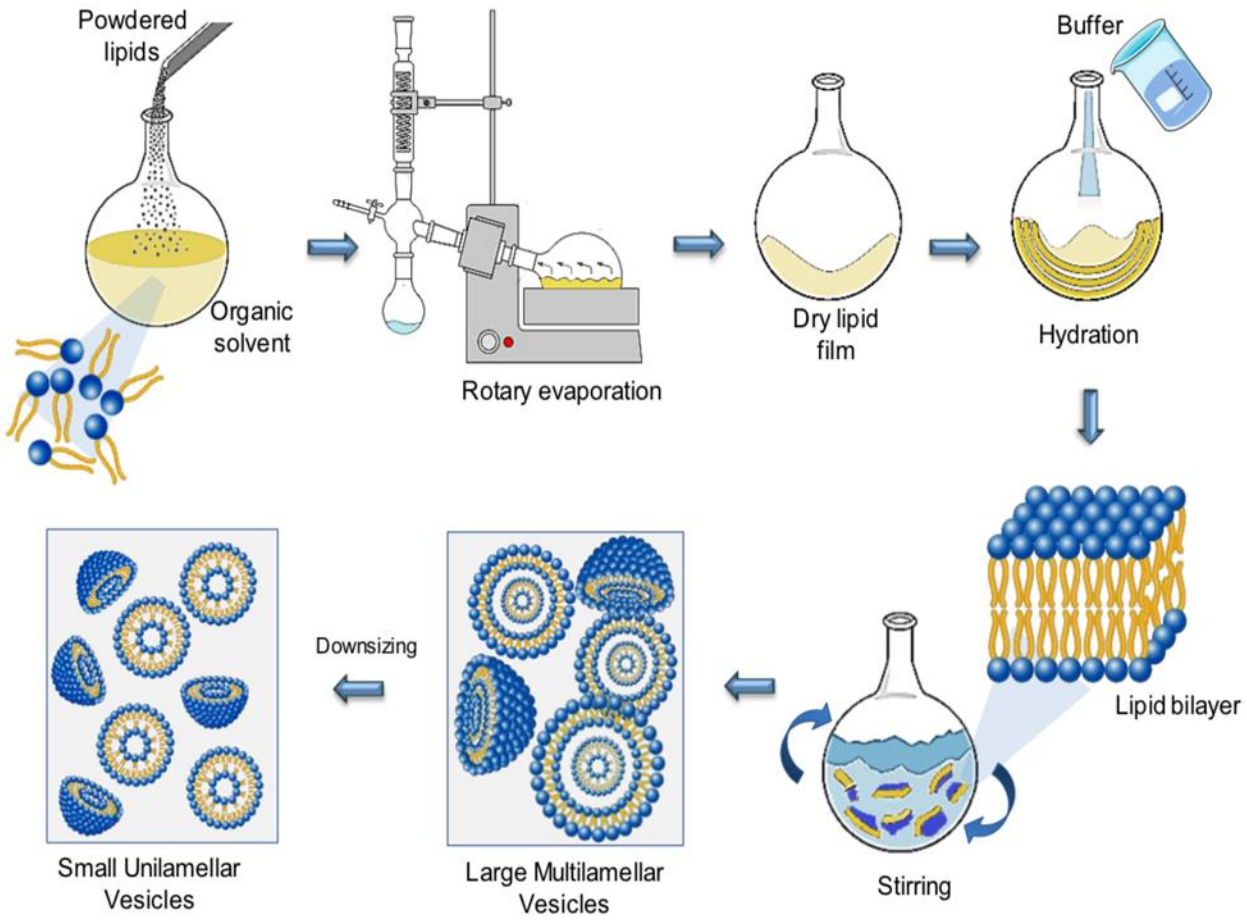


Figure 2.12: Schematic representation of the reverse-phase evaporation/thin film hydration method for liposome preparation. Reproduced from (de Araújo Lopes et al., 2013).

### 2.5.5.1 Passive encapsulation

In this method, the encapsulation of water-soluble hydrophilic drugs happens at the hydration stage, when lipids are forming a vesicle. The drug present in the hydrating buffer is passively loaded into the aqueous core of the liposome. However, this process has low drug uptake efficacy (Drummond, Noble, Hayes, Park, & Kirpotin, 2008; Sur, Fries, Kinzler, Zhou, & Vogelstein, 2014). If the drug is lipophilic, then it is entrapped inside the lipid bilayer of the liposomes. Drugs that are polyions are complexed with opposite charge to increase the loading efficacy (Drummond et al., 2008; Immordino et al., 2006).

### 2.5.5.2 Active encapsulation

In this method, the weakly acidic or basic drug is trapped in the liposomes via transmembrane gradient strategy (Ganai et al., 2011); the gradient is created between the aqueous core and the external environment of the liposomes. There are at least four techniques to create this gradient: 1) translocating potassium ions, 2) creating a pH gradient 3) creating a ($(NH_4)_2SO_4$) and ($(NH_4)_2HPO_4$) gradient (Fritze, Hens, Kimpfler, Schubert, & Peschka-Süss, 2006; Haran, Cohen, Bar, & Barenholz, 1993) and 4) creating an ethylenediaminetetraacetic acid (EDTA) gradient (Gubernator et al., 2010). Active encapsulation was successfully used in this study by creating a pH different through the use of a buffer at pH 4 inside and pH 8 outside the liposome bilayer. The drug molecules are uncharged before encapsulation; as a result, they are able to diffuse into the liposomes. When the drug reaches the acidic environment inside the intravehicular space, it becomes protonated and its chemical properties change. The charged molecules are less permeable; thus, the drug gets trapped inside the bilayer.

## 2.5.6 Liposomal SN38 formulation

To improve the solubility of CPT-11 and SN38 drugs in a stable and active condition, it is best to encapsulate them inside liposomes rather than using other cytotoxic organic solvents or for example, dimethylsulfoxide (DMSO) (Sadzuka, Takabe, & Sonobe, 2005; Szoka Jr, 1996; Xuan, Zhang, & Ahmad, 2006; J Allen Zhang et al., 2004).

Balancing the ratio of the administered drug-loaded liposomes versus the toxic side effects is a great concern when it comes to drug delivery.

Figure 2.13 illustrates the proposed encapsulation mechanism of SN38 into liposomes using a pH gradient strategy. The formation of crystals with ammonium sulfate inside the acidic interior makes the drug impermeable and keeps it active inside the core of the liposomes.

### 2.5.7 Drug release from liposomes

One of the main challenges in drug delivery is to control drug release after localization at the target site. Depending on the application, the environment of the tissue and the drug release mechanism type (e.g. temperature sensitive liposomes (Drummond et al., 2008; Sawant & Torchilin, 2010), pH-sensitive (Drummond et al., 2008; Sawant & Torchilin, 2010), enzymatic release (Andresen et al., 2005; Jørgensen, Davidsen, & Mouritsen, 2002; Panel et al., 2006), ultrasound sensitive (Schroeder, Kost, & Barenholz, 2009) and photosensitive (Drummond et al., 2008)), the physiochemical characteristics of liposomes can be manufactured differently.

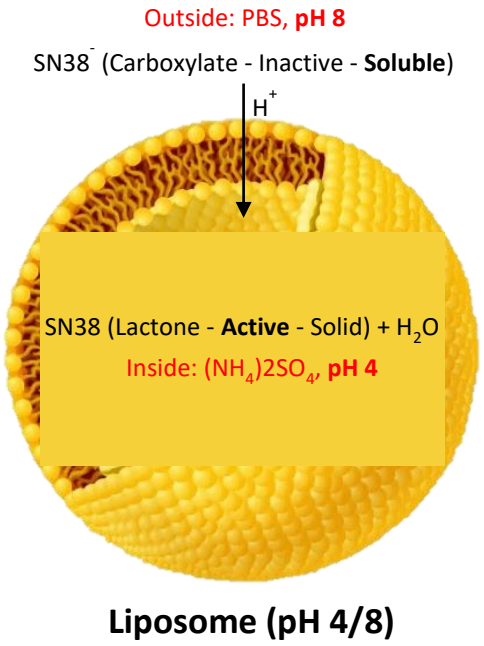


Figure 2.13: pH gradient strategy to accumulate SN38 drug inside the aqueous core of the liposome. At high pH, SN38 is in an inactive hydrophilic charged carboxylate form outside of the liposomes. At low pH, SN38 converts to the hydrophobic active closed lactone forms inside the liposomes.

In liposomes formulation, incorporating cholesterol with the saturated long-chain lipids would give retention. On the other hand, short and unsaturated acyl chains would make the liposomes leakier. Enzyme-activated liposome for the release of the drug in solid tumors is a promising technique in

which the tumor microenvironment contributes to the local degradation of the liposomal carriers through the release of lipases enzymes and oxidizing agents. Furthermore, the slightly acidic pH of the tumor tissue can contribute to the degradation of pH-sensitive liposomes without the need of any external means. Secretory phospholipase $A_2$ ($sPLA_2$) enzymes help in the destabilization and the cleavage of the lipids leading to lysolipids and fatty acids formulation (Andresen et al., 2005; Jørgensen et al., 2002; Panel et al., 2006). Size, charge, lipid composition (e.g. acyl-chain length and polymer coverage) and structural defects of the liposomes are factors that influence the activity of the $PLA_2$ enzyme. Adding anionic PEGylated lipids can enhance the $PLA_2$-catalyzed degradation of phospholipids membranes. However, when > 20 mol% of cholesterol is added to the liposome, it becomes non-degradable by $PLA_2$ and that limits the range of drugs that can be delivered to tumors (Jørgensen et al., 2002; Oude Blenke, 2012).

## 2.6 Bioconjugation methods

Attachment of various biomolecules such as drugs, antibodies, fluorescent dyes, nucleic acids, polymers, markers and different enzymes to nanoparticles produces hybrid materials. These materials can alter the stability, functionality, effectiveness and water-solubility of the biomolecules in the physiological environments. The commonly used methods for bioconjugation are (i) non-covalent interactions including physical adsorption (physisorption) and biological affinity-binding, (ii) covalent bonds (chemisorption) (Barar & Omidi, 2014; Sperling & Parak, 2010). Every method has its pros and cons and is used for specific applications, reagent requirements and timetables. Figure 2.14 shows some of the basic chemistry for attachment of biomolecules to particles. In this study, –COOH functionalized nanoparticles were covalently attached on the surface of the amine-containing ($–NH_2$) MTB cells.

### 2.6.1 Carbodiimide-mediated coupling

Among different zero-length bioconjugation techniques (Hermanson, 2013), carbodiimide agents are commonly used to activate carboxylic acid groups and to form amide or ester linkages. One of the benefits of the carbodiimide is that different types of amine-containing molecules such as antibodies, peptides, enzymes and DNA can directly be immobilized to the functionalized surface of the substrate without prior modification.

Carbodiimides activation agents that are commonly used are 1-ethyl-3-(3-dimethylaminopropyl)carbodiimide hydrochloride (EDC or EDAC), 1-cyclohexyl-3-(2-morpholinoethyl) carbodiimide (CMC), dicyclohexylcarbodiimide (DCC), diisopropyl carbodiimide (DIC)), Woodward's reagent K (N-ethyl-3-phenylisoxazolium-3′-sulfonate) and N,N′-carbonyldiimidazole (CDI) (Hermanson, 2013). They are categorized into two groups: (i) water-soluble and (ii) water-insoluble (soluble in organic solvents). For biochemical attachment, the water-soluble agents are favored as they allow direct reaction in physiologic solutions without the need for dissolution in organic solvents (Danila et al., 2009; Pattabiraman & Bode, 2011).

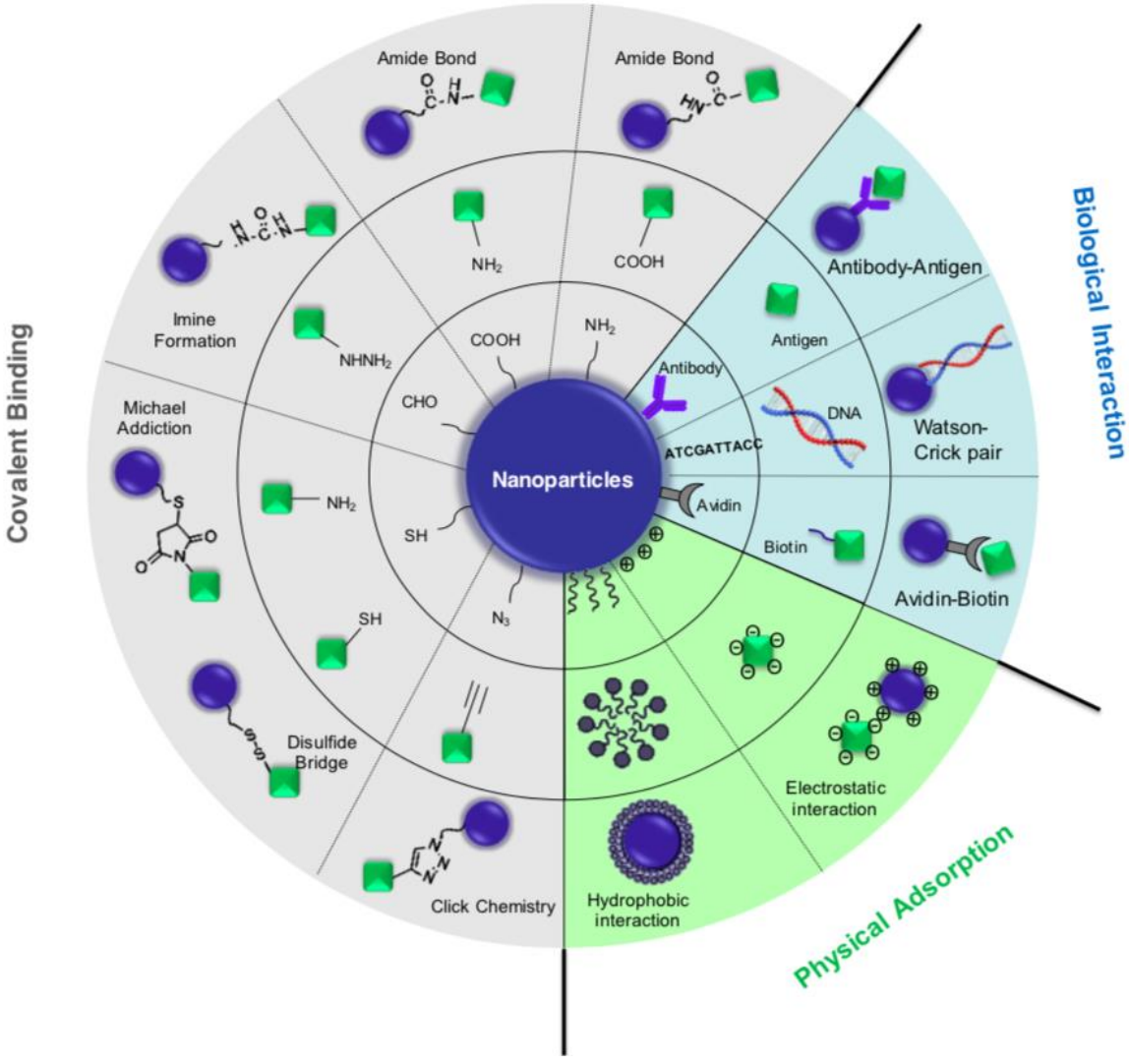


Figure 2.14: Schematic representation of bioconjugation methods based on the functional groups presented (Chen, 2014).

EDC carbodiimide and N–hydroxysuccinimide (NHS) or its analog (sulfo-NHS) are both water-soluble and are successfully used for creating zero-length crosslink (Grabarek & Gergely, 1990; Hermanson, 2013). For instance, EDC is used for direct conjugation of negatively charged carboxylates ($–COO^-$) to primary amines ($–NH_2$)-containing molecules, mediating the formation of amide linkages without becoming part of the final crosslink between the target molecules (Danila et al., 2009; Hermanson, 2013; Maruyama et al., 1997).

Figure 2.15 illustrates the basics of conjugation of an amine-containing molecule to a carboxylate-containing molecule using carbodiimide coupling method. This method consists of a single- or a two-steps process. In the single step process, an active ester (*O*-acylisourea) intermediate is produced when the carboxyl-containing molecule is activated with EDC. Then, this active agent can react with a primary amine containing species and form an amide bond (Figure 2.15a). In aqueous solutions, the reactive ester complex starts to lose activity and its reaction rate with amines decreases. Hydrolysis is the main competing reaction that split apart the activated ester intermediate to form an isourea while regenerating the carboxylate group (Figure 2.15b). To reach the desired coupling efficacy, it is recommended to prevent the hydrolysis of the reactive ester before the reaction with the target amine.

The two-steps procedure (Figure 2.15c), on the other hand, leads to a higher yield of amide bond formation compared with the later procedure. First, the carboxylate-containing agent forms an *O*-acylisourea intermediate reactive ester. To increase the stability of the active ester, NHS can be added. A considerably more stable sulfo-NHS ester intermediate can be formed from the reaction of the hydroxyl group of sulfo-NHS with the EDC active-ester complex. Sulfo-NHS ester is hydrophilic and it can rapidly bond with a nucleophilic amine on target molecules, increasing the efficiency of the amide bond formation. Sulfo-NHS increases the water-solubility of the activated carboxylate molecules and slows down the hydrolysis of generated ester intermediates. In addition, the sulfo-NHS ester intermediate has a negative charge and this help in maintaining the stability of molecules due to the repulsion force between the particles with the same charge. An effective washing step (e.g. gel filtration or dialysis) in a reasonable time frame is needed to get rid of excess reactants and by-products of the reaction (e.g. isourea). Even though sulfo-NHS is not fundamental in carbodiimide reactions, it can significantly enhance the solubility, stability and attachment efficiency by improving the yield of EDC-active intermediate and forming a more stable amine-reactive intermediate (Staros, Wright, & Swingle, 1986).

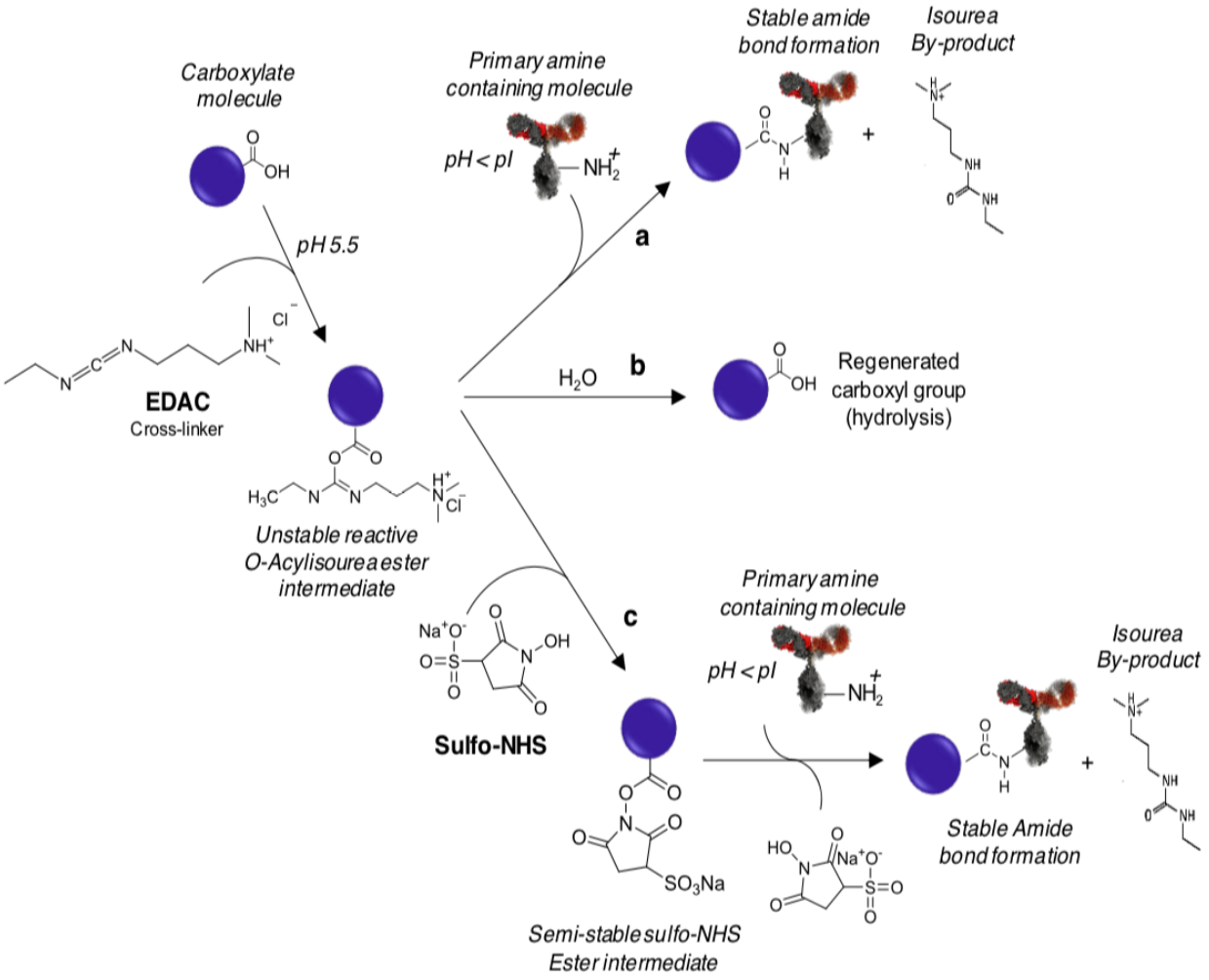


Figure 2.15: Carbodiimide EDC/NHS crosslinking. Molecules containing the carboxylate group can be activated with EDC and sulfo-NHS. By nucleophilic displacement, the activated generated esters can couple with amine-containing molecules to form amide bond linkages. Adapted from (Hermanson, 2013).

EDC hydrolysis takes place at an acidic pH and NHS-esters have a half-life of 4 - 5 h at pH 7, 1 h at pH 8 and just 10 min at pH 8.6 (S. S. Wong & Jameson, 2011). The rate of activation and efficiency of the conjugation directly depend on the pH, particle size, incubation time and the concentration of EDC/NHS used in activation. In general, for more effective results, in the two-steps crosslinking reactions, it is better to do the EDC and sulfo-NHS activation in a 0.1 M MES buffer for 30 min at room temperature at pH 4.5 - 6.0. This results in an efficient activation of EDC with less hydrolysis of the intermediates. Then, immediately prior to the reaction, the pH should

be elevated to neutral in order to increase the reaction of sulfo-NHS activated molecules with primary amines (Hermanson, 2013).

This approach has been implemented in different applications. For conjugation of biomolecules in targeted delivery purposes, this chemistry has also been used for the functionalization of various nanoparticles (Mahon, Salvati, Bombelli, Lynch, & Dawson, 2012), superparamagnetic iron oxide nanoparticles (Shamsipour et al., 2009), gold (Wei & Feng, 2009) and paramagnetic microparticles (Shang, Chang, Kan, Majetich, & Lee, 2006).

### 2.6.2 Immobilization of antibody on particles

Different direct and indirect methods have been implemented for the immobilization of antibodies at the surface of different particles (Hermanson, 2013). The functional groups present on the surface of an antibody could be primary amines ($–NH_2$), carboxylic acid (–COOH), sulfhydryl groups (–SH) or carbonyls (–CHO) (Figure 2.16) (Sesay, 2003).

Amine groups are present at the N-terminus of every polypeptide chain and in the side chains of lysine residues that are spread over the antibody surface. Because of the positive charge of the primary amines in physiologic environments, they are commonly outward-facing the proteins; thus, they are usually available for the immobilization without altering the protein structure. On the other hand, the carboxyl groups are present at the C-terminus of every polypeptide chain and in the side chains of aspartic acid and glutamic acid, while sulfhydryls occur in the side chains of cysteine residues joined by disulfide bonds (–S–S–).

In the direct bioconjugation, the activated particles with specific functional groups (e.g. carboxyl, amine, etc.) particularly react with the reactive groups of antibodies via suitable crosslinker (e.g. EDC) (Hermanson, 2013; Sesay, 2003). For biomolecules, antigen binding domains with appropriate orientation are required to increase antibody functionality. On the other hand, in the indirect antibody conjugation, a modified antibody with a functional group (e.g. biotin, thiol, etc.) can attach to the functionalized particles (e.g. aldehyde, avidin, etc.).

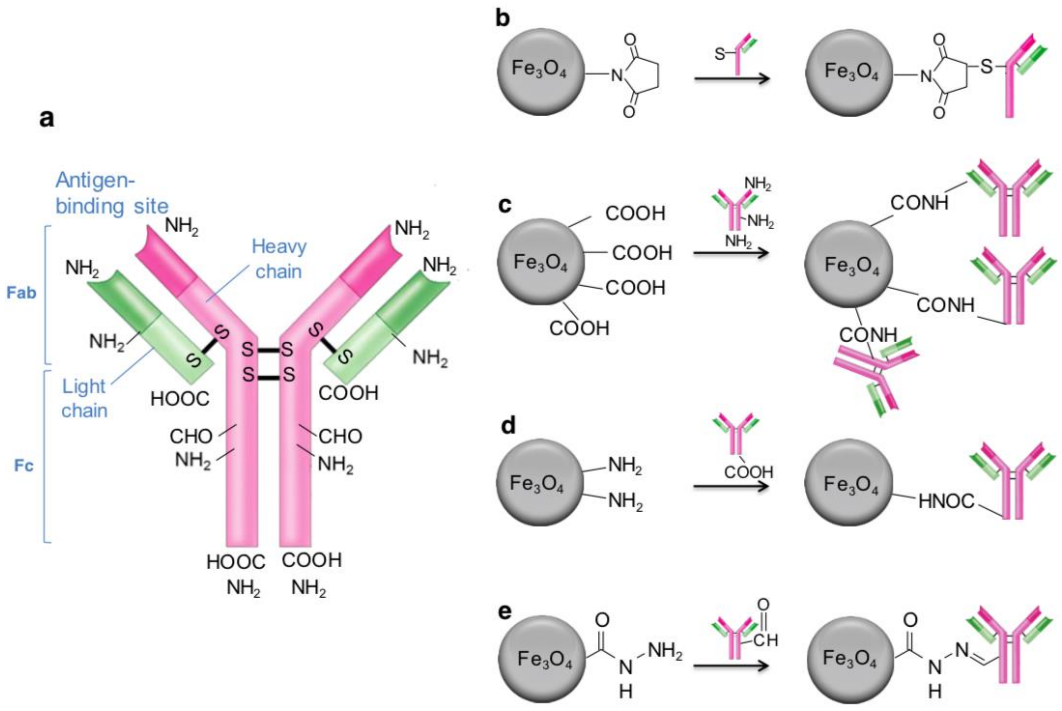


Figure 2.16: Attachment of an antibody on the surface of functionalized magnetite nanoparticles. (a) Antibody schematic structure. (b) Maleimide-particle covalently coupled with the thiol functional group of an antibody and forming a thioether bond. (c, d) Carbodiimide chemistry developing amide bond. (e) Hydrazide-particle conjugated to the aldehyde functional group of an antibody and forming a hydrazone bond. Adapted from (Hermanson, 2013).

## 2.7 Iron-oxide based MRI contrast agents

MRI is an imaging method with an excellent soft tissue contrast. However, it is not suitable for visualizing microstructures due to its low sensitivity and limited resolution characteristics. To overcome this, contrast agents are used.

### 2.7.1 Magnetic particles properties

Iron-oxide magnetic nanoparticles have been used in biomedicine applications such as contrast agents in MRI and drug delivery (Bulte & Kraitchman, 2004; Dennis et al., 2008; McBain, Yiu, & Dobson, 2008; Yiu, 2011; Yu et al., 2008). Generally, materials are categorized into four groups: diamagnetic (non-magnetic materials), paramagnetic, ferromagnetic and superparamagnetic.

Paramagnetic materials are slightly attracted by a magnetic field and their magnetism goes away when the field is removed. Paramagnetism is due to the presence of an odd number of valence electrons in the atoms of these materials. The unpaired electrons have a magnetic dipole moment due to their spin and they act like small magnets. An externally applied magnetic field causes the spins of the electrons to align parallel to the field and causing a net attraction.

Ferromagnetic materials, in contrast to paramagnetic materials, have their unpaired electron spins to line up parallel with each other in regions called domains. These materials are normally unmagnetized because of their multiple domains with random orientations. When a magnetic field is applied to these materials, all the individual domains align along the direction of the magnetic field. Consequently, these materials get completely magnetized. When the field is removed, the domains retain their orientation and tend to keep the fraction of the saturation magnetization or remanence magnetization ($M_r$) (Figure 2.17). The high magnetic susceptibility of ferromagnetic materials creates a high inhomogeneity in the magnetic field and consequently, they become properly traceable in MR imaging. However, the clinical applications of ferromagnetic materials with high magnetizations are limited because of their tendency to keep a high $M_r$ value.

Superparamagnetism occurs when the size of the multi-domain particles is smaller than the ferromagnetic domains. The size of the individual magnetic domains in these materials is in the range of tens of nanometers. The magnetization (M) initially rapidly increases when a magnetic field is applied until it reaches the maximum value called saturation magnetization ($M_s$). Superparamagnetic materials do not maintain any net magnetization when the magnetic field is removed.

### 2.7.2 Superparamagnetic iron oxide nanoparticles as MRI contrast agents

Superparamagnetic iron oxide (SPIONs) nanoparticles are widely used as MRI negative contrast agents in different biomedical applications such as imaging tumors angiogenesis (Allkemper, Bremer, Matuszewski, Ebert, & Reimer, 2002; Kinner et al., 2011) and molecular-cellular tracking and imaging (Bulte & Kraitchman, 2004; Demas & Lowery, 2011; Yu et al., 2008). Figure 2.17 shows the magnetization curve of iron oxide particles used as MRI contrast agents (A. G. Kolhatkar, Jamison, Litvinov, Willson, & Lee, 2013). A transition from ferromagnetic multi-domain to the superparamagnetic single-domain structure happens by the reduction of the size of the particles to approximately 30 nm; this leads to a decrease in the saturation magnetization

(Figure 2.17a). Although superparamagnetic materials have smaller magnetization than ferromagnetic particles, lower aggregation propensities in the absence of magnetic field make them best candidates as contrast agents in MR imaging for *in vivo* applications.

SPIONs contrast agents are categorized into two fundamental forms: magnetite ($Fe_3O_4$) and its oxidized form, maghemite ($\gamma$-$Fe_2O_3$) (Lin, Kim, El Haj, & Dobson, 2008). The core diameter is in the range of 4 - 12 nm. Both types consist of water-insoluble iron oxide particles and they need to be modified by polymer coating (Pouponneau et al., 2009) or encapsulation in liposomes (Mikhaylov et al., 2011) to increase their physicochemical stability, lower their aggregation, increase their circulating half-life and biocompatibility (Yallapu et al., 2010) (Mahmoudi, Sant, Wang, Laurent, & Sen, 2011) among other things. Ligands such as antibodies could be attached to the surface of the SPIONs to target a specific region in the body (McCarthy, Bhaumik, Karver, Sibel Erdem, & Weissleder, 2010; Tanabe, Zhang, Ito, Hatta, & Nishimoto, 2007).

The SPIONs have higher saturation magnetization than other contrast agents, resulting in a higher sensitivity and enhancing proton relaxation in the MRI field (Kinner et al., 2011). However, they do not have the highest saturation magnetization amongst all magnetic materials. Iron-cobalt nanocrystals coated with graphitic carbon, have the highest magnetization among all magnetic materials and can lead to the visualization of the smallest vessels in MRI (Brannon-Peppas & Blanchette, 2012). However, these materials can oxidize easily and cause toxicity. As a result, SPIONs are the most promising contrast agent known, so far (Jin, Lin, Li, & Ai, 2014).

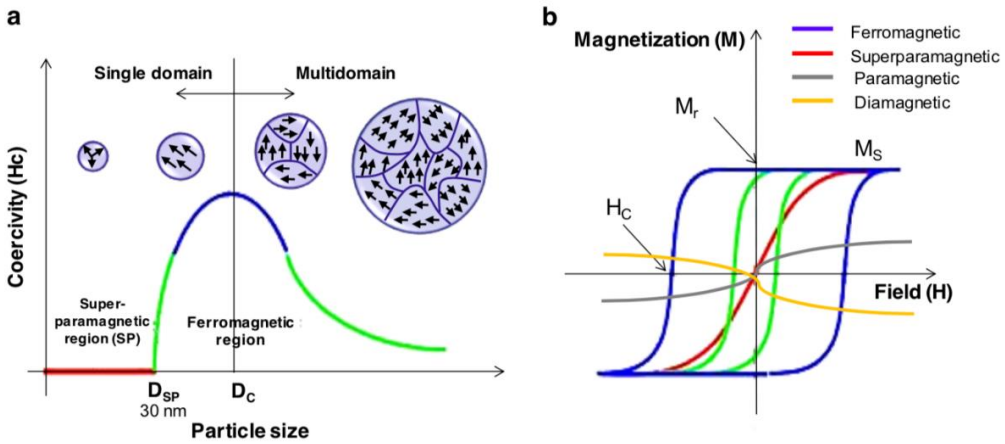


Figure 2.17: (a) Transition from multi-domain to single-domain to superparamagnetic regimes of iron oxide and also their magnetic domain organization. (b) Hysteresis in magnetic materials (A. G. Kolhatkar et al., 2013).

# CHAPTER 3 METHODOLOGY

## 3.1 MTB-LP-SN38 formulation

### 3.1.1 Reagents and chemicals

The 7-Ethyl-10-hydroxycamptothecin (SN38) drug was purchased from ABATRA Technology Co., Ltd. (Xi'an, Shaanxi, China). 1,2-distearoyl-sn-glycero-3-phosphocholine (DSPC) and 2-distearoyl-sn-glycero-3-phosphoethanolamine-N-[carboxy(polyethyleneglycol)2000] (DSPE-PEG2000-COOH) were purchased from Avanti Polar Lipids, Inc. (Alabaster, AL, USA). Cholesterol (Chol), chloroform, ammonium sulfate ((NH4)2SO4), Triton X-100, N-hydroxysulfosuccinimide sodium salt (sulfo-NHS), N-(3-Dimethylaminopropyl)-N'-ethylcarbodiimide hydrochloride (EDC), phosphate buffered saline (PBS), gel filtration media Sephadex G-50, sodium hydroxide solution (2 N), ferrous sulfate, FeSO4·7H2O and hydrogen chloride (1 N) solution were all obtained from Sigma-Aldrich (Sigma-Aldrich, Oakville, ON, Canada). All solvents and products were used without further purification. The water used in all experiments was pretreated with the Milli-Q® Plus System (Millipore Corp., Billerica, MA).

### 3.1.2 Culture growth conditions for BN-1 magnetotactic strain

As previously reported (Bazylinski et al., 2013), BN-1 strain from our laboratory stock was cultured in a microaerobic environment in the chemoheterolithotrophic liquid medium at room temperature. Cultures of bacteria (~ $10^7$ MTB/ml) were incubated under an oxygen concentration gradient of 0.1 - 0.5%, pH of 7.0 and a controlled input of 7.5% $CO_2$ in an iron-enriched medium supplied with 50 μM $FeSO_4$. The incubation lasted 48 hours (h) at room temperature, with no agitation and light to facilitate the biomineralization of bacterial magnetosomes. All of these parameters were controlled precisely to achieve the maximum swimming velocity and magnetic sensitivity essential for using MTB as bio-carrier agents in cancer drug delivery. The bacterial cells were harvested during the stationary phase of growth which is typically observed on the seventh day.

### 3.1.3 Preparation of SN38 saturated solution at high pH (loading solution)

This section describes the preparation of a saturated solution of SN38 at pH 11.3 (PBS 10 mM, NaCl 140 mM). The selected conditions ensure the optimal solubilization of the drug at high pH which is mainly based on the transformation of the lactone form (closed ring, insoluble form) into the carboxylate form (open ring, soluble).

To solubilize the drug at high pH, first, a certain amount of SN38 powder was added to PBS (pH 11.3) in order to reach a concentration of 500 µg/ml. The suspension was sonicated for 5 - 10 min until a bright yellow color was observed all over the solution. Then, the mixture was stirred for at least 2 h at 25.0 ± 0.5 °C. This step increased the brightness of the yellow color of the solution and led to the disappearance of the solid particles. The pH of the drug solution was measured and if any drop in the pH was detected, it was re-adjusted to ~ 11 with a very small amount of 2 N NaOH (in order not to dilute the drug). Then, the SN38 solution was ready for the loading step. Figure 3.1 illustrates the SN38 stock solution preparation.

### 3.1.4 Preparation of carboxylated nanoliposomes

This part describes the preparation of liposomes (LP) with a transmembrane pH gradient. Transmembrane pH gradients can be established by formulating large unilamellar vesicles (LUV) with an internal/external pH gradient of 4/8.

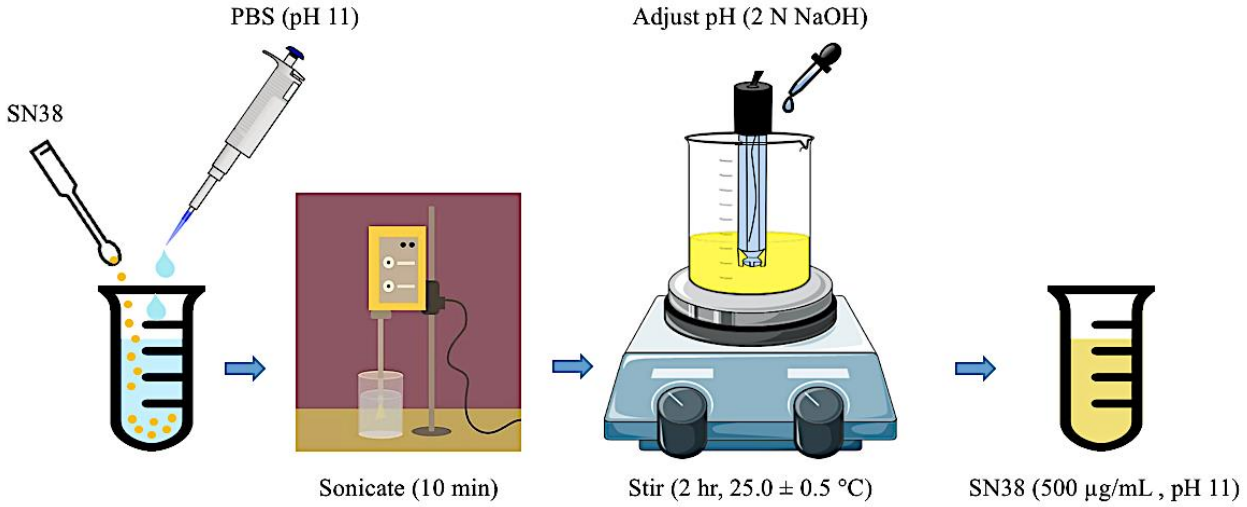


Figure 3.1: Preparation of SN38 saturated solution at high pH (loading solution).

First, LPs were prepared by the thin-film hydration method. Briefly, the lipids (ex. DSPC: Chol: DSPE-PEG-COOH; molar ratio 3:2:0.26) were dissolved in chloroform and were transferred into a round bottom flask. The flask was then connected to a rotary evaporator and a water bath with a temperature maintained at 60 °C. The solvent was then removed under vacuum for 1 h. The resulting dry lipid film was then hydrated with 1 ml ammonium sulfate solution [136 mM $(NH_4)_2SO_4$, pH 4] at 60 °C with continuous rotating for about 1 h. This led to a lipid concentration of 22.5 mg/ml. The suspension was then subjected to 5 cycles of freeze-thawing in liquid nitrogen and warm water (60 °C), to reduce multilamellarity, following by extrusion (Avanti Mini-Extruder, Avanti Polar Lipids) through 2 stacks of polycarbonate filters (Whatman, U.K.) with a defined pore size of 200 nm at least 20 times at ~ 60 °C. Then, the pH gradient was created by exchanging the external milieu with PBS (pH 8) using an exchange chromatography column. For each required batch, 200 µl of liposomes at pH 4 was loaded onto a Sephadex G-50 column equilibrated with PBS, pH 8. Then, a total of 2.5 ml of LP suspensions with pH (4/8) was collected. Figure 3.2 illustrates the carboxylated nanoliposomes preparation.

### 3.1.5 SN38 active loading in carboxylated nanoliposomes

Just immediately prior to the loading step, the pH of the SN38 solution in PBS (2.5 ml) was lowered from 11 to 8. Immediately after pH lowering step, 2.5 ml SN38 solution (0.5 mg/ml) in PBS (pH 8, with no precipitation) was added to the liposome suspension (2.5 ml, pH gradient 4/8) to achieve 0.1 wt/wt (drug/lipid). The mixture was incubated at 60 °C in a water bath for 20 min while mixing. Then, to eliminate the un-encapsulated drug, the LP-SN38 samples were passed over a spin column (the spin column was made of a 20 ml syringe filled with Sephadex G-50 column equilibrated with PBS (pH 8)). For each separation run, a 5 ml sample was loaded on top of the column and centrifuged (5 min, 3500 rpm). Figure 3.3 shows the steps for active loading of SN38 in the liposomes.

### 3.1.6 Covalent coupling of carboxylated nanoliposomes to MTB cells using carbodiimide chemistry

The attachment of the LP-SN38 to MTB bacteria cells was performed by pipetting 4 ml of LP-SN38 (stock liposome solution; 0.65 mM) into an Eppendorf tube. Just before use, carbodiimide activating reagents with EDC: NHS: DSPE-PEG-COOH molar ratio of = 30: 30: 3 were mixed

with 350 µl PBS (pH 6). The pH of the liposome external medium was reduced from 8 to 6 using 0.1 N HCl. Immediately, the EDC/NHS mixture was added to the liposomal suspension. The mixture was incubated for 20 min at room temperature with gentle agitation. Then, the activated LP-SN38 were passed over a spin column to eliminate the excess activating reagents (each spin column was made of a 1 ml syringe filled with Sephadex G-50 column equilibrated with PBS, pH 6). Then, activated liposomes were added to 50 ml of MTB bacteria (~ $10^7$ MTB/ml). The reaction was allowed to proceed for 2 h at room temperature with gentle agitation. The attached liposomes to MTB were separated from non-attached liposomes by applying a two dimensional (2D) magnetic field. The sample was washed three times with PBS (pH 7.4) and re-suspended in 100 µl of PBS (pH 7.4). The steps for the covalent coupling of the nanoliposomes to the MTB via carbodiimide is illustrated in Figure 3.4 while the schematic representation of LP-MTB formulation via carbodiimide is presented in Figure 3.5.

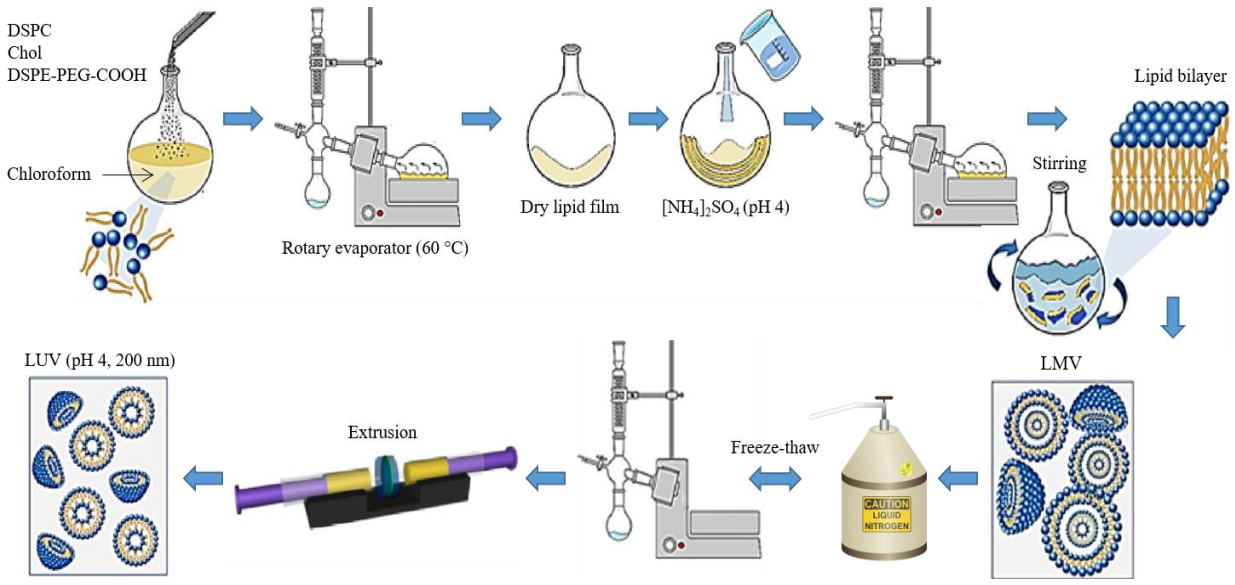


Figure 3.2: Preparation of carboxylated nanoliposomes by the thin-film hydration method. First, the lipids are dissolved in chloroform. Second, a rotary evaporator and a water bath are used to remove the solvent. The resulting dry lipid film is then hydrated with ammonium sulfate solution with continuous rotating. The suspension is then subjected to the freeze-thawing following by extrusion with a defined pore size. Reproduced from (de Araújo Lopes et al., 2013).

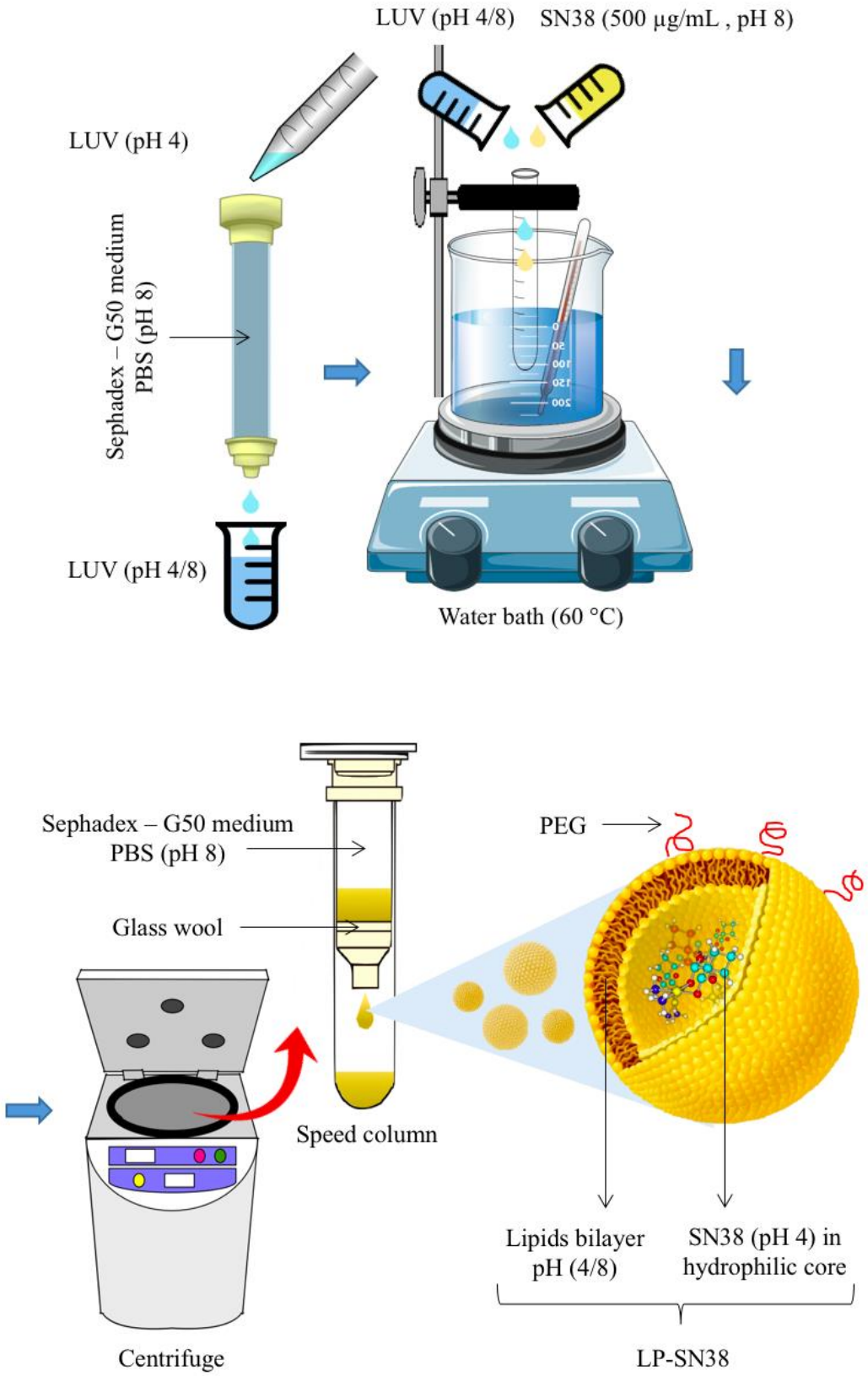


Figure 3.3: SN38 active loading in carboxylated nanoliposomes.

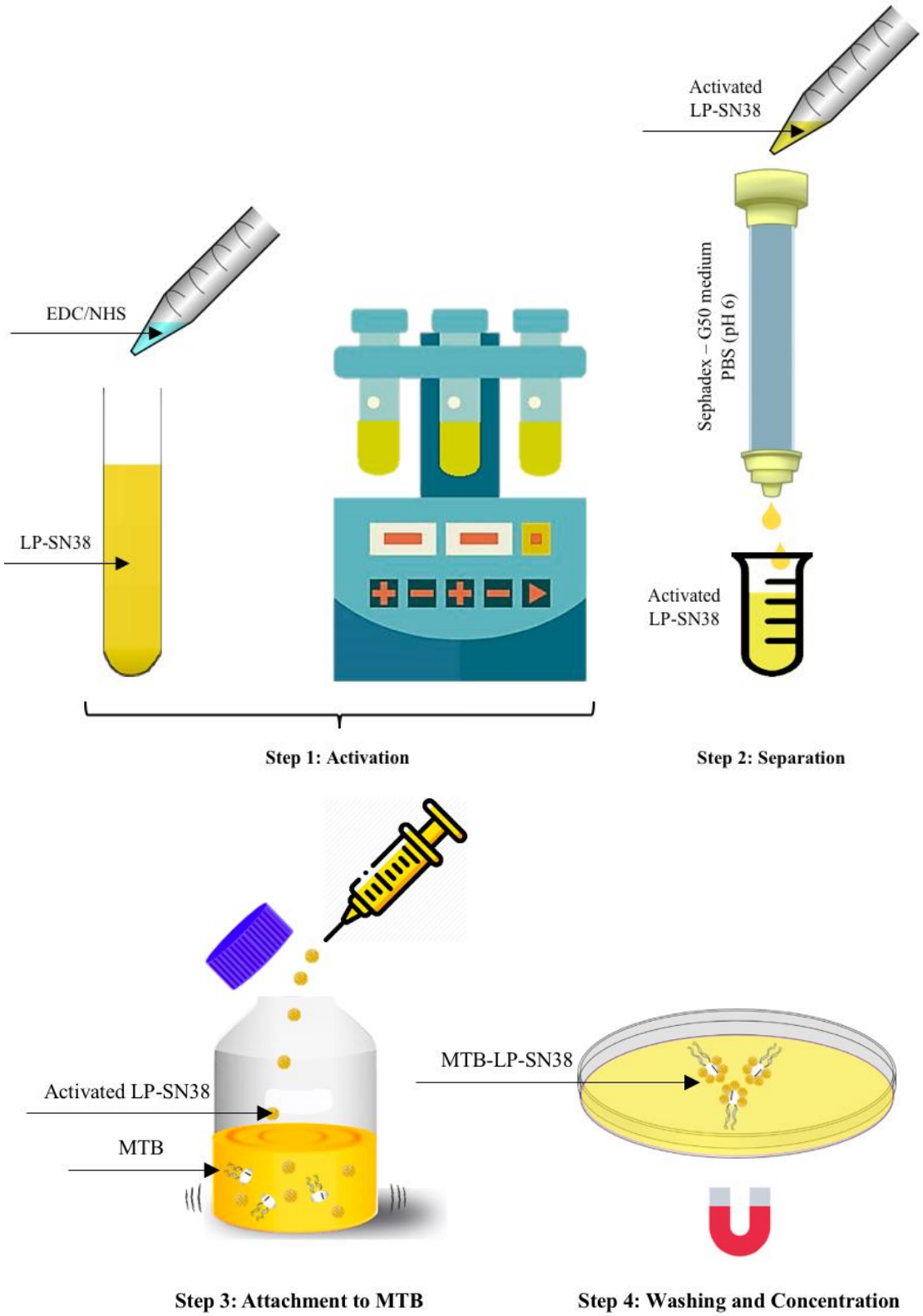


Figure 3.4: Covalent coupling of carboxylated nanoliposomes to MTB cells using carbodiimide chemistry.

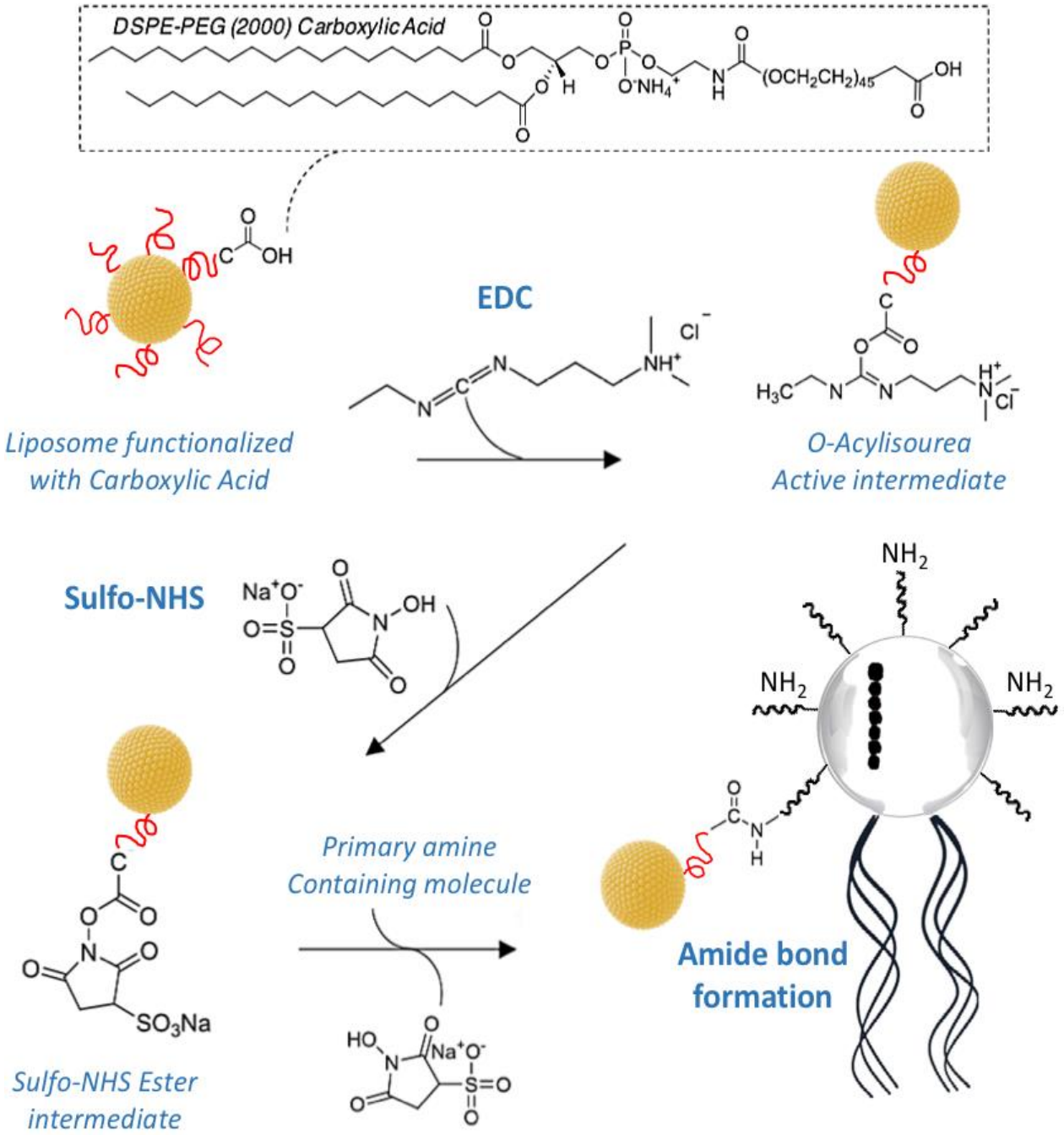


Figure 3.5: Schematic representation of LP-MTB formulating via carbodiimide chemistry. First, EDC/NHS reacts with the available carboxyl groups on the surface of the nanoliposomes. Then, the activated nanoliposomes, covalently attach to the amino groups at the surface of the MTB (Taherkhani, 2015).

### 3.1.7 Sample preparation for scanning electron microscopy (FE-SEM) imaging

For SEM imaging, a suspension of MTB-LP-SN38 sample was fixed in 2.5% glutaraldehyde overnight at 4 °C. A 20 µl of the fixed sample was placed on a grade II titanium discs (cp-Ti) of approximately 12 mm diameter and 2 mm thickness and incubated for 30 min. Subsequently, the plates were rinsed three times with 0.1 M sodium phosphate buffer (PB, pH 7.4) and incubated for 1 h in 1% osmium tetroxide at 4 °C. Samples were dehydrated in a series of ethanol (30%, 50%, 70%, 90%, 95% and two times 100%) followed by drying in a critical point dryer (Balzers CPD 030, Hudson, NH, USA) to remove the ethanol from the samples. High-resolution images of the complexes were obtained by the EOL JSM-7400F (JEOL Ltd, Tokyo, Japan) field-emission scanning electron microscope (FE-SEM) operated at an imaging voltage of 1.5 kV and a working distance of 8 mm.

## 3.2 MTB-MNP formulation

### 3.2.1 Reagents and chemicals

Fluid MAG-ARA-COOH superparamagnetic iron oxide nanoparticles (SPION) with a terminal carboxyl group are ferrofluid consisting of an aqueous dispersion of magnetic iron oxides particles ($Fe_3O_4$) coated with a polysaccharide layer (due to their biocompatibility and water solubility are most commonly used for coating the SPIONs) with a diameter of 200 nm, a density of 25 mg/ml and a number of particles $2.2\times10^{14}$/g was purchased from ChemiCell (ChemiCell GmbH, Germany). Lyophilized fluorescein isothiocyanate (FITC) conjugated rabbit anti-BN-1 antibodies was provided from GenScript. Other chemicals were obtained as indicated at the section 3.1.1.

### 3.2.2 Magnetotaxis platform

A 2D magnetotaxis platform consisting of four coreless solenoid electrical coils arranged in a square configuration was used in this project (Figure 3.6 and Figure 3.7) (Loghin, Tremblay, & Martel, 2016; Loghin, Tremblay, Mohammadi, & Martel, 2017). The coils work at a frequency up to 1 kHz. In order to control the MTB swimming direction, each coil was fed with 10 volts, by an H-bridge circuit, in order to alternate the direction of 0.034 amperes current set every second. Each coil induces 0.8 mT at the center of the platform. In every experiment, MTB-MNPs were washed with PBS (pH 7.4) buffer and concentrated in a custom magnetic separator. This separator was

made by a small vertical electromagnet located below the bacteria culture in a petri dish, attracting the live north-seeking MTB (Figure 3.9). About 10 µl of the bacterial suspension was placed between two custom made coverslips and placed on the magnetotaxis platform in such a way that it was coplanar with the platform's xz-plane. The platform is perfectly designed to fit the space under the optical microscope lens and the center of the microscope field of view (Figure 3.8). In order to normalize the bacteria replication variability, a control sample of control MTB was also systematically observed.

An optical microscope (AxioImager Z1, Imaging Solutions Carl ZEISS) equipped with a 20× Apochromat objective and a camera, Sony HRC-1000, of 720×480 resolution at 30 FPS was used to acquire images of the MTB. The field of view size captured by the camera is (727.92 × 436.85) mm where the pixel height and width densities are 0.9101 pixels/mm and 1.011 pixels/mm, respectively. For every observation, a 20 sec video was captured and every single MTB motion was tracked frame by frame using a custom software that was specially developed for bacteria tracking (Loghin et al., 2017).

### 3.2.3 Covalent immobilization of anti-BN-1 antibody on magnetic particles

The carboxylic acid terminal group of the magnetic nanoparticles facilitates the covalent immobilization to biomolecules. The experimental steps are shown in Figure 3.10. Immunoglobulin G (IgG) antibody (AB) specific against the BN-1 MTB has amino terminal groups that can covalently bind to the distal terminal group of the carboxylated MNP via the carbodiimide chemistry technique and make MNP-AB complexes, as shown in Figure 3.11.

The carboxyl groups of MNP were activated by EDC activating/coupling reagent. EDC along with sulfo-NHS can be used to convert the carboxyl groups to amine-reactive sulfo-NHS esters (Hermanson, 2013) for efficient AB attachment (Figure 3.11b). Similar to what reported in (Taherkhani, 2015), 2 mg of fluidMAG-ARA particles were washed repeatedly with 1 ml MES buffer (0.1 M, pH 5.5) using a magnetic separator (MagnetoPURE, ChemiCell) and then dispersed in 2.5 ml MES buffer solution. Then, in order to attach the antibody to the MNPs, the particles were incubated for 30 min in 4 mg EDC and 6 mg NHS for 30 minutes in 2.5 ml MES buffer. The solution was purified from excess activating reagents by washing with MES buffer using the separator. Next, a solution of 2 mg/ml of FITC BN-1 antibodies (AB) was prepared and 50 µl was added to the activated particles. The solution was incubated for 4 h on a laboratory shaker at room

temperature. Unconjugated antibodies were removed by washing three times with BPS buffer (0.01 M, pH 7.4). Finally, the MNP-AB was dispersed in PBS buffer (0.01 M, pH 7.4) with a final concentration of 400 μg/ml and stored at 4 °C until use.

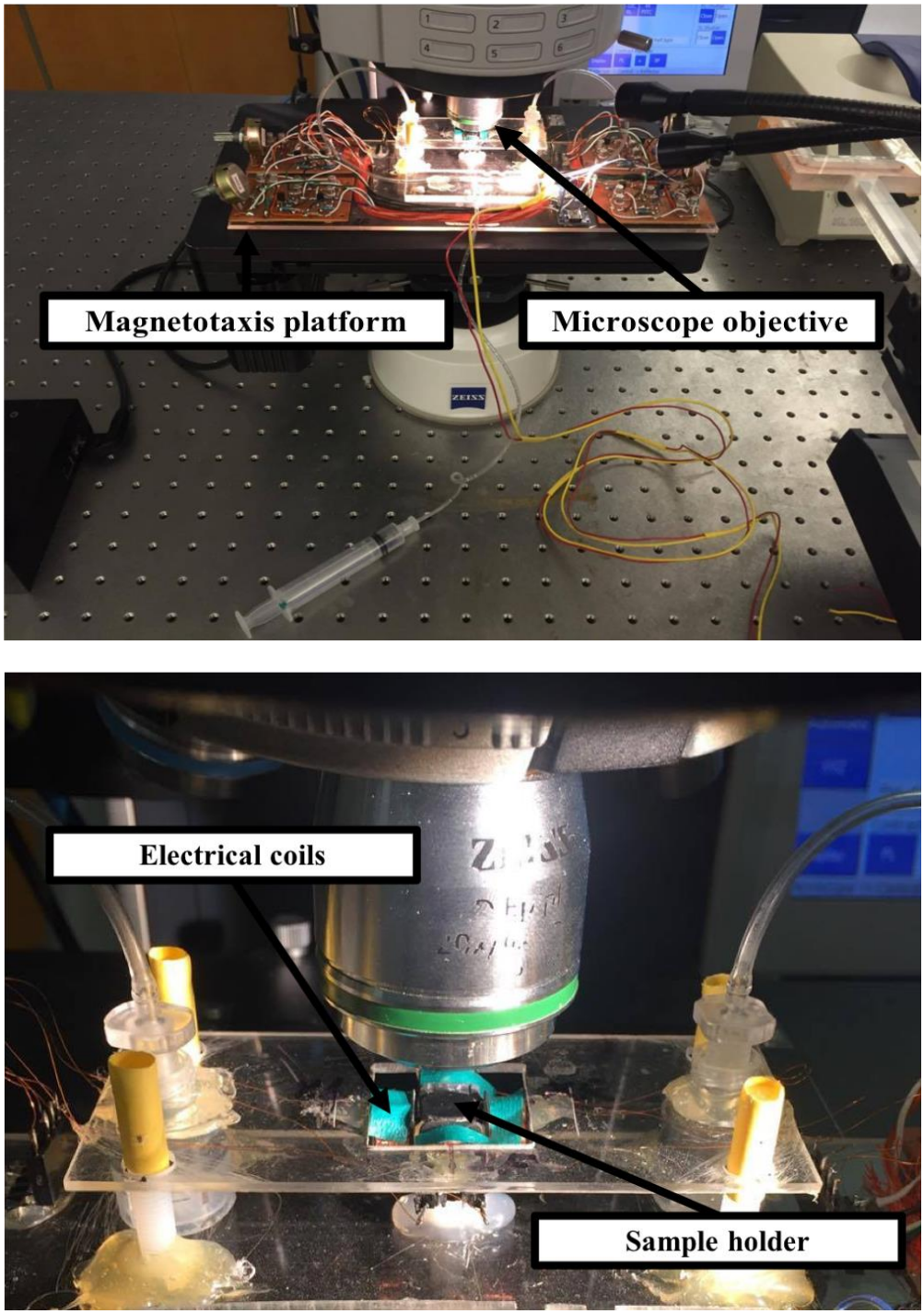


Figure 3.6: Magnetotactic platform installed under the microscope objective (Top). Zoomed in view of the platform (Bottom). The labels show different parts of the experimental setup.

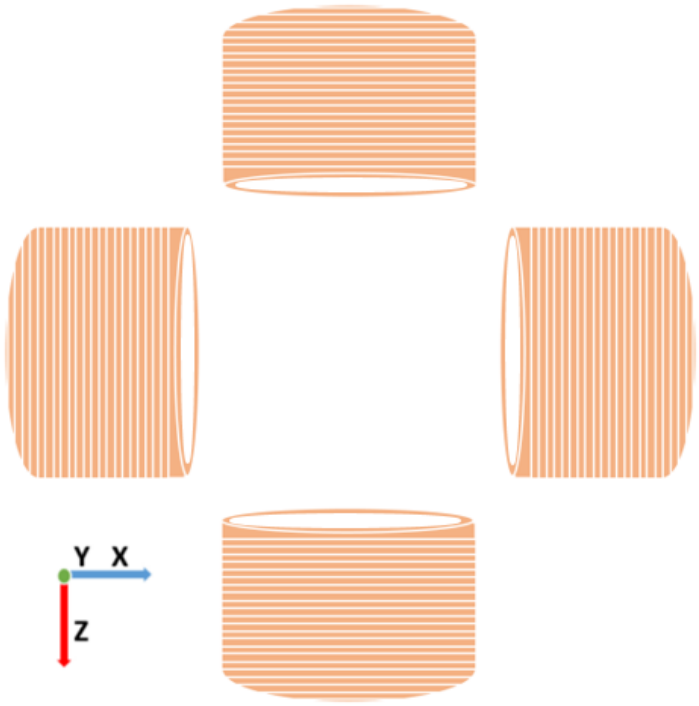


Figure 3.7: Schematic representation of the four-coiled magnetotaxis platform. This platform is based on two pairs of coils placed in an orthogonal square configuration along the X-Y axis.

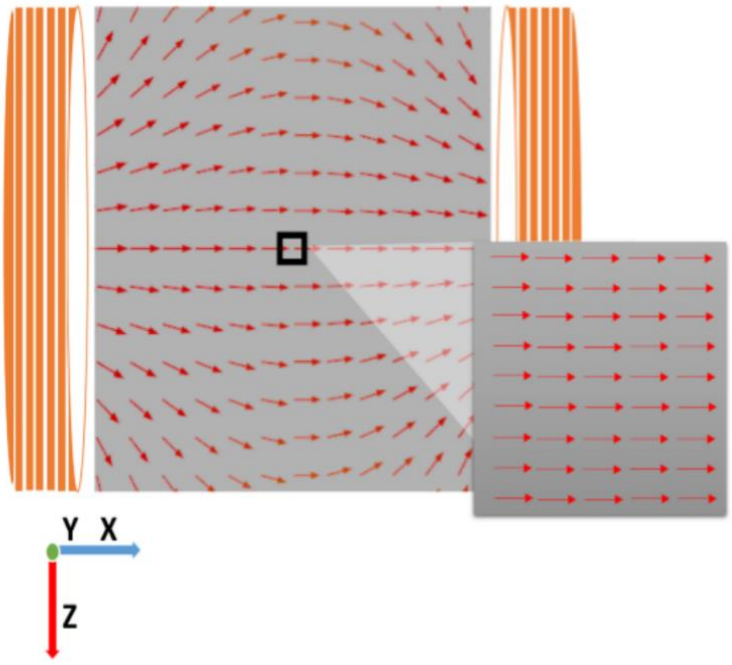


Figure 3.8: Magnetic Field Configurations vector field illustration (uniform). Adapted from (Majedi, Loghin, Mohammadi, & Martel, 2017).

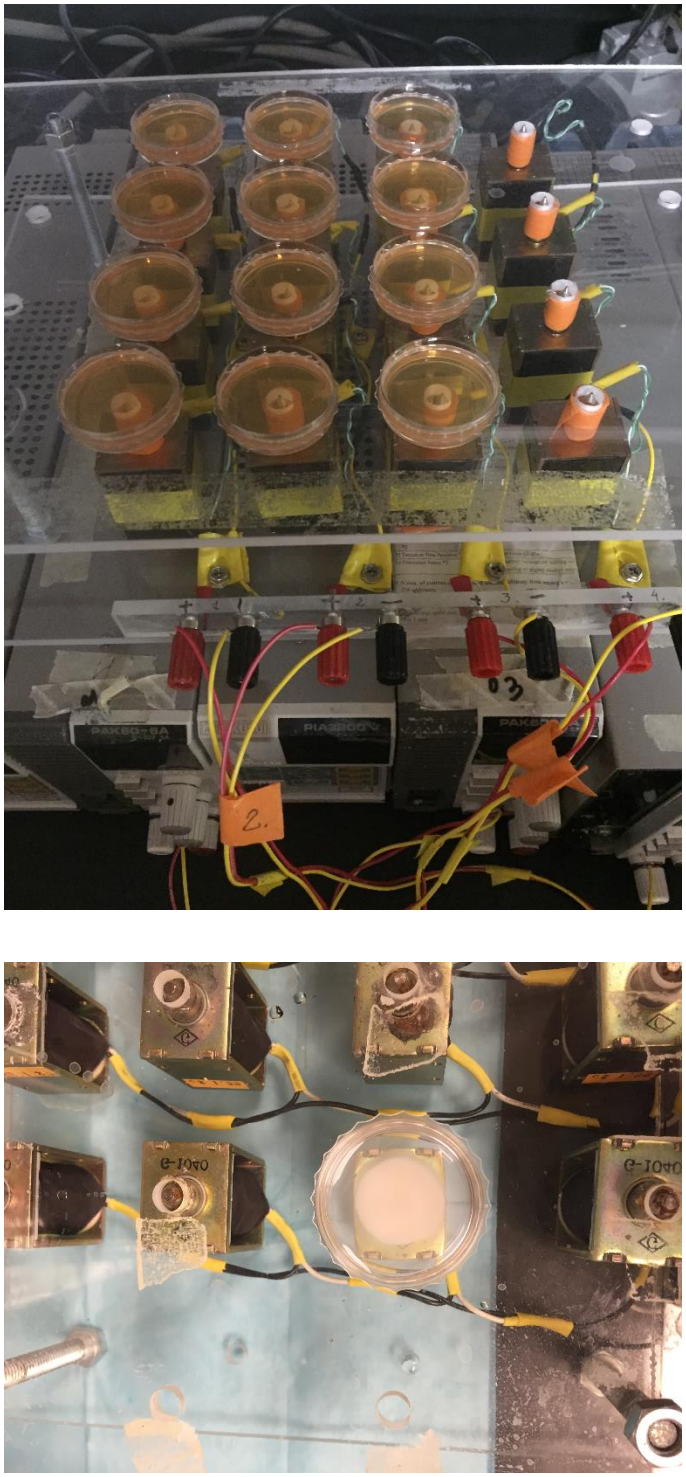

Figure 3.9: The two-dimensional magnetic setup connected to a power supply for concentrating and washing cultures of the MTB and/or their complexes (Top). Zoomed in view of a swarm of the MTB-MNP complex (Bottom).

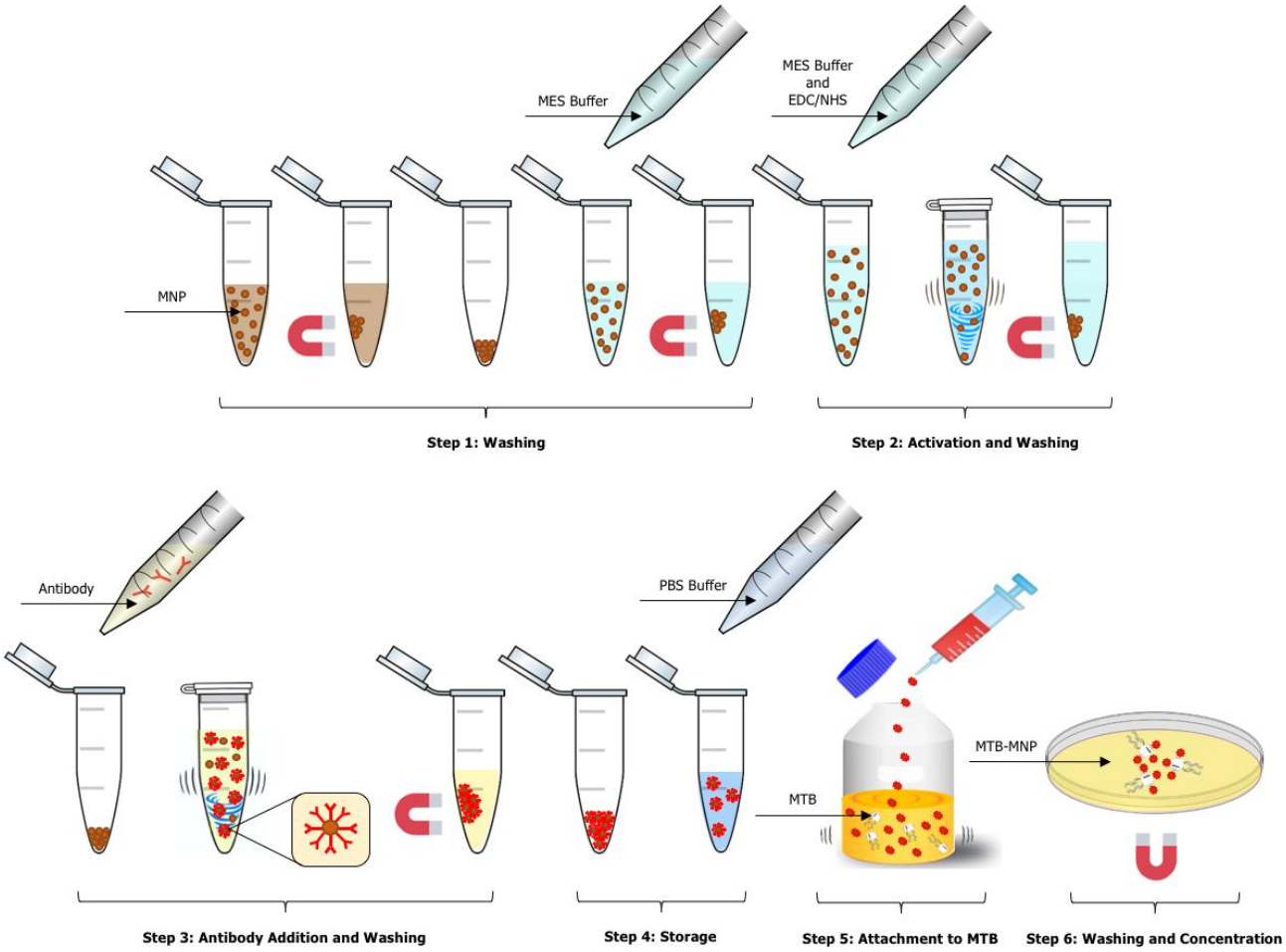


Figure 3.10: Covalent immobilization of anti-BN-1 antibody on magnetic particles.

### 3.2.4 MNP-AB attachment to the MTB membrane to form MTB-MNP complexes

In order to attach the MNP-AB to MTB, 3 ml of the MNP-AB was injected to 50 ml MTB ($10^7$ MTB/ml). Then, the bioconjugation was successfully achieved by incubating MTB with activated MNPs solution for 2 h in dark, at room temperature and with gentle agitation.

The obtained complexes were washed three times with PBS (pH 7.4) using the magnetic setup in order to remove the free particles (Figure 3.9). This system generates a homogeneous magnetic gradient in 2D that decreases from 60 Gauss at the edges to zero Gauss at the center of the sample holders. The magnetic field was applied towards the center of each petri dish where the MTB-MNP complexes are collected.

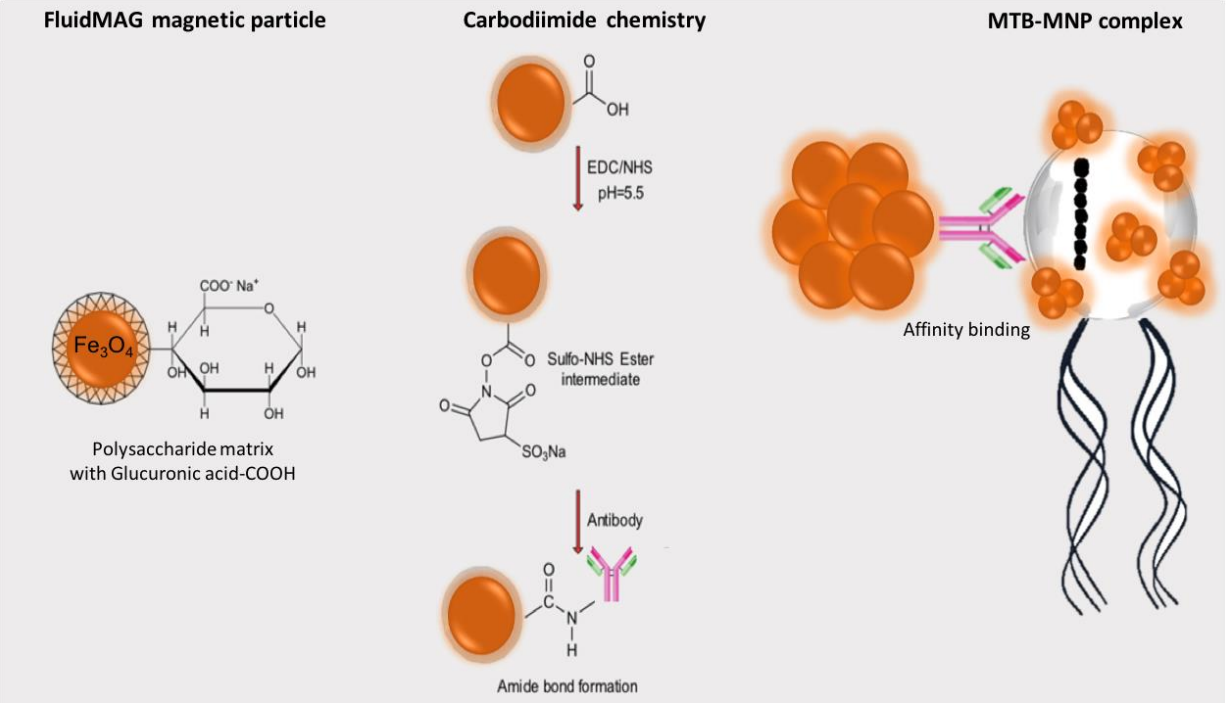


Figure 3.11: Schematic representation of the steps to prepare the MTB-MNP complex. FluidMAG magnetic nanoparticle with terminal carboxyl groups (left). Covalent attachment of the amino group-containing antibody to the carboxylated MNPs by the carbodiimide activation (middle). Attachment of the MNP-AB to the MTB cell membrane (right) (Taherkhani, 2015).

### 3.2.5 Characterization of the MTB-MNP complexes

To validate the success of the experiment, the MTB-MNPs solution was concentrated and washed with PBS buffer (pH 7.4) on the magnetic concentrator (Figure 3.9) to get rid of unattached particles and free salts. The same amount of control MTB solution was also concentrated and washed from its medium with the same buffer, at the same time and conditions for testing.

Olympus FLUOVIEW FV1000 confocal microscope and JEM-2100F transmission electron microscope were used for qualitatively analyzing the attachment of MNP-AB to MTB, while a ZEISS optical microscope and a four coils magnetotaxis setup connected to the microscope along with a bacteria tracking software was used for characterization (Figure 3.6).

### 3.2.5.1 Sample preparation for transmission electron microscopy (TEM) imaging

The structure of the MTB-MNPs was characterized by a transmission electron microscopy (TEM, JEM 2100F, operating at 200 kV). For TEM imaging, the MTB-MNPs suspension and the bacteria complex were washed with unsalted 0.1 M sodium phosphate buffer (pH 7.4) and concentrated on the magnetic concentrator (Figure 3.6 and 3.8), separately. A 5 µl of the suspension of each sample was dropped onto 200 mesh formvar-coated copper TEM grid with a carbon film (FCF200-Cu, Electron Microscopy Sciences) and left under ambient conditions. The excess of the solution was removed by a piece of blotting paper. Finally, the grids were gently dipped in distilled water to get rid of any remaining impurities.

### 3.2.5.2 Bacteria transition under an applied magnetic field ($B_o$)

In the magnetotaxis platform (Figure 3.6), the two opposite electrical coils in a Helmholtz configuration were each fed with 10 volts causing both coils to induce 1.6 mT magnetic field for the straightforward and U-turn paths. When the two coils are fed at the same time, the platform is able to produce a nearly homogenous magnetic field at the center of the xz-plane (Figure 3.8) where the sample is located. In order to characterize the bacteria, this platform repeatedly produces sequences of predefined Magnetic Field Configurations (MFC) to orient MTB forward then backward. The exposure time for each sequence was a few seconds. In order to track the bacteria trajectory, 10 bacteria that were in the focus were selected and their paths were tracked frame by frame until the tracked bacterium was out of the focus or invisible.

The motion of a bacterium is governed by Equation 1 (Bahaj & James, 1993). Where the first and the second terms represent the field induced torque and the viscous drag torque, respectively. m is the magnetic moment [$A.m^2$], $B_o$ is the applied magnetic field (T), $\eta$ is the viscosity of the medium (Pa.s), R is the radius of a sphere.

$$mB_{\circ} \sin\theta - 8\pi\eta R^3 \frac{d\theta}{dt} = 0 \qquad (1)$$

The U-turn diameter (L) depends on the total magnetic moment (m) and is given by Equations 2. Where L is the U-turn diameter [m] and v is the mean velocity at an applied magnetic field [m/s].

$$L = \frac{8\pi^2 R^3 v \eta}{m B_\circ} \qquad (2)$$

Magnetic moment ratio of the attached over control samples can be obtained using Equation 3. Where the subscripts a and c stand for the attached and the control samples, respectively.

$$\frac{m_a}{m_c} = \frac{L_c R_a^3 v_a}{L_a R_c^3 v_c} \qquad (3)$$

# CHAPTER 4 RESULTS AND DISCUSSION

## 4.1 Analytical assessment of SN38 content in MTB-LP-SN38 complex

The samples (LP, LP-SN38 and the MTB-LP-SN38 complexes) were analyzed with LC/MS, UV-Spectroscopy, DLS and Zeta potential.

**Liquid/Liquid Extraction.** An extraction method had to be carried out to determine the concentration of encapsulated/attached SN38. In these cases,10 µl of the liposome or complex were diluted with 200 µl of a camptothecin solution in PBS buffer (pH 11) (10.4 µg/ml) used as an internal standard. The samples were mixed on a vortex. 800 µl of chloroform was added and the samples were vortexed and centrifuged (1 min at 6000 rpm). Then, the aqueous layer was transferred to a clean tube and the sample was dried with an $N_2$ flow. The sample was reconstituted in 800 µl of MeOH 0.5% formic acid followed by vortexing and centrifugation (1 min at 6000 rpm). Finally, the supernatant was injected into the LC/MS system.

**Quantification of SN38 by Liquid Chromatography/Mass Spectroscopy (LC/MS)**

LC/MS was used to evaluate the SN38 concentration in each sample. All reagents used for LC/MS analyses were HPLC grade. The analyses were performed on Waters Xevo instrument and Agilent Eclipse Plus C18 RRHD column (1.8 µm, 2.1 × 50 mm). After the injection of 2 µl of the sample, a linear gradient elution, using 0.1% (v/v) formic acid in water (mobile phase A) and 0.1% (v/v) formic acid in methanol (mobile phase B) was performed at a flow rate of 0.25 ml/min for a total run time of 15 min (Table 4.1). The detection was made in positive electrospray using two multiple reaction monitoring transitions by the compound. The relative peak area of the chromatograms was used to quantify the SN38 in the samples.

**MTB Complex Calibration Curve.** To prepare the calibration curve, a stock solution of SN38 in PBS buffer (pH 11, 0.5 mg/ml) was diluted in PBS (pH 8) at different concentrations. 1 µl of each standard solution was then added to 10 µl of MTB to obtain concentrations ranging from 0.86 to 15.38 µg/ml. A 5.22 µg/ml internal standard solution was prepared in PBS (pH 11). Then, from the chromatograms the calibration curve was traced. The system's responses were obtained from the peak area ratio of the SN38 to the IS of the chromatograms.

Table 4.1: SN38 samples were eluted with a gradient of mobile phase A and B.

| **Time (min)** | **%A** | **%B** |
|---|---|---|
| 0.0 | 60 | 40 |
| 6.5 | 10 | 90 |
| 8.0 | 10 | 90 |
| 8.5 | 60 | 40 |
| 15.0 | 60 | 40 |

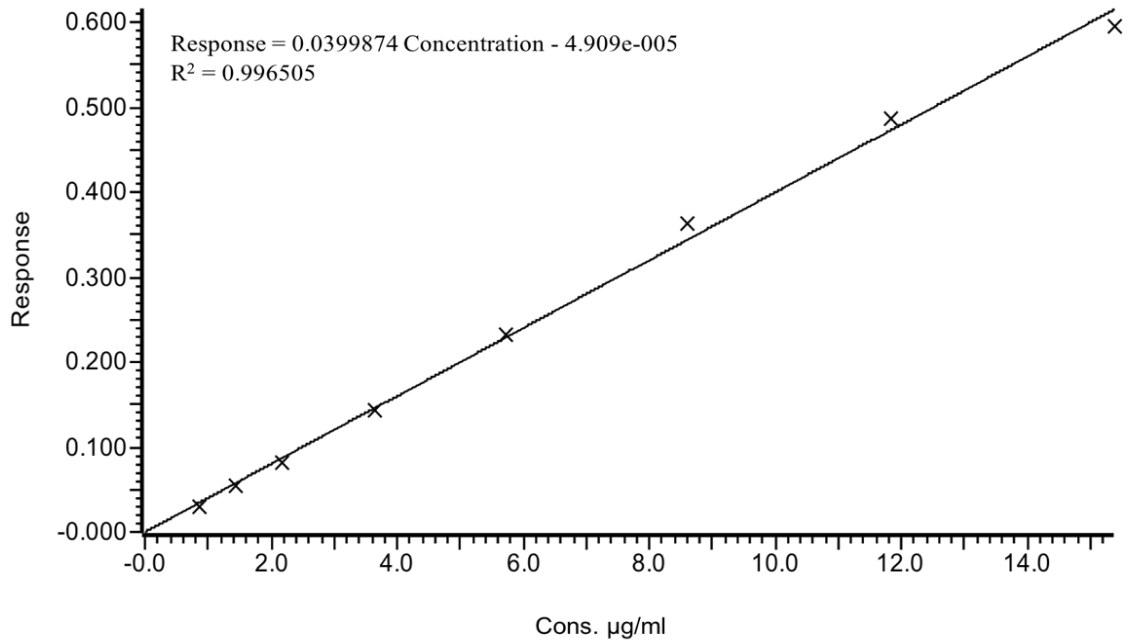


Figure 4.1: Calibration curve of SN38 in the MTB complex.

**Liposomes Calibration Curve.** An empty-liposome suspension (6 mM) was diluted to 0.7 mM using PBS buffer (pH 8). A stock solution of SN38 (0.5 mg/ml) in PBS (pH 11) was diluted in PBS (pH 8) to obtain concentrations ranging from 5.5 to 35.7 µg/ml. 10 µl of each standard solution was then added to 100 µl of liposome solution and vortexed. (Figure 4.2).

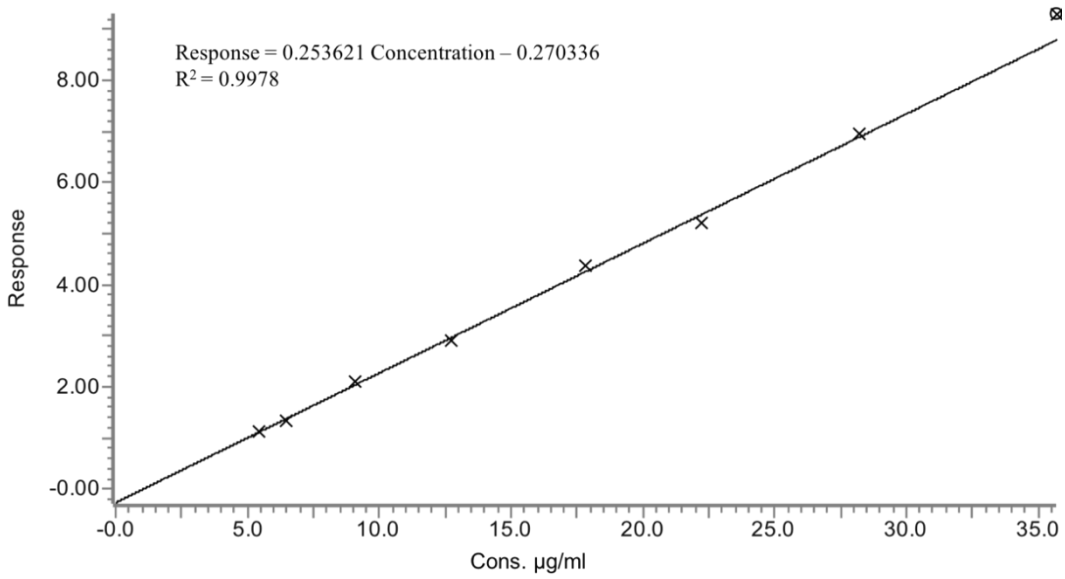


Figure 4.2: Calibration curve of the liposome solution.

Table 4.2 shows the calculated concentrations of SN38 for the samples. The average calculated concentration of the SN38 attached to the MTB complex was determined to be 14 µg/ml. The limit of detection (LOD) was extrapolated from the calibration curve. In brief, the signal to noise ratio (S/N) of the smallest concentration from the curve was evaluated and extrapolated what it would be for 3× S/N ratio.

Table 4.2: Calculated SN38 concentrations in samples (n = 3).

| **Sample** | **SN38 concentration (µg/ml)** |
|---|---|
| MTB-LP-SN38 | 14 |
| MTB | < LOD |
| LP (pH 4/8) | < LOD |
| SN38 (pH 11) | 5.04 |

< LOD: below limit of detection (0.33 µg/ml)

Figure 4.3 shows the chromatograms of the SN38 in different samples. In Figure 2d, the peaks are corresponding to the internal standard and the SN38, respectively.

To determine the amount of SN38 attached to each MTB cell, 25 ml of the MTB-LP-SN38 complex was concentrated in 110 µl PBS (pH 7.4). The MTB was counted using an optical microscope. The amount of SN38 attached per MTB was estimated to 1.3 µg using LC/MS method which is corresponding to ~ $1.46 \times 10^8$ MTB/ml. The MTB concentration was determined by counting under optical microscopy (AxioImager Z1, Imaging Solutions Carl ZEISS).

**UV-Spectroscopy Analysis**

In addition to LC/MS, the SN38 concentration was also analyzed with UV-Spectroscopy. First, a certain amount of SN38 powder was dissolved into PBS buffer (pH 11) to reach a concentration of 0.5 mg/ml. SN38 standard solutions (0.15 - 320 µg/ml) were prepared. 1 µl of Triton X-100 1% wt/wt (in PBS pH 11) was added to the LP-SN38 and MTB-LP-SN38 samples to make sure that the vesicles are broken and the loaded drug is released entirely. The absorbance of SN38 was read at 385 nm and compared to that of the standards to determine the amount of loaded drug into LP and MTB-LP. Figure 4.4 shows the calibration curve of the SN38. The concentration of the encapsulated drug was calculated to be 14.4 µg/ml. UV results were in compliance with LC/MS.

**Particle size and zeta potential analysis of carboxylated nanoliposomes**

Immediately after preparation, the average particle size (PS), the size distribution and the zeta potential (ZP) of the liposomes were determined using dynamic light scattering (DLS) techniques, using a Malvern Zetasizer (Malvern Instruments, Malvern, UK). Each sample was analyzed in triplicate at 25 °C. The particle size was found to be ~ 200 nm (Figure 4.5) with a polydispersity index (PDI) of 0.16. The surface charge of the liposomes was found to be -16 mV, consistent with the presence of the carboxyl group.

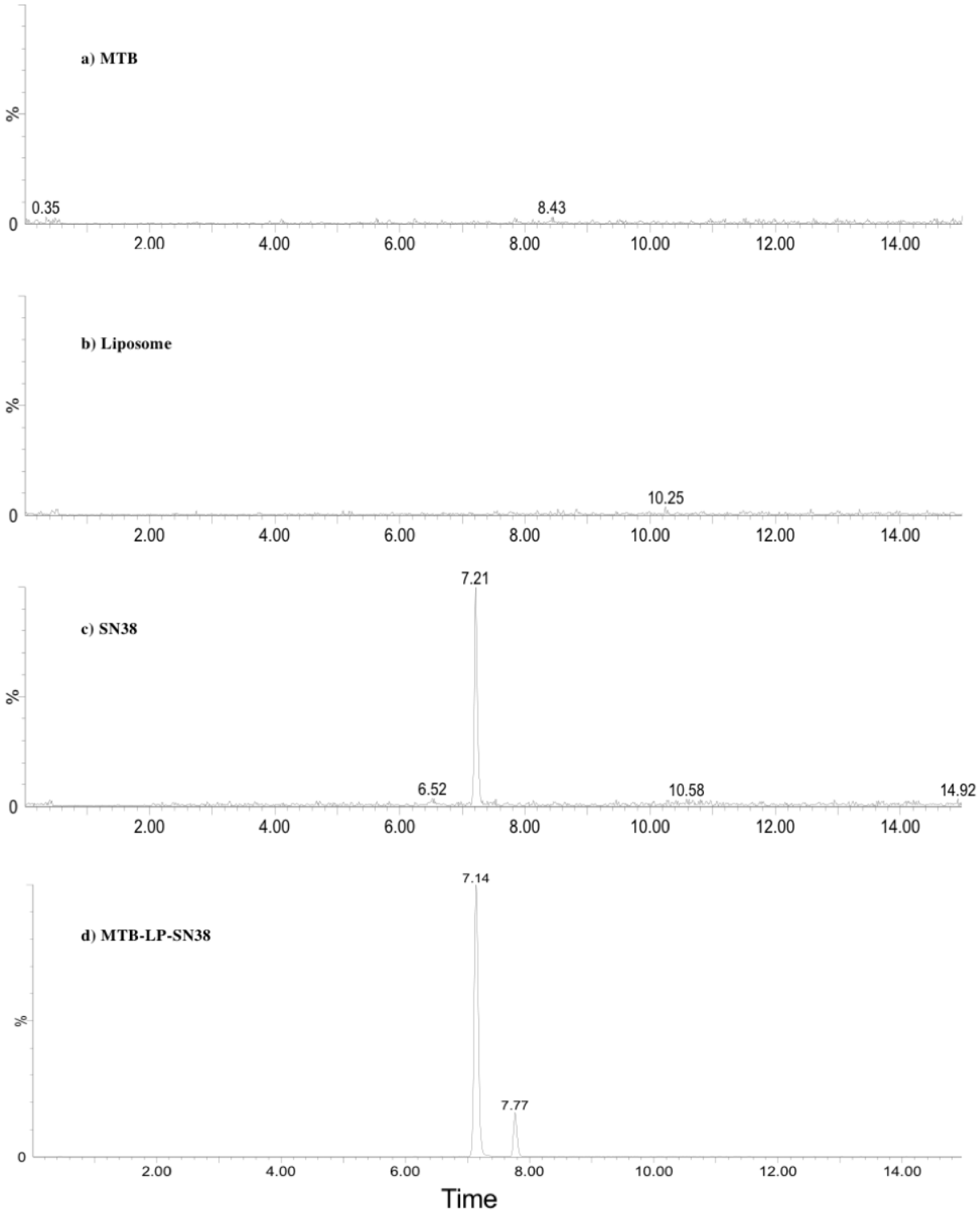


Figure 4.3: (a) Chromatograms of SN38 in MTB. (b) LP (pH 4/8). (c) SN38 lowest standard at 0.86 µg/ml. (d) Camptothecin and MTB-LP-SN38.

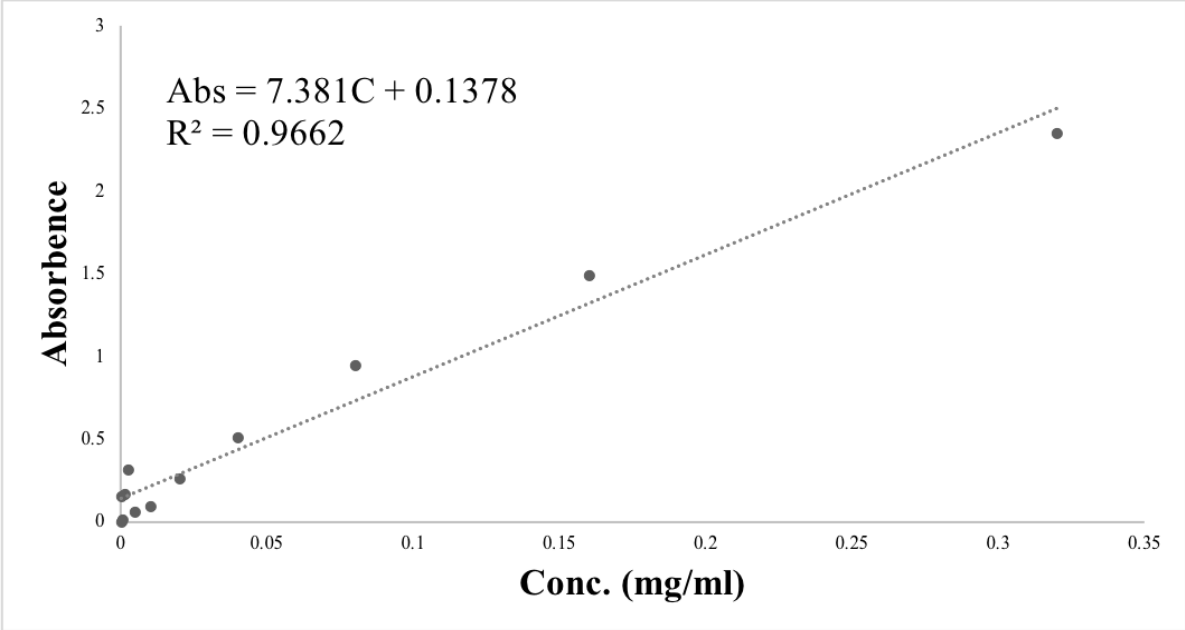


Figure 4.4: Calibration curve of SN38 (n = 3).

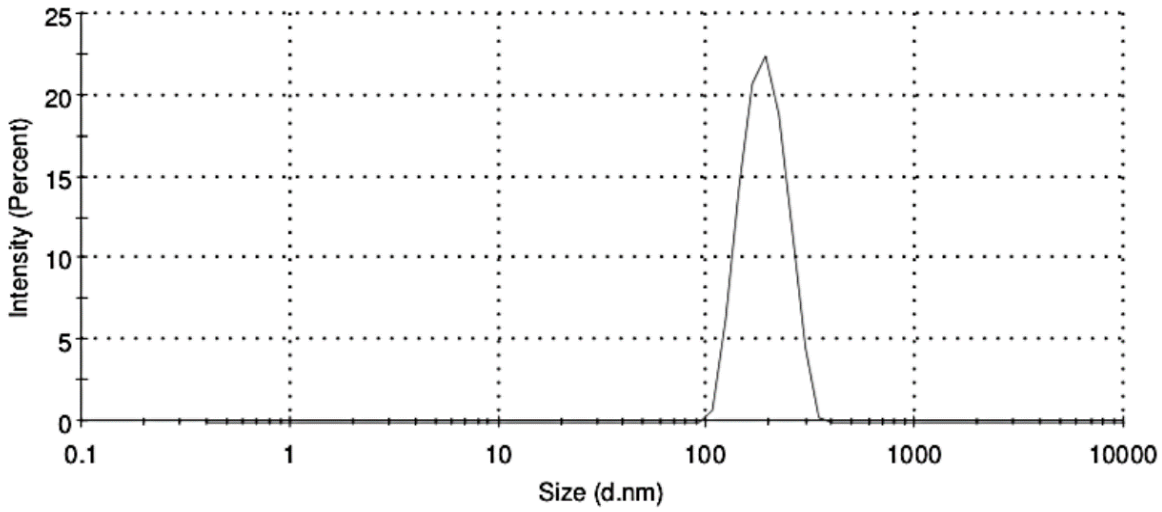


Figure 4.5: Size distribution analysis obtained by dynamic light scattering (DLS) of LP-SN38.

## 4.2 Characterization of the MTB-MNP complexes

The attachment of the MTB-MNPs was examined by a single photon confocal microscope (Figure 4.6), with excitation/emission wavelengths of 488/519 nm, and a JEOL 2100-F filed emission gun transmission electron microscope (TEM) operated at 200 kV to acquire bright filed images (Figure 4.7). In the confocal microscope, both the fluorescent image (from the FITC BN-1 AB attached on

the MNPs in the MTB-MNPs samples) and the visible image via differential interference contrast are displayed. The image obtained by differential interference contrast indicated the location of the bacteria while the fluorescent spots, observed from the window beside it, showed the presence of the fluorescent antibody. All the bacteria presented in the bright field condition (Figure 4.6-Right) showed fluorescence under fluorescent light (Figure 4.6-Left) validating the success of the attachment of the antibody on the bacteria. In addition, clusters of MNPs attached on the surface of MTB can be seen in Figure 4.7.

The obtained results, using a bacteria tracking software (Loghin et al., 2017), showed that the swimming MTB-MNPs complexes, in all sequences, clearly respond faster to the change in the external magnetic field and they well align with the applied magnetic field orientation compared with the control MTB bacteria (Figure 4.8) while they have less speed (Table 4.3). As can be seen, the MTB-MNPs complexes in Figure 4.8b illustrate relatively straight lines compared with the path lines of the control MTB in Figure 4.8a. Similarly, the U-turn diameters (L) are narrower in MTB-MNPs in Figure 4.8d in contrast with control MTB in Figure 4.8c. In the U-turn configuration of MTB-MNPs, as depicted in Figure 4.8d, some tangled paths were detected that could be due to the uneven distribution of the MNPs on the surface of MTB. The tracking software calculated the displacement over the time of each bacterium. Table 4.3 compares the average speeds of the MTB versus MTB-MNPs in both straightforward and U-turn sequences in physiological PBS buffer solution (pH 7.4) at room temperature. In all experiments, the speed of the control bacteria was found to be almost double the speed of MTB-MNPs. By employing Equation 2 the magnetic moment of both the control MTB and MTB-MNPs were calculated to be $1.53 \times 10^{-}14$ A.m$^2$ and $4.0 \times 10^{-}14$ A.m$^2$, respectively. Equation 3 showed that the magnetic moment in the MTB-MNPs was ×3 higher, approximately.

Table 4.3: Average speeds of control MTB versus MTB-MNPs. Adapted from (Majedi et al., 2017).

| **Sequence** | **U-turn** | | **Straightforward** | |
|---|---|---|---|---|
| **Sample** | ***Control*** | ***Attached*** | ***Control*** | ***Attached*** |
| **Average Speed (μm/s)** | 100 | 66 | 102 | 57 |

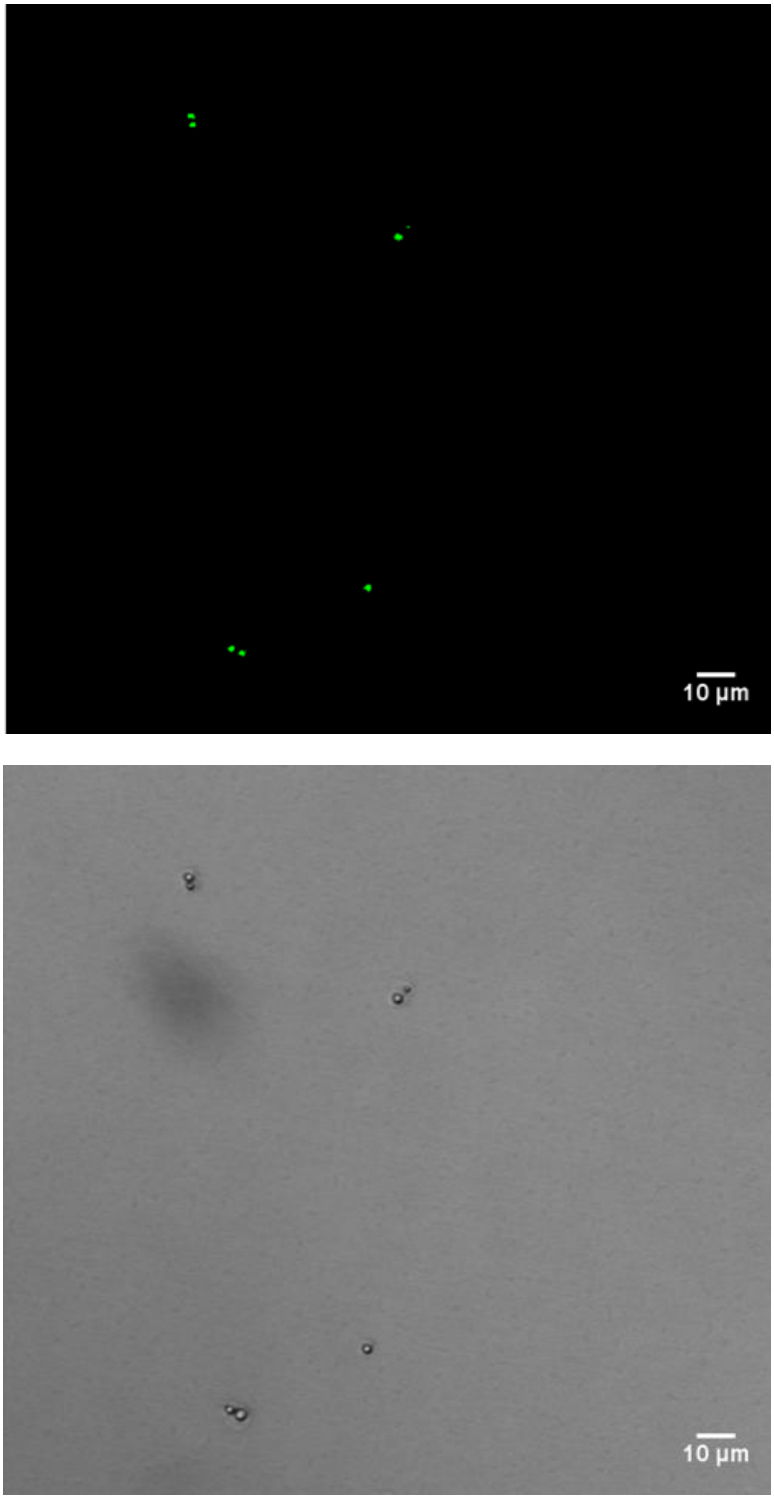


Figure 4.6: Confocal microscopy images of MTB-MNPs complexes: bottom image corresponds to the visible image whereas the top image was obtained by fluorescence confocal microscopy with FITC BN-1 AB label (excitation/emission wavelength of 488/519 nm). Adapted from (Majedi et al., 2017).

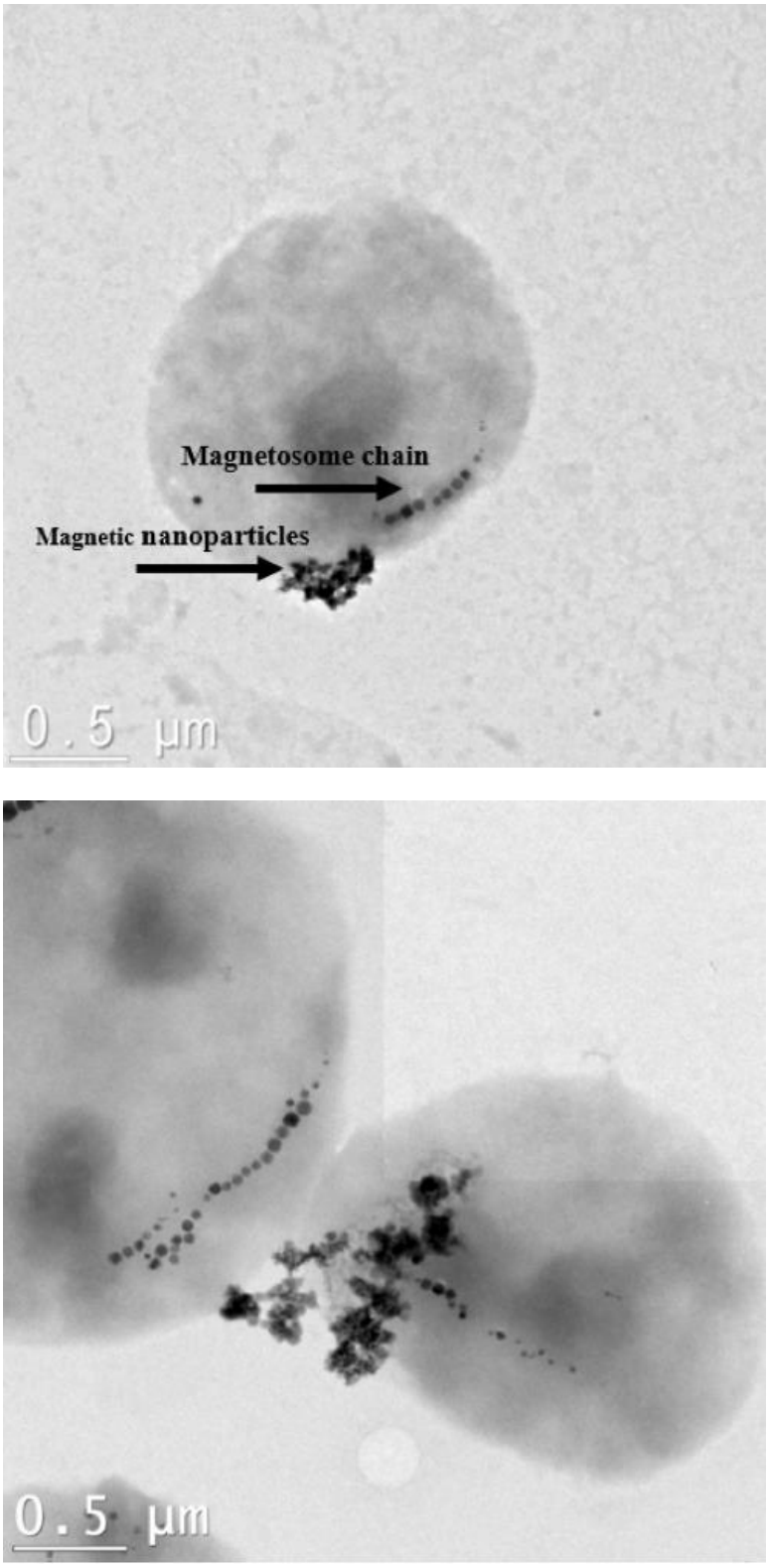


Figure 4.7: Transmission electron microscopy images of MTB-MNPs complexes. Adapted from (Majedi et al., 2017).

There are a number of factors contributing to the U-turn motion of bacteria in the applied magnetic field (e.g. viscosity of the medium and the size of the organism) (Bahaj & James, 1993). One reason explaining the increase in sensitivity of the directional magnetic torque of the MTB-MNPs complex is attributed to the anisotropy of the clusters of magnetic nanoparticles being attached to the surface of the BN-1 cell. Indeed, if the respective easy axis of such clusters would be parallel to the chain of magnetosomes in the BN-1 cells, then this could be the cause of such increase in sensibility along the natural swimming path of the bacteria. On the other hand, attached clusters with the easy axis perpendicular to the axis of the chain of magnetosomes could potentially help in turning the motion of the bacteria. Microscopy examination of the clusters configurations being attached to the BN-1 cells and additional tests on various MTB-MNPs complexes would be required to really explain and validate such results. Moreover, the volume of the MTB-MNPs due to the MNPs attached to MTB surface increases, the viscosity of the medium increases, consequently resulting in the difference in speed and traveling path of the bacteria samples. Therefore, as the viscosity increases, the speed of the MTB-MNPs should decrease. The magnetic moment of the MTB-MNPs is more due to the magnetic particles contributions in the total magnetic moment. Therefore, this causes the MTB-MNPs to respond quickly to the change in the magnetic field and L decreases when compared with the control bacteria (Figure 4.8c and Figure 4.8d).

In the U-turn configuration, the U-turn diameter (L), and the distances traveled by the bacteria (a) were measured for a number of randomly selected bacteria once MFC is applied and the bacteria adapted to the field (Figure 4.9 and 4.10). The average displacement was found to be higher in MTB-MNPs while the U-turn diameter was greater for the control MTB (Figure 4.10). Figure 4.10 shows that the MTB-MNPs responded faster to the magnetic field, causing them to travel a further distance ($\bar{a}_{\mathrm{MTB-MNPs}} > \bar{a}_{\mathrm{Control\ MTB}}$) while, for the same time interval and conditions, the control MTB spent more time adjusting to the field direction change and propelled for a shorter distance ($\bar{L}_{\mathrm{MTB-MNPs}} < \bar{L}_{\mathrm{Control\ MTB}}$).

This study shows clear evidence that there are differences between the MTB and the MTB-MNPs and it opens a door to study if the MNPs are contributed in the response of bacteria to the magnetic field. MTB-MNPs could be a promising factor in enhancing the steering of bacteria in hypoxic regions of solid tumors, however, extensive observations are required.

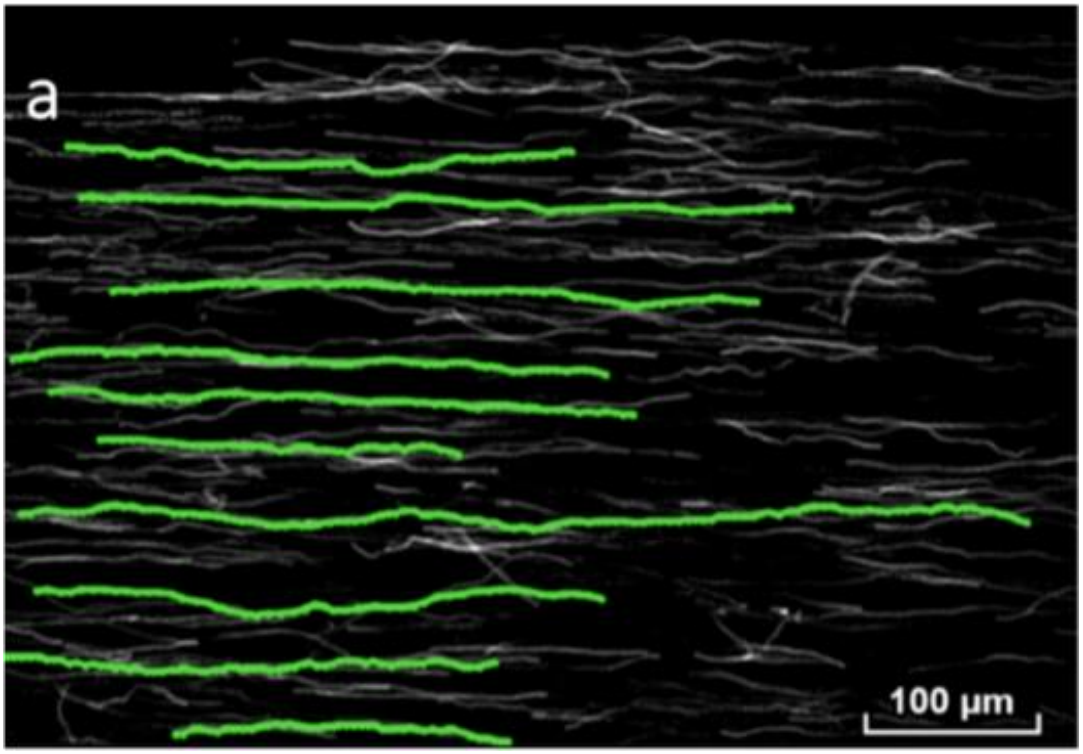
a
100 µm

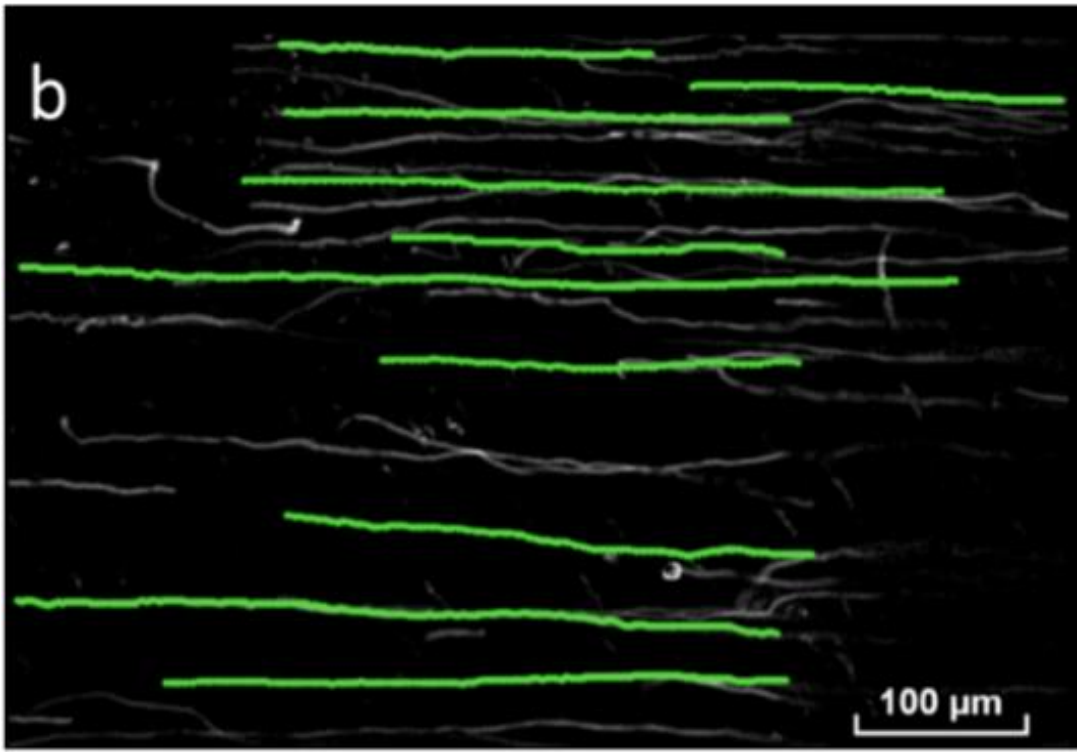
b
100 µm

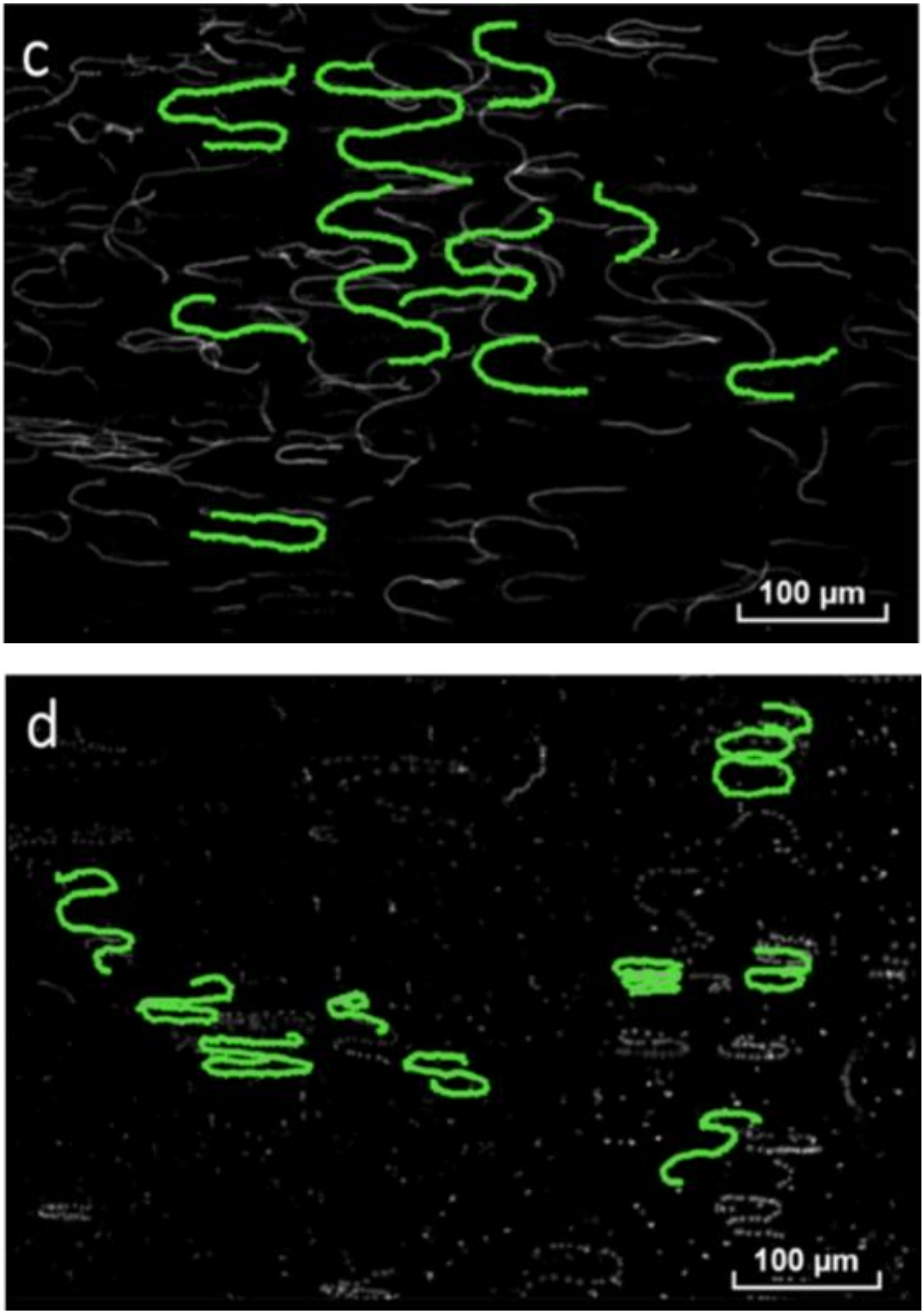


Figure 4.8: Straightforward displacements of control MTB (a) versus MTB-MNPs complexes (b) and U-turn displacements of control MTB (c) versus MTB-MNPs complexes (d). Adapted from (Majedi et al., 2017).

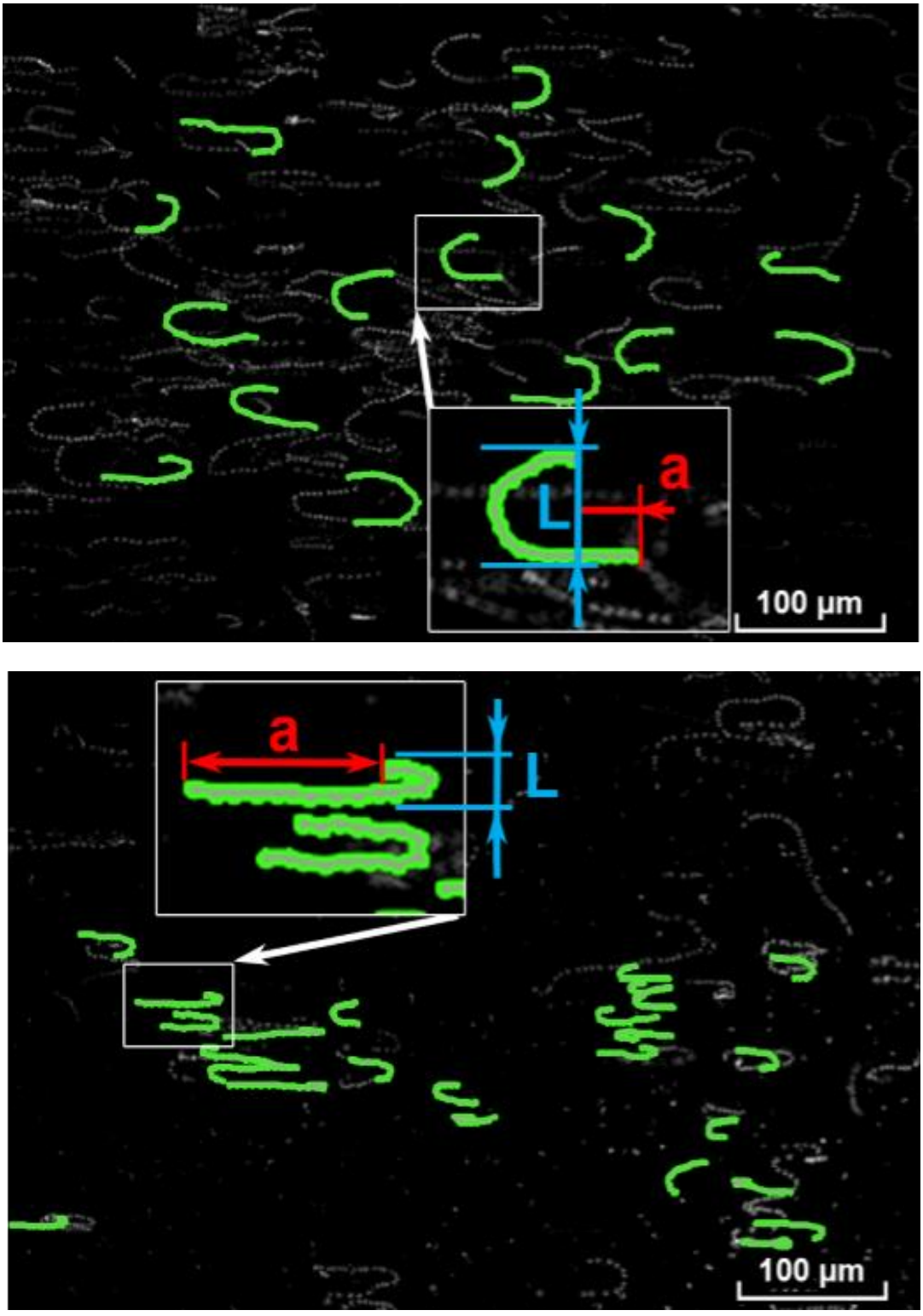


Figure 4.9: Distance traveled by a bacterium (a) and U-turn diameter (L) during the field change in control MTB (Top) versus MTB-MNPs (Bottom). Adapted from (Majedi et al., 2017).

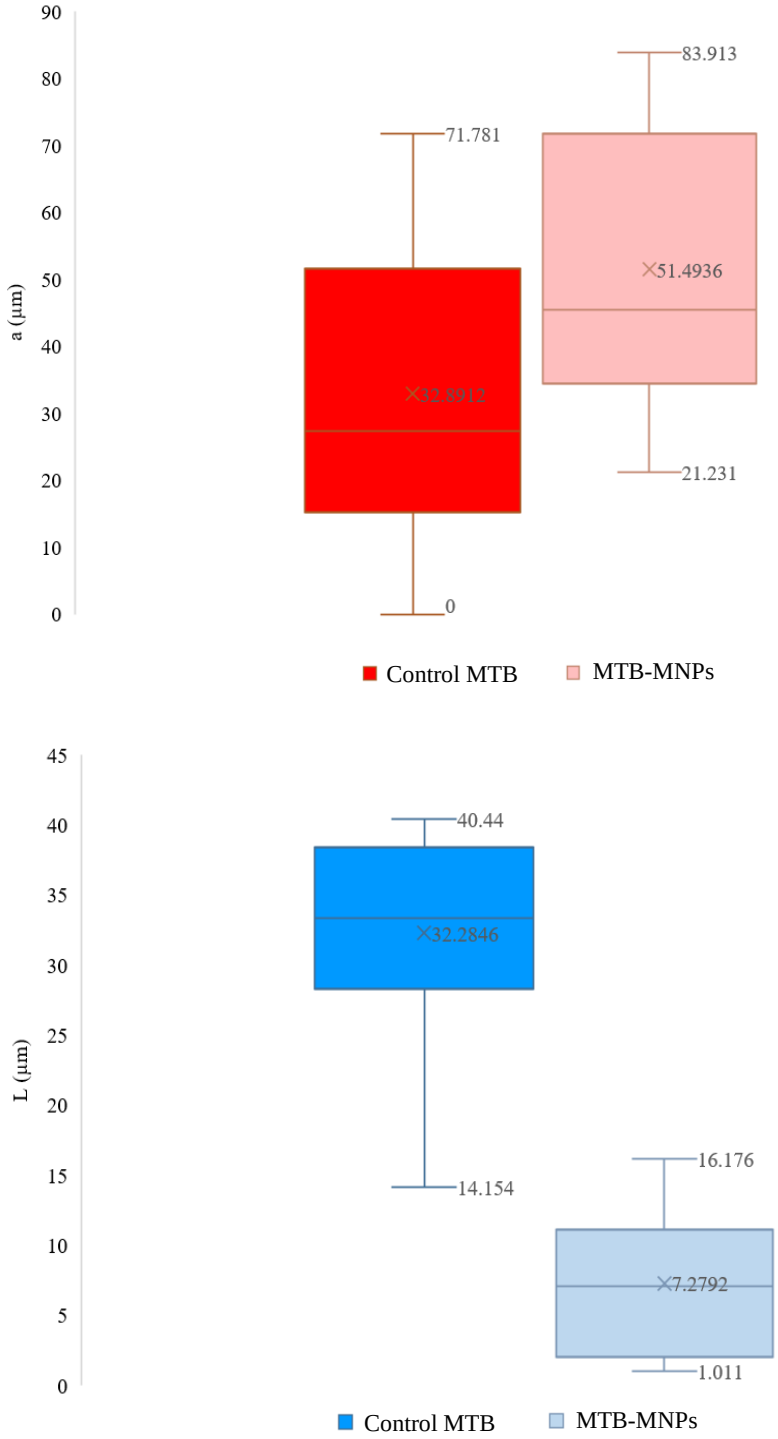


Figure 4.10: Distance traveled (a) by bacteria for the control MTB versus MTB-MNPs (Top) and U-turn diameter (L) for the control MTB versus MTB-MNPs (Bottom). The box-and-whisker plot shows the range and (25th percentile/median ($\bar{a}$)/75th percentile) box for the control MTB and the MTB-MNPs groups.

# CHAPTER 5 CONCLUSION AND RECOMMENDATIONS

For treating cancer through the targeted delivery using the MR-navigable carrier based on magnetotactic bacteria or MTB, payloads of therapeutic and imaging agents were attached to the surface of the MTB and the complexes were characterized. The results demonstrated that SN38 loaded nanoliposomes can covalently attach to the surface of MTB via carbodiimide cross-linking chemistry without altering the bacteria cells' magnetic characteristics. The average concentration of the SN38 attached to the MTB-LP-SN38 complex was found to be 14 µg/ml. Samples prepared through this study were used in a couple of *in vivo* studies. The results are not discussed here due to confidentiality matters.

In addition, we demonstrated that 200 nm SPIONs were successfully attached to the surface of MTB cells and the prepared MTB-MNP complexes were guided in MFC. Results showed the difference in the behavior of the MTB-MNPs and the control MTB trajectory in the applied magnetic field as expected. The MTB-MNPs were better aligned in the direction of the field and had lower velocity compared to the control MTB. The reason behind this difference, whether it is the contribution of the MNPs to the overall field or other factors needs further investigation. U-turn technique can be used to validate the success of the experiment.

These initial findings based on the attachment of cargos on the MTB bio-carrier may influence medical interventions and provide opportunities for the development of new agents to achieve maximum effectiveness in drug, gene and vaccine delivery.

**Future perspective, recommendation, limitation and economic impact**

In this work, we were able to successfully attach therapeutic and imaging nanoparticles to the magnetotactic bacteria cells to act as microrobots or targeting and tracking agents in the field of cancer therapy. The techniques presented here may open further opportunities in diverse disciplines including clinical oncology, chemistry and immunology for non-invasive delivering of other agents (e.g. tumor markers, genetic materials, enzymes, proteins and vaccines).

Further studies can be done on the attachment of a combination of the therapeutic and magnetic agents together to the surface of MTB to access their magnetic behavior, characteristics and multifunctionality for targeting, tracking and treating tumoral cells.

*In vitro* and *in vivo* tests should be administrated to assess the safety, inflammatory responses and effectiveness of this technique in treating cancer.

In addition, two techniques developed by our team (magnetotactic bacteria as carriers and MRI-based transport) should be combined to be applicable where the peritumoral injection is not practical. The main approach is to develop techniques and protocols to encapsulate drug-load MTBs in large temperature-sensitive magnetic vesicles compatible with our MRI-actuated transport and the appropriate release mechanism when these vesicles are in the peritumoral region. This would allow a reduction of the treatment-related toxicity by decreasing the dose of anticancer drugs for cancers where injections near the tumors are not practical. This might not only decrease the cost of some cancer treatments but might also contribute to ensuring quality care in comparison to other conventional treatment options.

# BIBLIOGRAPHY

Afergan, E., David, M. B., Epstein, H., Koroukhov, N., Gilhar, D., Rohekar, K., . . . Golomb, G. (2010). Liposomal simvastatin attenuates neointimal hyperplasia in rats. *The AAPS Journal, 12*(2), 181-187.

Al-Jamal, W. T., & Kostarelos, K. (2011). Liposomes: from a clinically established drug delivery system to a nanoparticle platform for theranostic nanomedicine. *Accounts of Chemical Research, 44*(10), 1094-1104.

Allkemper, T., Bremer, C., Matuszewski, L., Ebert, W., & Reimer, P. (2002). Contrast-enhanced blood-pool MR angiography with optimized iron oxides: effect of size and dose on vascular contrast enhancement in rabbits. *Radiology, 223*(2), 432-438.

Andresen, T. L., Jensen, S. S., & Jørgensen, K. (2005). Advanced strategies in liposomal cancer therapy: problems and prospects of active and tumor specific drug release. *Progress in Lipid Research, 44*(1), 68-97.

Ariffin, A. B., Forde, P. F., Jahangeer, S., Soden, D. M., & Hinchion, J. (2014). Releasing pressure in tumors: what do we know so far and where do we go from here? A review. *Cancer Research, 74*(10), 2655-2662.

Au, J. L.-S., Jang, S. H., & Wientjes, M. G. (2002). Clinical aspects of drug delivery to tumors. *Journal of Controlled Release, 78*(1-3), 81-95.

Baban, C. K., Cronin, M., O'Hanlon, D., O'Sullivan, G. C., & Tangney, M. (2010). Bacteria as vectors for gene therapy of cancer. *Bioengineered Bugs, 1*(6), 385-394.

Bae, Y. H., & Park, K. (2011). Targeted drug delivery to tumors: myths, reality and possibility. *Journal of Controlled Release, 153*(3), 198.

Bahaj, A., & James, P. (1993). Characterisation of magnetotactic bacteria using image processing techniques. *IEEE Transactions on Magnetics, 29*(6), 3358-3360.

Bangham, A., Standish, M. M., & Watkins, J. C. (1965). Diffusion of univalent ions across the lamellae of swollen phospholipids. *Journal of Molecular Biology, 13*(1), 238-IN227.

Barar, J., & Omidi, Y. (2014). Surface modified multifunctional nanomedicines for simultaneous imaging and therapy of cancer. *BioImpacts, 4*(1), 3.

Bazylinski, D. A., Williams, T. J., Lefèvre, C. T., Berg, R. J., Zhang, C. L., Bowser, S. S., . . . Beveridge, T. J. (2013). Magnetococcus marinus gen. nov., sp. nov., a marine, magnetotactic bacterium that represents a novel lineage (Magnetococcaceae fam. nov., Magnetococcales ord. nov.) at the base of the Alphaproteobacteria. *International Journal of Systematic and Evolutionary Microbiology, 63*(3), 801-808.

Bettegowda, C., Dang, L. H., Abrams, R., Huso, D. L., Dillehay, L., Cheong, I., . . . Watson, E. L. (2003). Overcoming the hypoxic barrier to radiation therapy with anaerobic bacteria. *Proceedings of the National Academy of Sciences, 100*(25), 15083-15088.

Blakemore, R. P. (1982). Magnetotactic bacteria. *Annual Reviews in Microbiology, 36*(1), 217-238.

Bodurka, D. C., Levenback, C., Wolf, J. K., Gano, J., Wharton, J. T., Kavanagh, J. J., & Gershenson, D. M. (2003). Phase II Trial of Irinotecan in Patients With Metastatic Epithelial Ovarian Cancer or Peritoneal Cancer. *Journal of Clinical Oncology, 21*(2), 291-297.

Brannon-Peppas, L., & Blanchette, J. O. (2012). Nanoparticle and targeted systems for cancer therapy. *Advanced Drug Delivery Reviews, 64*, 206-212.

Brown, J. M., & Wilson, W. R. (2004). Exploiting tumour hypoxia in cancer treatment. *Nature Reviews Cancer, 4*(6), 437.

Bulte, J. W., & Kraitchman, D. L. (2004). Iron oxide MR contrast agents for molecular and cellular imaging. *NMR in Biomedicine, 17*(7), 484-499.

Bussink, J., Kaanders, J. H., & van der Kogel, A. J. (2003). Tumor hypoxia at the micro-regional level: clinical relevance and predictive value of exogenous and endogenous hypoxic cell markers. *Radiotherapy and Oncology, 67*(1), 3-15.

Canadian Cancer Society. (2017). Nearly 1 in 2 Canadians expected to get cancer: report. Retrieved from http://www.cancer.ca/en/about-us/for-media/media-releases/national/2017/canadian-cancer-statistics/?region=bc

Channarong, S., Chaicumpa, W., Sinchaipanid, N., & Mitrevej, A. (2011). Development and evaluation of chitosan-coated liposomes for oral DNA vaccine: the improvement of Peyer's patch targeting using a polyplex-loaded liposomes. *AAPS Pharmscitech, 12*(1), 192-200.

Chen, L. (2014). *Surface Functionalization and Bioconjugation of Nanoparticles for Biomedical Applications*. Ph.D. Thesis, University of Western Ontario, London, Ontario, Canada.

Cheong, I., Huang, X., Bettegowda, C., Diaz, L. A., Kinzler, K. W., Zhou, S., & Vogelstein, B. (2006). A bacterial protein enhances the release and efficacy of liposomal cancer drugs. *Science, 314*(5803), 1308-1311.

Choi, I.-K., Strauss, R., Richter, M., Yun, C.-O., & Lieber, A. (2013). Strategies to increase drug penetration in solid tumors. *Frontiers in Oncology, 3*, 193.

Coley, W. B. (1891). II. Contribution to the knowledge of sarcoma. *Annals of Surgery, 14*(3), 199.

Cunningham, D., Pyrhönen, S., James, R. D., Punt, C. J. A., Hickish, T. F., Heikkila, R., . . . Herait, P. (1998). Randomised trial of irinotecan plus supportive care versus supportive care alone after fluorouracil failure for patients with metastatic colorectal cancer. *The Lancet, 352*(9138), 1413-1418.

Dang, L. H., Bettegowda, C., Huso, D. L., Kinzler, K. W., & Vogelstein, B. (2001). Combination bacteriolytic therapy for the treatment of experimental tumors. *Proceedings of the National Academy of Sciences, 98*(26), 15155-15160.

Danila, D., Partha, R., Elrod, D. B., Lackey, M., Casscells, S. W., & Conyers, J. L. (2009). Antibody-labeled liposomes for CT imaging of atherosclerotic plaques: in vitro investigation of an anti-ICAM antibody-labeled liposome containing iohexol for molecular imaging of atherosclerotic plaques via computed tomography. *Texas Heart Institute Journal, 36*(5), 393.

de Araújo Lopes, S. C., dos Santos Giuberti, C., Rocha, T. G. R., dos Santos Ferreira, D., Leite, E. A., & Oliveira, M. C. (2013). *Liposomes as carriers of anticancer drugs*. Rijeka, Croatia: Cancer Treatment-Conventional and Innovative Approaches.

De Lanauze, D. (2013). *Contrôle tridimensionnel de bactéries magnétotactiques agissant comme microrobots pour le transport actif de médicament vers une tumeur.* Montréal, Canada: École Polytechnique de Montréal.

De Lanauze, D., Felfoul, O., Turcot, J.-P., Mohammadi, M., & Martel, S. (2014). Three-dimensional remote aggregation and steering of magnetotactic bacteria microrobots for drug delivery applications. *The International Journal of Robotics Research, 33*(3), 359-374.

Demas, V., & Lowery, T. J. (2011). Magnetic resonance for in vitro medical diagnostics: superparamagnetic nanoparticle-based magnetic relaxation switches. *New Journal of Physics, 13*(2), 025005.

Denham, C., Blakemore, R., & Frankel, R. (1980). Bulk magnetic properties of magnetotactic bacteria. *IEEE Transactions on Magnetics, 16*(5), 1006-1007.

Dennis, C., Jackson, A., Borchers, J., Ivkov, R., Foreman, A., Hoopes, P., . . . Lau, J. (2008). The influence of magnetic and physiological behaviour on the effectiveness of iron oxide nanoparticles for hyperthermia. *Journal of Physics D: Applied Physics, 41*(13), 134020.

Drummond, D. C., Noble, C. O., Hayes, M. E., Park, J. W., & Kirpotin, D. B. (2008). Pharmacokinetics and in vivo drug release rates in liposomal nanocarrier development. *Journal of pharmaceutical sciences, 97*(11), 4696-4740.

Duan, K., Zhang, X., Tang, X., Yu, J., Liu, S., Wang, D., . . . Huang, J. (2010). Fabrication of cationic nanomicelle from chitosan-graft-polycaprolactone as the carrier of 7-ethyl-10-hydroxy-camptothecin. *Colloids and Surfaces B: Biointerfaces, 76*(2), 475-482.

Ebrahimnejad, P., Dinarvand, R., Jafari, M. R., Tabasi, S. A. S., & Atyabi, F. (2011). Characterization, blood profile and biodistribution properties of surface modified PLGA nanoparticles of SN-38. *International Journal of Pharmaceutics, 406*(1–2), 122-127.

Felfoul, O. (2011). *MRI-based tumour targeting enhancement with magnetotactic bacterial carriers.* Montréal, Canada: École Polytechnique de Montréal.

Felfoul, O., Mathieu, J.-B., & Martel, S. (2008). A comparative study between BN-1 Cells and magnetic microparticles used for enhanced target delivery of therapeutic agents in the microvasculature. Paper presented at the *2nd IEEE RAS & EMBS International Conference on Biomedical Robotics and Biomechatronics*. (pp. 606-611). Scottsdale, AZ, USA.

Felfoul, O., Mohammadi, M., Taherkhani, S., De Lanauze, D., Xu, Y. Z., Loghin, D., . . . Lafleur, M. (2016). Magneto-aerotactic bacteria deliver drug-containing nanoliposomes to tumour hypoxic regions. *Nature Nanotechnology, 11*(11), 941.

Felfoul, O., Pouponneau, P., Mathieu, J.-B., & Martel, S. (2007). MR imaging of Fe-Co nanoparticles, magnetotactic bacteria and Fe3O4 microparticles for future drug delivery applications. Paper presented at the *7th IEEE Conference on Nanotechnology*. (pp. 308-311). Hong Kong, Hong Kong.

Felgner, S., Kocijancic, D., Frahm, M., & Weiss, S. (2016). Bacteria in cancer therapy: renaissance of an old concept. *International Journal of Microbiology, 2016*, 1-14.

Forbes, N. S. (2010). Engineering the perfect (bacterial) cancer therapy. *Nature Reviews Cancer, 10*(11), 785.

Forbes, N. S., Munn, L. L., Fukumura, D., & Jain, R. K. (2003). Sparse initial entrapment of systemically injected Salmonella typhimurium leads to heterogeneous accumulation within tumors. *Cancer Research, 63*(17), 5188-5193.

Fox, M., Lemmon, M., Mauchline, M., Davis, T., Giaccia, A., Minton, N., & Brown, J. (1996). Anaerobic bacteria as a delivery system for cancer gene therapy: in vitro activation of 5-fluorocytosine by genetically engineered clostridia. *Gene Therapy, 3*(2), 173-178.

Frankel, R. B., Bazylinski, D. A., Johnson, M. S., & Taylor, B. L. (1997). Magneto-aerotaxis in marine coccoid bacteria. *Biophysical Journal, 73*(2), 994-1000.

Frankel, R. B., & Blakemore, R. (1980). Navigational compass in magnetic bacteria. *Journal of Magnetism and Magnetic Materials, 15*(3), 1562.

Frese, S., & Diamond, B. (2011). Structural modification of DNA—a therapeutic option in SLE? *Nature Reviews Rheumatology, 7*(12), 733.

Fritze, A., Hens, F., Kimpfler, A., Schubert, R., & Peschka-Süss, R. (2006). Remote loading of doxorubicin into liposomes driven by a transmembrane phosphate gradient. *Biochimica et Biophysica Acta (BBA)-Biomembranes, 1758*(10), 1633-1640.

Furlani, E. J., & Furlani, E. P. (2007). A model for predicting magnetic targeting of multifunctional particles in the microvasculature. *Journal of Magnetism and Magnetic Materials, 312*(1), 187-193.

Ganai, S., Arenas, R. B., Sauer, J. P., Bentley, B., & Forbes, N. S. (2011). In tumors Salmonella migrate away from vasculature toward the transition zone and induce apoptosis. *Cancer Gene Therapy, 18*(7), 457.

Garcia-Carbonero, R., & Supko, J. G. (2002). Current Perspectives on the Clinical Experience, Pharmacology, and Continued Development of the Camptothecins. *Clinical Cancer Research, 8*(3), 641-661.

Gardlik, R., Behuliak, M., Palffy, R., Celec, P., & Li, C. (2011). Gene therapy for cancer: bacteria-mediated anti-angiogenesis therapy. *Gene Therapy, 18*(5), 425.

Gil, P. R., & Parak, W. J. (2008). Composite nanoparticles take aim at cancer. *ACS Nano, 2*(11), 2200-2205.

Gleich, B., Hellwig, N., Bridell, H., Jurgons, R., Seliger, C., Alexiou, C., . . . Weyh, T. (2007). Design and evaluation of magnetic fields for nanoparticle drug targeting in cancer. *IEEE Transactions on Nanotechnology, 6*(2), 164-170.

Grabarek, Z., & Gergely, J. (1990). Zero-length crosslinking procedure with the use of active esters. *Analytical Biochemistry, 185*(1), 131-135.

Gray, L. H., Conger, A. D., Ebert, M., Hornsey, S., & Scott, O. (1953). The concentration of oxygen dissolved in tissues at the time of irradiation as a factor in radiotherapy. *The British Journal of radiology, 26*(312), 638-648.

Gubernator, J., Chwastek, G., Korycińska, M., Stasiuk, M., Grynkiewicz, G., Lewrick, F., . . . Kozubek, A. (2010). The encapsulation of idarubicin within liposomes using the novel EDTA ion gradient method ensures improved drug retention in vitro and in vivo. *Journal of Controlled Release, 146*(1), 68-75.

Haran, G., Cohen, R., Bar, L. K., & Barenholz, Y. (1993). Transmembrane ammonium sulfate gradients in liposomes produce efficient and stable entrapment of amphipathic weak bases. *Biochimica et Biophysica Acta (BBA)-Biomembranes, 1151*(2), 201-215.

Hermanson, G. T. (2013). *Bioconjugate Techniques*: Academic Press.

Hernández-Zapata, E., Martínez-Balbuena, L., & Santamaría-Holek, I. (2010). Thermodynamics and Dynamics of the Formation of Spherical Lipid Vesicles. *Biophysical Journal, 98*(3), 481a.

Hobbs, S. K., Monsky, W. L., Yuan, F., Roberts, W. G., Griffith, L., Torchilin, V. P., & Jain, R. K. (1998). Regulation of transport pathways in tumor vessels: role of tumor type and microenvironment. *Proceedings of the National Academy of Sciences, 95*(8), 4607-4612.

Hong, M., Zhu, S., Jiang, Y., Tang, G., & Pei, Y. (2009). Efficient tumor targeting of hydroxycamptothecin loaded PEGylated niosomes modified with transferrin. *Journal of Controlled Release, 133*(2), 96-102.

Hood, R. R., DeVoe, D. L., Atencia, J., Vreeland, W. N., & Omiatek, D. M. (2014). A facile route to the synthesis of monodisperse nanoscale liposomes using 3D microfluidic hydrodynamic focusing in a concentric capillary array. *Lab on a Chip, 14*(14), 2403-2409.

Immordino, M. L., Dosio, F., & Cattel, L. (2006). Stealth liposomes: review of the basic science, rationale, and clinical applications, existing and potential. *International Journal of Nanomedicine, 1*(3), 297.

Jain, R. K. (Dec 2012). Delivery of molecular and cellular medicine to solid tumors. *Advanced Drug Delivery Reviews, 64*, 353-365.

Jesorka, A., & Orwar, O. (2008). Liposomes: technologies and analytical applications. *Annual Review of Anaytical Chemistry, 1*, 801-832.

Jhaveri, A. M., & Torchilin, V. P. (2014). Multifunctional polymeric micelles for delivery of drugs and siRNA. *Frontiers in Pharmacology, 5*, 77.

Jin, R., Lin, B., Li, D., & Ai, H. (2014). Superparamagnetic iron oxide nanoparticles for MR imaging and therapy: design considerations and clinical applications. *Current opinion in pharmacology, 18*, 18-27.

Jørgensen, K., Davidsen, J., & Mouritsen, O. G. (2002). Biophysical mechanisms of phospholipase A2 activation and their use in liposome-based drug delivery. *FEBS Letters, 531*(1), 23-27.

Junttila, M. R., & de Sauvage, F. J. (2013). Influence of tumour micro-environment heterogeneity on therapeutic response. *Nature, 501*(7467), 346-354.

Kaminskas, L. M., McLeod, V. M., Kelly, B. D., Sberna, G., Boyd, B. J., Williamson, M., . . . Porter, C. J. (2012). A comparison of changes to doxorubicin pharmacokinetics, antitumor activity, and toxicity mediated by PEGylated dendrimer and PEGylated liposome drug delivery systems. *Nanomedicine: Nanotechnology, Biology and Medicine, 8*(1), 103-111.

Kasinskas, R. W., & Forbes, N. S. (2006). Salmonella typhimurium specifically chemotax and proliferate in heterogeneous tumor tissue in vitro. *Biotechnology and Bioengineering, 94*(4), 710-721.

Kinner, S., Maderwald, S., Parohl, N., Albert, J., Corot, C., Robert, P., . . . Vogt, F. M. (2011). Contrast-enhanced magnetic resonance angiography in rabbits: evaluation of the gadolinium-based agent p846 and the iron-based blood pool agent p904 in comparison with gadoterate meglumine. *Investigative Radiology, 46*(8), 524-529.

Koçer, A. (2010). Functional liposomal membranes for triggered release. In *Liposomes* (pp. 243-255): Springer.

Koizumi, F., Kitagawa, M., Negishi, T., Onda, T., Matsumoto, S.-i., Hamaguchi, T., & Matsumura, Y. (2006). Novel SN-38–Incorporating Polymeric Micelles, NK012, Eradicate Vascular Endothelial Growth Factor–Secreting Bulky Tumors. *Cancer Research, 66*(20), 10048-10056.

Kolhatkar, A. G., Jamison, A. C., Litvinov, D., Willson, R. C., & Lee, T. R. (2013). Tuning the magnetic properties of nanoparticles. *International Journal of Molecular Sciences, 14*(8), 15977-16009.

Kolhatkar, R., Swaan, P., & Ghandehari, H. (2008). Potential Oral Delivery of 7-Ethyl-10-Hydroxy-Camptothecin (SN-38) using Poly(amidoamine) Dendrimers. *Pharmaceutical Research, 25*(7), 1723-1729.

Koumoutsakos, P., Pivkin, I., & Milde, F. (2013). The fluid mechanics of cancer and its therapy. *Annual Review of Fluid Mechanics, 45*.

Kuh, H.-J., Jang, S. H., Wientjes, M. G., Weaver, J. R., & Au, J. L.-S. (1999). Determinants of paclitaxel penetration and accumulation in human solid tumor. *Journal of Pharmacology and Experimental Therapeutics, 290*(2), 871-880.

Kumari, A., Yadav, S. K., & Yadav, S. C. (2010). Biodegradable polymeric nanoparticles based drug delivery systems. *Colloids and Surfaces B: Biointerfaces, 75*(1), 1-18.

Lin, M. M., Kim, D. K., El Haj, A. J., & Dobson, J. (2008). Development of superparamagnetic iron oxide nanoparticles (SPIONS) for translation to clinical applications. *IEEE Transactions on Nanobioscience, 7*(4), 298-305.

Liu, S., Xu, X., Zeng, X., Li, L., Chen, Q., & Li, J. (2014). Tumor-targeting bacterial therapy: A potential treatment for oral cancer. *Oncology Letters, 8*(6), 2359-2366.

Liu, Z., Robinson, J. T., Sun, X., & Dai, H. (2008). PEGylated Nanographene Oxide for Delivery of Water-Insoluble Cancer Drugs. *Journal of the American Chemical Society, 130*(33), 10876-10877.

Loghin, D., Tremblay, C., & Martel, S. (2016). Improved three-dimensional remote aggregations of magnetotactic bacteria for tumor targeting. Paper presented at the *IEEE International Conference on Manipulation, Automation and Robotics at Small Scales (MARSS)*. (pp. 1-6). Paris, France.

Loghin, D., Tremblay, C., Mohammadi, M., & Martel, S. (2017). Exploiting the responses of magnetotactic bacteria robotic agents to enhance displacement control and swarm formation for drug delivery platforms. *The International Journal of Robotics Research, 36*(11), 1195-1210.

Mahapatro, A., & Singh, D. K. (2011). Biodegradable nanoparticles are excellent vehicle for site directed in-vivo delivery of drugs and vaccines. *Journal of Nanobiotechnology, 9*(1), 55.

Maherani, B., Arab-Tehrany, E., R Mozafari, M., Gaiani, C., & Linder, M. (2011). Liposomes: a review of manufacturing techniques and targeting strategies. *Current Nanoscience, 7*(3), 436-452.

Mahmoudi, M., Sant, S., Wang, B., Laurent, S., & Sen, T. (2011). Superparamagnetic iron oxide nanoparticles (SPIONs): development, surface modification and applications in chemotherapy. *Advanced Drug Delivery Reviews, 63*(1-2), 24-46.

Mahon, E., Salvati, A., Bombelli, F. B., Lynch, I., & Dawson, K. A. (2012). Designing the nanoparticle–biomolecule interface for "targeting and therapeutic delivery". *Journal of Controlled Release, 161*(2), 164-174.

Majedi, Y., Loghin, D., Mohammadi, M., & Martel, S. (2017). Characterizations of magnetotactic bacteria conjugated versus unconjugated with carboxylate-Functionalized superparamagnetic iron oxide nanoparticles for tumor targeting purposes. Paper presented at the *IEEE International Conference on Manipulation, Automation and Robotics at Small Scales (MARSS)*. (pp. 1-6). Montreal, QC, Canada.

Malam, Y., Loizidou, M., & Seifalian, A. M. (2009). Liposomes and nanoparticles: nanosized vehicles for drug delivery in cancer. *Trends in Pharmacological Sciences, 30*(11), 592-599.

Malam, Y., Loizidou, M., & Seifalian, A. M. (Nov 2009). Liposomes and nanoparticles: nanosized vehicles for drug delivery in cancer. *Trends in Pharmacological Sciences, 30*(11), 592-599.

Maleux, G., van Malenstein, H., Vandecaveye, V., Heye, S., Vaninbroukx, J., Nevens, F., & Verslype, C. (2009). Transcatheter chemoembolization of unresectable hepatocellular carcinoma: current knowledge and future directions. *Digestive Diseases, 27*(2), 157-163.

Manaspon, C., Hongeng, S., Boongird, A., & Nasongkla, N. (2012). Preparation and in vitro characterization of SN-38-loaded, self-forming polymeric depots as an injectable drug delivery system. *Journal of Pharmaceutical Sciences*, 101(10), 3708-3717.

Martel, S. (2006). Controlled bacterial micro-actuation. Paper presented at the IEEE *International Conference on Microtechnologies in Medicine and Biology*. (PP. 89-92). Okinawa, Japan.

Martel, S. (2012). Magnetotactic bacteria for microrobotics. In *Microbiorobotics* (pp. 201-210): Elsevier.

Martel, S. (2013a). Combining pulsed and DC gradients in a clinical MRI-based microrobotic platform to guide therapeutic magnetic agents in the vascular network. *International Journal of Advanced Robotic Systems, 10*(1), 30.

Martel, S. (2013b). Magnetic navigation control of microagents in the vascular network: Challenges and strategies for endovascular magnetic navigation control of microscale drug delivery carriers. *IEEE Control Systems, 33*(6), 119-134.

Martel, S. (2014). Magnetic therapeutic delivery using navigable agents. *Therapeutic Delivery, 5*(2), 189-204.

Martel, S. (2014). Presenting a New Paradigm in Cancer Therapy: Delivering therapeutic agents using navigable microcarriers. *IEEE Pulse, 5*(3), 48-55.

Martel, S. (2017). Beyond imaging: Macro-and microscale medical robots actuated by clinical MRI scanners. *Science Robotics, 2*(3), eaam8119.

Martel, S., Felfoul, O., Mathieu, J.-B., Chanu, A., Tamaz, S., Mohammadi, M., . . . Tabatabaei, N. (2009). MRI-based medical nanorobotic platform for the control of magnetic nanoparticles and flagellated bacteria for target interventions in human capillaries. *The International Journal of Robotics Research, 28*(9), 1169-1182.

Martel, S., Mathieu, J.-B., Felfoul, O., Chanu, A., Aboussouan, E., Tamaz, S., . . . Soulez, G. (2007). Automatic navigation of an untethered device in the artery of a living animal using a conventional clinical magnetic resonance imaging system. *Applied Physics Letters, 90*(11), 114105.

Martel, S., Mohammadi, M., de Lanauze, D., & Felfoul, O. (2013). *Magnetotactic bacteria as dispatched oxygen sensors.* Paper presented at the Sensing Technology (ICST), 2013 Seventh International Conference on.

Martel, S., Mohammadi, M., Felfoul, O., Lu, Z., & Pouponneau, P. (2009). Flagellated magnetotactic bacteria as controlled MRI-trackable propulsion and steering systems for medical nanorobots operating in the human microvasculature. *The International Journal of Robotics Research, 28*(4), 571-582.

Martel, S., Tremblay, C. C., Ngakeng, S., & Langlois, G. (2006). Controlled manipulation and actuation of micro-objects with magnetotactic bacteria. *Applied Physics Letters, 89*(23), 233904.

Maruyama, K., Takizawa, T., Takahashi, N., Tagawa, T., Nagaike, K., & Iwatsuru, M. (1997). Targeting efficiency of PEG-immunoliposome-conjugated antibodies at PEG terminals. *Advanced Drug Delivery Reviews, 24*(2-3), 235-242.

Massing, U., Cicko, S., & Ziroli, V. (2008). Dual asymmetric centrifugation (DAC)—A new technique for liposome preparation. *Journal of Controlled Release, 125*(1), 16-24.

Mathieu, J.-B., & Martel, S. (2007). Magnetic microparticle steering within the constraints of an MRI system: proof of concept of a novel targeting approach. *Biomedical microdevices, 9*(6), 801-808.

McBain, S. C., Yiu, H. H., & Dobson, J. (2008). Magnetic nanoparticles for gene and drug delivery. *International Journal of Nanomedicine, 3*(2), 169.

McCarthy, J. R., Bhaumik, J., Karver, M. R., Sibel Erdem, S., & Weissleder, R. (2010). Targeted nanoagents for the detection of cancers. *Molecular Oncology, 4*(6), 511-528.

McDonald, D. M., & Baluk, P. (2002). Significance of blood vessel leakiness in cancer. In: AACR.

Meure, L. A., Foster, N. R., & Dehghani, F. (2008). Conventional and dense gas techniques for the production of liposomes: a review. *AAPS Pharmscitech, 9*(3), 798.

Mikhaylov, G., Mikac, U., Magaeva, A. A., Itin, V. I., Naiden, E. P., Psakhye, I., . . . Zeiser, R. (2011). Ferri-liposomes as an MRI-visible drug-delivery system for targeting tumours and their microenvironment. *Nature Nanotechnology, 6*(9), 594.

Minchinton, A. I., & Tannock, I. F. (2006). Drug penetration in solid tumours. *Nature Reviews Cancer, 6*(8), 583.

Mishima, F., Takeda, S.-i., Izumi, Y., & Nishijima, S. (2006). Three dimensional motion control system of ferromagnetic particles for magnetically targeted drug delivery systems. *IEEE Transactions on Applied Superconductivity, 16*(2), 1539-1542.

Mitchell, N., Kalber, T. L., Cooper, M. S., Sunassee, K., Chalker, S. L., Shaw, K. P., . . . Blower, P. J. (2013). Incorporation of paramagnetic, fluorescent and PET/SPECT contrast agents into liposomes for multimodal imaging. *Biomaterials, 34*(4), 1179-1192.

Moeller, B. J., Richardson, R. A., & Dewhirst, M. W. (2007). Hypoxia and radiotherapy: opportunities for improved outcomes in cancer treatment. *Cancer and Metastasis Reviews, 26*(2), 241-248.

Moese, J., & Moese, G. (1964). Oncolysis by clostridia. I. Activity of Clostridium butyricum (M-55) and other nonpathogenic clostridia against the Ehrlich carcinoma. *Cancer research, 24*(2 Part 1), 212-216.

Nadkarni, R., Barkley, S., & Fradin, C. (2013). A comparison of methods to measure the magnetic moment of magnetotactic bacteria through analysis of their trajectories in external magnetic fields. *PloS one, 8*(12), e82064.

Noda, K., Nishiwaki, Y., Kawahara, M., Negoro, S., Sugiura, T., Yokoyama, A., . . . Saijo, N. (2002). Irinotecan plus Cisplatin Compared with Etoposide plus Cisplatin for Extensive Small-Cell Lung Cancer. *New England Journal of Medicine, 346*(2), 85-91.

Nogueira, E., Gomes, A. C., Preto, A., & Cavaco-Paulo, A. (2015). Design of liposomal formulations for cell targeting. *Colloids and Surfaces B: Biointerfaces, 136*, 514-526.

O'Connell, M. J., Martenson, J. A., Wieand, H. S., Krook, J. E., Macdonald, J. S., Haller, D. G., . . . Rich, T. A. (1994). Improving adjuvant therapy for rectal cancer by combining protracted-infusion fluorouracil with radiation therapy after curative surgery. *New England Journal of Medicine, 331*(8), 502-507.

Oude Blenke, E. (2012). *Strategies for triggered drug release from liposomes: in search of "smart" lipids and "smart" triggers.* Utrecht, Netherlands: University of Utrecht.

Panel, V., Boëlle, P.-Y., Ayala-Sanmartin, J., Jouniaux, A.-M., Hamelin, R., Masliah, J., . . . Wendum, D. (2006). Cytoplasmic phospholipase A2 expression in human colon adenocarcinoma is correlated with cyclooxygenase-2 expression and contributes to prostaglandin E2 production. *Cancer Letters, 243*(2), 255-263.

Papahadjopoulos, D., & Miller, N. (1967). Phospholipid model membranes. I. Structural characteristics of hydrated liquid crystals. *Biochimica et Biophysica Acta (BBA)-Biomembranes, 135*(4), 624-638.

Papahadjopoulos, D., Nir, S., & Ohki, S. (1972). Permeability properties of phospholipid membranes: effect of cholesterol and temperature. *Biochimica et Biophysica Acta (BBA)-Biomembranes, 266*(3), 561-583.

Pattabiraman, V. R., & Bode, J. W. (2011). Rethinking amide bond synthesis. *Nature, 480*(7378), 471.

Patyar, S., Joshi, R., Byrav, D. P., Prakash, A., Medhi, B., & Das, B. (2010). Bacteria in cancer therapy: a novel experimental strategy. *Journal of Biomedical Science, 17*(1), 21.

Peddareddigari, V. G., Wang, D., & DuBois, R. N. (2010). The tumor microenvironment in colorectal carcinogenesis. *Cancer Microenvironment, 3*(1), 149-166.

Polyak, B., & Friedman, G. (2009). Magnetic targeting for site-specific drug delivery: applications and clinical potential. *Expert Opinion on Drug Delivery, 6*(1), 53-70.

Pouponneau, P., Leroux, J.-C., & Martel, S. (2009). Magnetic nanoparticles encapsulated into biodegradable microparticles steered with an upgraded magnetic resonance imaging system for tumor chemoembolization. *Biomaterials, 30*(31), 6327-6332.

Quanrong, G., James, Z. X., Min, H., Chuan, H., & Jie, C. (2012). SN-38 loaded polymeric micelles to enhance cancer therapy. *Nanotechnology, 23*(20), 205101.

Roizin-Towle, L., & Hall, E. (1978). Studies with bleomycin and misonidazole on aerated and hypoxic cells. *British Journal of Cancer, 37*(2), 254.

Rotariu, O., & Strachan, N. J. (2005). Modelling magnetic carrier particle targeting in the tumor microvasculature for cancer treatment. *Journal of Magnetism and Magnetic Materials, 293*(1), 639-646.

S. A. Hussain, D. R. F., G. El-Gazzaz, D. F. Mirza, N. D. James, P. McMaster, et al. (Feb 2001). Hepatocellular carcinoma. *Annals of Oncology, 12*, 161-172.

Sadzuka, Y., Takabe, H., & Sonobe, T. (2005). Liposomalization of SN-38 as active metabolite of CPT-11. *Journal of Controlled Release, 108*(2-3), 453-459.

Sawant, R. R., & Torchilin, V. P. (2010). Liposomes as 'smart'pharmaceutical nanocarriers. *Soft Matter, 6*(17), 4026-4044.

Schroeder, A., Kost, J., & Barenholz, Y. (2009). Ultrasound, liposomes, and drug delivery: principles for using ultrasound to control the release of drugs from liposomes. *Chemistry and Physics of Lipids, 162*(1), 1-16.

Sesay, M. A. (2003). Monoclonal antibody conjugation via chemical modification. *Biopharm International, 16*(12), 32-39.

Shamsipour, F., Zarnani, A. H., Ghods, R., Chamankhah, M., Forouzesh, F., Vafaei, S., . . . Jeddi-Tehrani, M. (2009). Conjugation of monoclonal antibodies to super paramagnetic iron

oxide nanoparticles for detection of her2/neu antigen on breast cancer cell lines. *Avicenna Journal of Medical Biotechnology, 1*(1), 27.

Shang, H., Chang, W.-S., Kan, S., Majetich, S. A., & Lee, G. U. (2006). Synthesis and characterization of paramagnetic microparticles through emulsion-templated free radical polymerization. *Langmuir, 22*(6), 2516-2522.

Slatter, J. G., Su, P., Sams, J. P., Schaaf, L. J., & Wienkers, L. C. (1997). Bioactivation of the anticancer agent CPT-11 to SN-38 by human hepatic microsomal carboxylesterases and the in vitroassessment of potential drug interactions. *Drug Metabolism and Disposition, 25*(10), 1157-1164.

Sperling, R. A., & Parak, W. J. (2010). Surface modification, functionalization and bioconjugation of colloidal inorganic nanoparticles. *Philosophical Transactions of the Royal Society of London A: Mathematical, Physical and Engineering Sciences, 368*(1915), 1333-1383.

St Jean, A. T., Zhang, M., & Forbes, N. S. (2008). Bacterial therapies: completing the cancer treatment toolbox. *Current Opinion in Biotechnology, 19*(5), 511-517.

Staros, J. V., Wright, R. W., & Swingle, D. M. (1986). Enhancement by N-hydroxysulfosuccinimide of water-soluble carbodiimide-mediated coupling reactions. *Analytical Biochemistry, 156*(1), 220-222.

Sur, S., Fries, A. C., Kinzler, K. W., Zhou, S., & Vogelstein, B. (2014). Remote loading of preencapsulated drugs into stealth liposomes. *Proceedings of the National Academy of Sciences, 111*(6), 2283-2288.

Szoka Jr, F. C. (1996). *U.S. Patent No. 5,567,434*. Washington, DC: U.S. Patent and Trademark Office.

Taherkhani, S. (2015). *Attachment of Therapeutic and Imaging Agents to Magnetotactic Bacteria Acting as Self-Propelled Bio-Carriers for Cancer Treatment.* Montréal, Canada: École Polytechnique de Montréal.

Tallman, M. N., Ritter, J. K., & Smith, P. C. (2005). Differential rates of glucuronidation for 7-ethyl-10-hydroxy-camptothecin (SN-38) lactone and carboxylate in human and rat microsomes and recombinant udp-glucuronosyltransferase isoforms. *Drug Metabolism and Disposition, 33*(7), 977-983.

Tanabe, K., Zhang, Z., Ito, T., Hatta, H., & Nishimoto, S.-i. (2007). Current molecular design of intelligent drugs and imaging probes targeting tumor-specific microenvironments. *Organic & Biomolecular Chemistry, 5*(23), 3745-3757.

Tobin, P., Clarke, S., Seale, J. P., Lee, S., Solomon, M., Aulds, S., . . . Rivory, L. (2006). The in vitro metabolism of irinotecan (CPT-11) by carboxylesterase and β-glucuronidase in human colorectal tumours. *British Journal of Clinical Pharmacology, 62*(1), 122-129.

Torchilin, V. P. (2005). Recent advances with liposomes as pharmaceutical carriers. *Nature Reviews Drug Discovery, 4*(2), 145.

Toso, J. F., Gill, V. J., Hwu, P., Marincola, F. M., Restifo, N. P., Schwartzentruber, D. J., . . . Stock, F. (2002). Phase I study of the intravenous administration of attenuated Salmonella typhimurium to patients with metastatic melanoma. *Journal of clinical oncology: Official Journal of the American Society of Clinical Oncology, 20*(1), 142.

Trédan, O., Galmarini, C. M., Patel, K., & Tannock, I. F. (2007). Drug resistance and the solid tumor microenvironment. *Journal of the National Cancer Institute, 99*(19), 1441-1454.

WEI, W., & FENG, J. (2009). Immobilization of anti-transferrin on nano-gold and its immune recognition of transferrin. *Spectroscopy and Spectral Analysis, 29*(5), 1398-1401.

Weiss, G. J., Infante, J. R., Chiorean, E. G., Borad, M. J., Bendell, J. C., Molina, J. R., . . . Jones, S. F. (2011). Phase 1 study of the safety, tolerability, and pharmacokinetics of TH-302, a hypoxia-activated prodrug, in patients with advanced solid malignancies. *Clinical Cancer Research, 17*(9), 2997-3004.

Williams, J., Lansdown, R., Sweitzer, R., Romanowski, M., LaBell, R., Ramaswami, R., & Unger, E. (2003). Nanoparticle drug delivery system for intravenous delivery of topoisomerase inhibitors. *Journal of Controlled Release, 91*(1–2), 167-172.

Wong, C., Stylianopoulos, T., Cui, J., Martin, J., Chauhan, V. P., Jiang, W., . . . Fukumura, D. (2011). Multistage nanoparticle delivery system for deep penetration into tumor tissue. *Proceedings of the National Academy of Sciences, 108*(6), 2426-2431.

Wong, S. S., & Jameson, D. M. (2011). *Chemistry of protein and nucleic acid cross-linking and conjugation*: CRC Press.

World Health Organization. (2017). World's health ministers renew commitment to cancer prevention and control. Retrieved from http://www.who.int/cancer/media/news/cancer-prevention-resolution/en/

Xuan, T., Zhang, J. A., & Ahmad, I. (2006). HPLC method for determination of SN-38 content and SN-38 entrapment efficiency in a novel liposome-based formulation, LE-SN38. *Journal of Pharmaceutical and Biomedical Analysis, 41*(2), 582-588.

Yallapu, M. M., Foy, S. P., Jain, T. K., & Labhasetwar, V. (2010). PEG-functionalized magnetic nanoparticles for drug delivery and magnetic resonance imaging applications. *Pharmaceutical Research, 27*(11), 2283-2295.

Yang, S.-y., Zheng, Y., Chen, J.-y., Zhang, Q.-y., Zhao, D., Han, D.-e., & Chen, X.-j. (2013). Comprehensive study of cationic liposomes composed of DC-Chol and cholesterol with different mole ratios for gene transfection. *Colloids and Surfaces B: Biointerfaces, 101*, 6-13.

Yang, X., Hu, Z., Chan, S. Y., Goh, B. C., Duan, W., Chan, E., & Zhou, S. (2005). Simultaneous determination of the lactone and carboxylate forms of irinotecan (CPT-11) and its active metabolite SN-38 by high-performance liquid chromatography: Application to plasma pharmacokinetic studies in the rat. *Journal of Chromatography B, 821*(2), 221-228.

Yin, X., Yu, B., Tang, Z., He, B., Ren, J., Xiao, X., & Tang, W. (2013). Bifidobacterium infantis-mediated HSV-TK/GCV suicide gene therapy induces both extrinsic and intrinsic apoptosis in a rat model of bladder cancer. *Cancer Gene Therapy, 20*(2), 77.

Yiu, H. H. (2011). Engineering the multifunctional surface on magnetic nanoparticles for targeted biomedical applications: a chemical approach. *Nanomedicine, 6*(8), 1429-1446.

Yu, M. K., Jeong, Y. Y., Park, J., Park, S., Kim, J. W., Min, J. J., . . . Jon, S. (2008). Drug-loaded superparamagnetic iron oxide nanoparticles for combined cancer imaging and therapy in vivo. *Angewandte Chemie, 120*(29), 5442-5445.

Yun, X., Maximov, V. D., Yu, J., Vertegel, A. A., & Kindy, M. S. (2013). Nanoparticles for targeted delivery of antioxidant enzymes to the brain after cerebral ischemia and reperfusion injury. *Journal of Cerebral Blood Flow & Metabolism, 33*(4), 583-592.

Zeghari-Squalli, N., Raymond, E., Cvitkovic, E., & Goldwasser, F. (1999). Cellular Pharmacology of the Combination of the DNA Topoisomerase I Inhibitor SN-38 and the Diaminocyclohexane Platinum Derivative Oxaliplatin. *Clinical Cancer Research, 5*(5), 1189-1196.

Zhang, J. A., Xuan, T., Parmar, M., Ma, L., Ugwu, S., Ali, S., & Ahmad, I. (2004). Development and characterization of a novel liposome-based formulation of SN-38. *International Journal of Pharmaceutics, 270*(1-2), 93-107.

Znati, C. A., Rosenstein, M., Boucher, Y., Epperly, M. W., Bloomer, W. D., & Jain, R. K. (1996). Effect of radiation on interstitial fluid pressure and oxygenation in a human tumor xenograft. *Cancer Research, 56*(5), 964-968.